Available online at www.sciencedirect.com

ScienceDirect

Procedia Engineering 00 (2017) 000–000

Procedia Engineering

www.elsevier.com/locate/procedia

Sustainable Civil Engineering Structures and Construction Materials, SCESCM 2016

Forensic Assessment on Near Surface Landslide using Electrical Resistivity Imaging (ERI) at Kenyir Lake area in Terengganu, Malaysia

Mohd Hazreek Zainal Abidin[a,*], Aziman Madun[b], Saiful Azhar Ahmad Tajudin[c], Mohd Fakhrurrazi Ishak[d]

[a,b]*Faculty of Civil and Environmental Engineering, Universiti Tun Hussein Onn Malaysia, Johor 84600, Malaysia*
[c]*Research Center for Soft Soil, Universiti Tun Hussein Onn Malaysia, Johor 84600, Malaysia*
[d]*Faculty of Engineering Technology, Universiti Malaysia Pahang, Pahang 26600, Malaysia*

Abstract

Electrical resistivity method which was championed by geophysicist has increasingly popular in civil engineering application due to its efficiency in term of cost, time and data coverage. In the past, conventional forensic assessment related to the landslide has experienced several limitations due to expensive, time consuming and limited data coverage. Hence, this study performed an alternative technique with particular reference to electrical resistivity imaging (ERI) in evaluating the slope failure at Kenyir Lake, Malaysia. During the data acquisition, two lines of ERI was performed using ABEM Terrameter LS set of equipment based on Schlumberger array. According to the ERI results produced, it was found that the subsurface profiles consist of completely weathered to highly weathered material (1 – 150 ohm.m), highly weathered to moderately weathered material (150 – 300 ohm.m), moderately weathered to hard material (300 – 2400 ohm.m) and fresh, hard and dry material (>2400 ohm.m). Moreover, electrical resistivity anomaly was managed to detect the presence of geological structure with particular reference to fault and rock discontinuities which associated to low resistivity anomaly. The heterogeneous of the subsurface material presented using integrated analysis of ERI and borehole data enabled forensic assessment of the landslide to be evaluated. The combination of heavy rainfall and existing geological structure (weakness zone) was believed to be a major factor which triggered this slope to be failed. This result was applicable to assist the geotechnical engineer in design concept recommendation of the slope remediation with fast, less cost and wide data coverage. Finally, ERI results with borehole verification was applicable to be adopted in landslide forensic assessment based on slope geomaterials stiffness variations generated after the slope movement. Furthermore, this electrical resistivity method adopts a surface technique that can minimize the disruption and damage to the site thus preserving a sustainable environment during the site data acquisition assessment.

* Corresponding author. Tel.: +0-000-000-0000 ; fax: +0-000-000-0000 .
E-mail address: hazreek@uthm.edu.my

Peer-review under responsibility of the organizing committee of SCESCM 2016.

Peer-review under responsibility of the organizing committee of SCESCM 2016.

Keywords: Electrical resistivity method ; electrical resistivity imaging ; forensic assessment ; landslide ; resistivity anomaly ; geological structure.

1. Introduction

Forensic assessment in engineering is the investigation of materials, products, structures or breakdown components which may cause injury or property damage. Engineering forensic investigation used to identify causes of failure for rehabilitation or mitigation purposes or to assist a court in determining the facts of an incident. The process of engineering forensic assessment involve with investigation and data collection related to the materials, products, structures or components that failed such as inspections, collecting evidence, testing and measurements, developing models, obtaining prototype model and conducting experiments. Specifically in geotechnical forensic engineering, it involves analysis of a project, site conditions, or construction from a geotechnical point of view which can be performed during the design phase (e.g. checking calculations and engineering assumptions) or during or after the construction of the project (e.g. providing quality assurance or address issues that arise during or after construction) for rehabilitation purposes. Common related issues involving geotechnical forensic evaluation were ground settlement, slope instability, foundation failure, excavation failure, collapsible soil, soil corrosion, etc. Forensic geotechnical engineering is growing increasing important in most of the countries where the foundation failures may lead to litigation and even criminal action [1].

Conventionally, site investigation data used in ground instability assessment was based on borehole exploration method [2-4]. However, several limitations have been experienced related to conventional method due to its high cost, time consuming and limited data coverage. Furthermore, conventional method was based on the drilling data which represent only single point information (1-D) at the actual drilling location thus enables some degree of uncertainties due to the boring interpolation which consider critical in a complex geological area [5-7]. Lots number of drilling point was required in order to obtain higher accuracy of the subsurface results thus increasing cost and time of the project. Moreover, conventional method was based on drilling process which able to increased site damageability due to its destructive approach in field exploration. Therefore, the solutions to these challenges will require multidisciplinary research across the social and physical sciences and engineering [8]. Hence, geophysical method offers the chance to overcome some of the problems inherent in more conventional ground investigation techniques [9]. Geophysical techniques contributes several advantages such as it can be performed fast and low cost and has the ability to cover greater areas more thoroughly [10-13] and [6].

As reported by [14], Cummings and Clark have found that geophysical instruments used in landslides evaluation were heavily based on seismic refraction and electrical resistivity methods thru basis of interpretation of obvious different physical properties of the sliding materials compared to the underlying undisturbed sediments or bedrock. However, seismic refraction method experienced several limitations due to its physics fundamental constraint such as hidden and thin layer, inadequate sources, noisy and involve lots of data reduction thus promoting to increase the results ambiguity. Nowadays, electrical resistivity imaging (ERI) has greatly being improved in term of survey coverage, field measurement, processing techniques thus applicable to resolve complex geological structure compared to the previous sounding technique [15]. From the past, electrical resistivity survey has widely used as a tool for investigating the condition of the slope especially in landslide studies during the pre and post construction stages [16-21]. According to [22], landslides areas has widely being investigated using ERT technique with the aim to reconstruct the slope and body geometry, to locate the possible sliding surface, to identify vulnerability surfaces, to estimate the slide material thickness and to detect areas with high water content. According to [21-24] and [25], geophysical method such as the electrical resistivity can be practically adopted to determine the internal distribution of materials within a slope, identifying sliding surface geometry, water effect on slope, landslide material physical properties and mass movement. Furthermore, electrical resistivity data was able to show a two layer system in which the low resistivity landslide mass cross-cuts the resistivity layering in the higher resistivity sediments [26]. However, the standard performance of individual geophysical method always depends on fundamental physical limitation (e.g. penetration, resolution, and signal to-noise ratio) [21] and [27] Moreover, geophysical methods are unable to stand

alone in order to provide solutions to any particular problems [28] and [29]. Hence, strong verification from direct test (field test, experimental test, etc.) was important to support the electrical resistivity anomaly interpretation. A number of researchers have shown that the integration of geophysical survey and geotechnical data can provide a meaningful data and interpretation for subsurface profile characterization [30-32] and [20]

Hence, this study performed a forensic assessment on near surface landslide using electrical resistivity imaging (ERI) at Kenyir Lake area in Terengganu, Malaysia. Finally, this study aims to contribute those related parties regarding the good prospect of ERI as an alternative tool in forensic landslide investigation.

2. Methodology

This study involves three phases via desk study, field measurement and data processing. Desk study begins with gathering of previous information regarding study area thru existing report, maps, etc. due to obtained early information such as sites geology, topography, etc. in global and localize scale as presented in subsection 2.1. Then, field measurement was performed using electrical resistivity imaging (ERI) and finally raw data from field measurement was analyzed and processed using RES2DINV software as explained in subsection 2.2.

Study area and geologic setting

This study was located at north eastside of Peninsular Malaysia consist of an artificial lake (largest man-made lake in South East Asia) in the state of Terengganu created in 1985. Generally, the site study has mix topography of undulating hilly terrain which surrounds the existing reservoir. The localize site study was performed at Kenyir Lake, Terengganu specifically at Pengkalan Gawi as shown in Figure 1.

The general geology of Malaysia has been well documented by Minerals and Geoscience Department Malaysia (1985). Geological map in Figure 2 shows distribution the bedrock in this studied area which specifically located at Pengkalan Gawi, Kenyir Lake. According to Figure 1, Pengkalan Gawi, Kenyir Lake is situated at intrusive rock formation which is granitic rock consist of fault zone. In addition, Figure 3 shows positive lineament of satellite image as evidence that Pengkalan Gawi, Kenyir Lake was located in a fault zone. This fault may possibly presents and influencing the investigated area, thus provide a groundwater regime in the rock formation. Site observation indicated the granitic outcrop and boulder. Based on boreholes results, it was found that this area has been a mixture of sandy silt, silty sand, clayey silt and gravelly sand. Borehole records (BH 1 and BH 2) also revealed that this area was formed by granitic bedrock.

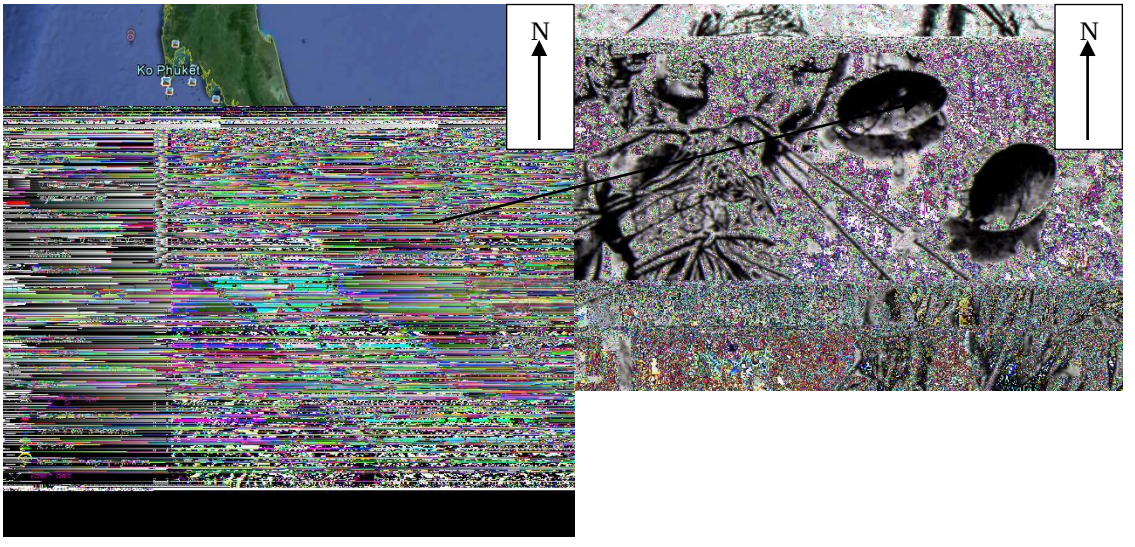

Fig. 1. Study area.

Fig 2. Geology of the study area [33].

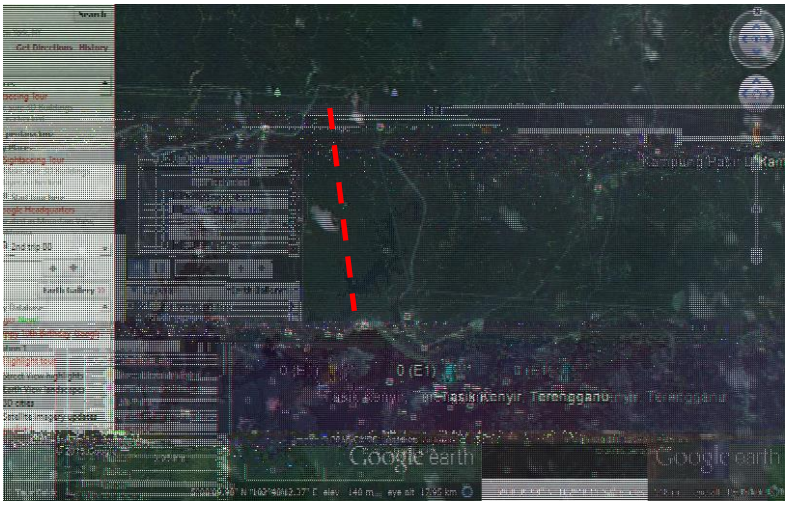

Fig. 3. Positive lineament from satellite image as an evidence that Pengkalan Gawi, Kenyir Lake located in a fault zone.

1. Equipment

The electrical resistivity equipment consists of three main components; viz. source, inducer and record. The electrical resistivity source was generated using a 12 volt of DC battery. A 53 steel electrode was used as a current inducer medium while ABEM Terrameter LS was used to record the apparent resistivity value. The raw data measured on site was analyzed and interpreted by RES2DINV software.

2. Data acquisition and processing

Electrical resistivity imaging (ERI) was performed using ABEM Terrameter LS equipment set. Two (2) spread lines of electrical resistivity survey were performed across the problematic study area as shown in Figure 4. Testing configuration was based on Schlumberger array using three resistivity land cables, fifty one (51) numbers of electrode and fifty three (53) numbers of jumper cable. Equal electrode spacing of 3.0 m was used for all 51 electrodes producing total electrical resistivity survey length of 180 m. Field arrangement of the electrical resistivity imaging was given in Figure 5. Schlumberger array was used during the data acquisition since it able to provide dense near-surface cover of resistivity data. As reported by [34], the array provides a good vertical resolution and can give a clear image of groundwater and sand-clay boundaries as horizontal structures. Furthermore, the array able to provide greater depth of subsurface profiles within limited spaced area during the resistivity data acquisition. Raw data obtained from data acquisition were firstly being processed using commercialize RES2DINV software of [35] to provide an inverse model that approximates the actual subsurface structure. The inversion algorithm of RES2DINV was used to process the data, as proposed by [36] in order to obtain the 2-D resistivity section. The inversion routine used by the program RES2DINV was based on the robust constrained method due to the target interest (subsurface deformation) and site condition.

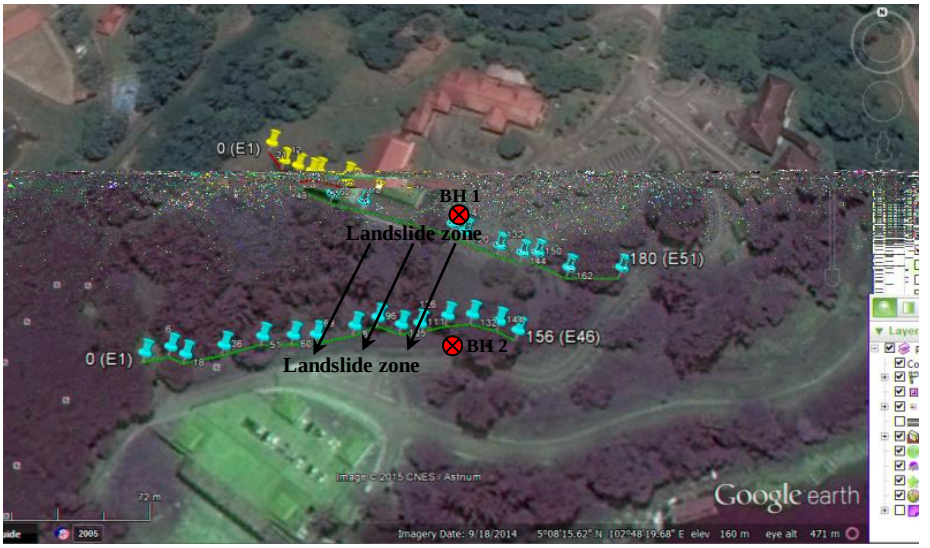

Fig. 4. Location of the entire electrical resistivity lines (spread lines) performed at Pengkalan Gawi Tasik Kenyir, Terengganu.

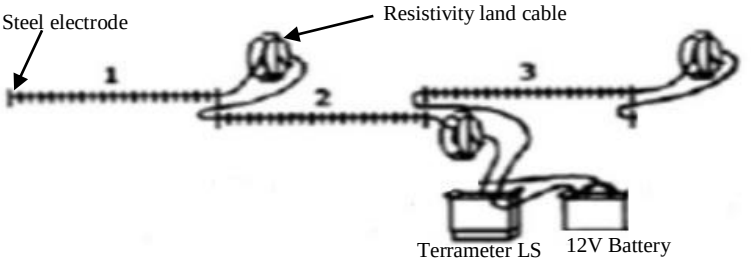

Fig. 5. Field arrangement of electrical resistivity imaging (ERI) based on three cables configuration.

3. Results and Discussions

Two (2) profiles of two-dimensional (2D) electrical resistivity tomography (ERT) were obtained from the field surveys at the selected area in Kenyir Lake Terengganu, Malaysia. Subsurface profile mapping generated by surface mapping of electrical resistivity method was produced thru ERT as given in Figure 6 and 7 respectively. The ERT result and interpretation spread lines 1 and 2 was verified thru the existing boreholes (BH 1 and BH 2) located along of each spread lines as shown in Figure 6 and 7 respectively. Generally, both ERT at Figure 6 and 7 composed of materials from completely weathered to highly weathered zone (1 – 150 ohm.m), highly weathered to moderately weathered (150 – 300 ohm.m), moderately weathered to hard material (300 – 2400 ohm.m) and fresh, hard and dry material (2400 ohm.m & over). Electrical resistivity value (ERV) was determined by measuring the potential difference at points on the ground surface which caused the propagation of direct current through the subsurface [37]. Electrical resistivity value can be influenced by several factors such as the concentration and type of ions in pore fluid and grain matrix of geomaterials via the process of electrolysis where the current was carried by ions at a comparatively slow rate [38]. According to [12], a soil's electrical resistivity value generally varies inversely proportional to the water content and dissolved ion concentration as clayey soil exhibit high dissolved ion concentration, wet clayey soils have lowest resistivity of all soil materials while coarse, dry sand and gravel deposits and massive bedded and hard bedrocks have the highest ERV. As reported by [39], a decrease of ERV was results from an increase of metal ions or inorganic elements in geomaterials. As reported by [40-42], [5] and [43], soil resistivity value can be varied due to the variation of basic geotechnical properties such as moisture content, densities, void ratio, porosity and grain size fraction. Furthermore, condition such as porosity, degree of saturation, salt concentration in pore fluid, grain size, size gradation, temperature and activity may influence to the electrical resistivity value variations [44].

The resistivity image (ERT) for spread line 1 was able to obtain the maximum depth of penetration with up to 20 m. Figure 6 shows the vast range of resistivity value within for spread line 1 shows that highly heterogenous material. At the center of resistivity line, blue color of ERV (< 150 ohm.m) has been classify as completely weathered to highly weathered zone. This zone was possibly composed of soil with water and weak cohesive soil and highly fractured rock. According to BH 1, soil profile consists of sandy SILT to clayey SILT which represented by ERV of 150 ohm.m and below subjected to moisture and grain size variations. According to [45], ERV of clayey and silty soils was varies from 1 – 150 ohm.m. Moreover, [14] was reported that the ERV of clay and silt material can be varied from 1 – 500 ohm.m subjected to moisture and grain size variations. Both sides of the ERT (Figure 6) consists of moderately weathered to hard material (300 – 2400 ohm.m) which possibly derived from moderately fractured to hard/dry material with dry soil filled cracks; sand and gravel with layers of silt & weathered rock [45]. The resistivity value larger than 2400 ohm.m was classified as fresh, hard and dry material which possibly composed from massive bedded and hard bedrock; coarse dry and gravel deposits [45]. According to BH 1, inconsistent layer of soil consistency was varied from medium-stiff-medium-soft (SPT (N) = 6 – 9 – 8 – 4). Furthermore, shallow rock head was detected at depth of 7.5 m with its poor-fair-good description of rock quality designation (RQD = 40% – 60%– 80%). Hence, the results obtained from BH 1 shows that the subsurface profile consist of heterogeneous profile thus verified the ERT result and interpretation for spread line 1. According to BH 1, groundwater table was detected at 6.3 m which also indicates that the ground can possibly instable.

The resistivity image (ERT) for spread line 2 was able to obtain the maximum depth of penetration with up to 20 m. Figure 7 shows the vast range of resistivity value within for spread line 2 shows that highly heterogeneous material. At the center of resistivity line, blue color of ERV (< 150 ohm.m) has been classified as completely weathered to highly weathered zone. This zone was possibly composed of soil with water and weak cohesive soil and highly fractured rock. According to BH 2, soil profile consist of sandy SILT and silty SAND which represented by ERV of 150 ohm.m and below subjected to moisture and grain size variations. According to [45], ERV of silty and sandy soils was varies from 3 – 150 ohm.m. Moreover, [14] was reported that the ERV of clay and silt material can be varied from 1 – 500 ohm.m subjected to moisture and grain size variations. Both sides of the ERT (Figure 7)

consists of highly weathered to moderately weathered zone (150 – 300 ohm.m) which possibly consists of well fractured to moderately fractured bedrock with moist soil filled cracks [45]. The resistivity value larger than 2400 ohm.m has been classified as fresh, hard and dry material which possibly composed of massive bedded and hard bedrock; coarse dry and gravel deposits [45]. According to BH 2, inconsistent layer of soil consistency was varied from medium-stiff-very stiff (SPT (N) = 9 – 12 – 14 – 12 – 15 – 14 – 8 – 11 – 10 – 13 – 15 – 12 – 18). Furthermore as referred to BH 1-2, it was found that the subsurface profile consist of deep rock head (21.1 m) with fair rock quality designation (RQD = 65%). Hence, the results obtained from BH 2 shows that the subsurface profile consist of heterogeneous profile thus verified the ERT result and interpretation for spread line 2. According to BH 2, groundwater table was detected at 5.03 m which also indicates that the ground can possibly instable.

Generally, the entire ERT (Figure 8) has shown that the subsurface profile has been dominated by weak materials at the center of each profile continuously. Historically, this area presents geological structure with particular reference to fault line (Figure 3) which consider weak due to its heterogeneous geomaterials. Hence, landslides phenomenon in this area was possibly triggered by heavy precipitation due to rain water that flow and seep thru the geological structure with particular reference to fault zone. This landslide tragedy was occurred during the raining season (December 2015) thus influencing the activation of weakness zone (fault zone) due to excessive pore water pressure. This judgment was made due to the verification thru established geological map [33] which indicates the existing of fault line symbol as shown in Figure 2. Commonly, low electrical resistivity value (ERV) will indicate the existing of the weak zone, which may contain high water content or highly conductive materials. As a result, it is possible to think that weak zone of subsurface geomaterials in natural slope is likely to show a low resistivity value due to the high conductive zone which commonly contained water [46]. Based on Figure 8, deformation zone geometry due to the water and fault line influences was able to be approximated by 36 m (width) and 40 m and over (depth). According to [26], reduction of ERV may related to increased water content that would lower the ERV of sheared materials, development of shear zones that lower the ERV for the sliding materials and alteration through weathering may reduce the ERV in the sliding zone. This study has demonstrated that the ERT (2D) result from Figure 8 was able to contribute to the estimation of destructive zone (landslides due to the fault line) in contrast to the boreholes (1D) method. As reported by [47], geophysical surveys supplemented shallow boreholes to extend the subsurface data to greater depths. It was highly recommended that the resistivity survey need to be performed earlier than the borehole drilling exploration due to decide the most suitable point location of boreholes.

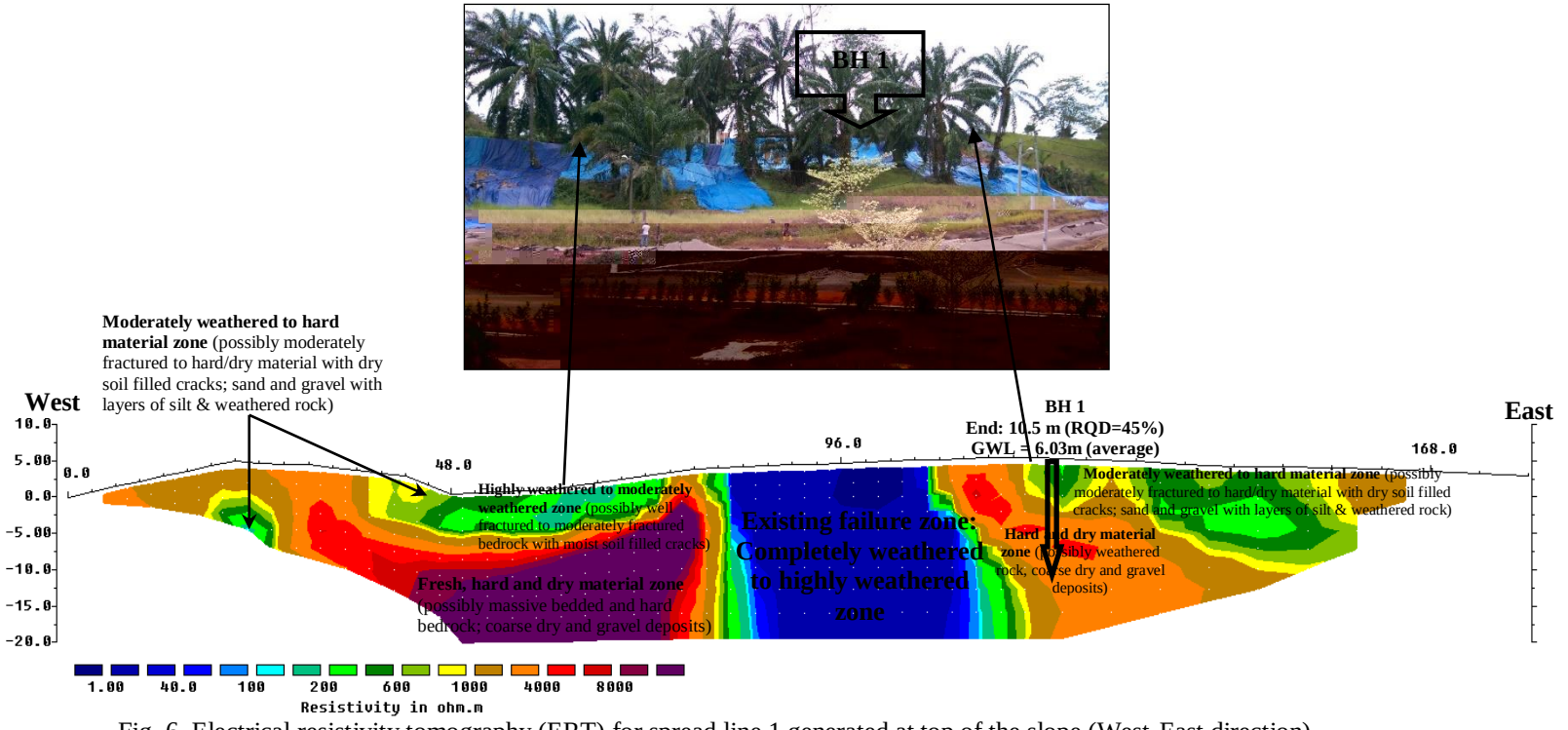

Fig. 6. Electrical resistivity tomography (ERT) for spread line 1 generated at top of the slope (West-East direction).

Peer-review under responsibility of the organizing committee of SCESCM 2016.

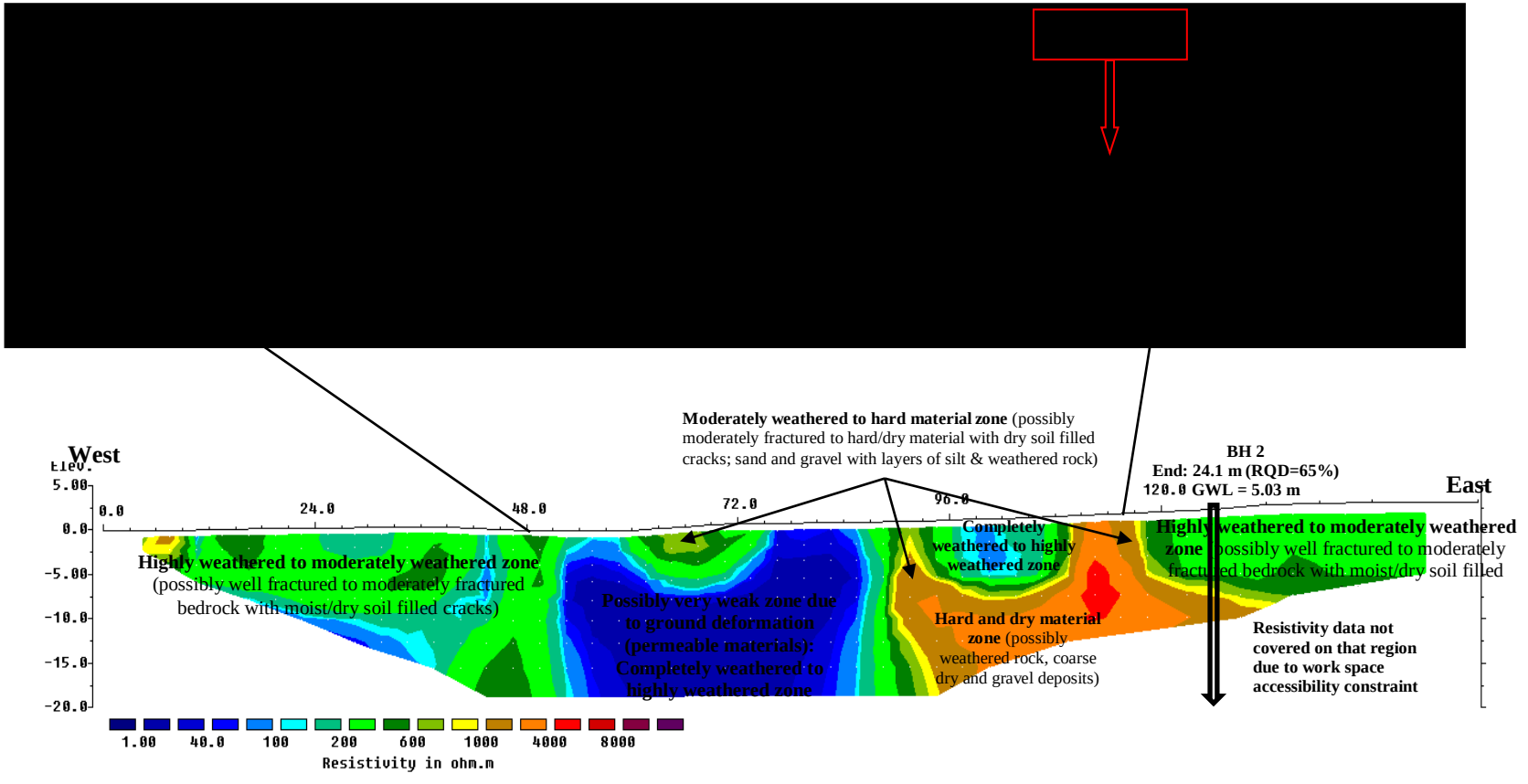

Fig. 7: Electrical resistivity tomography (ERT) for spread line 2 generated at toe of the slope (West-East direction).

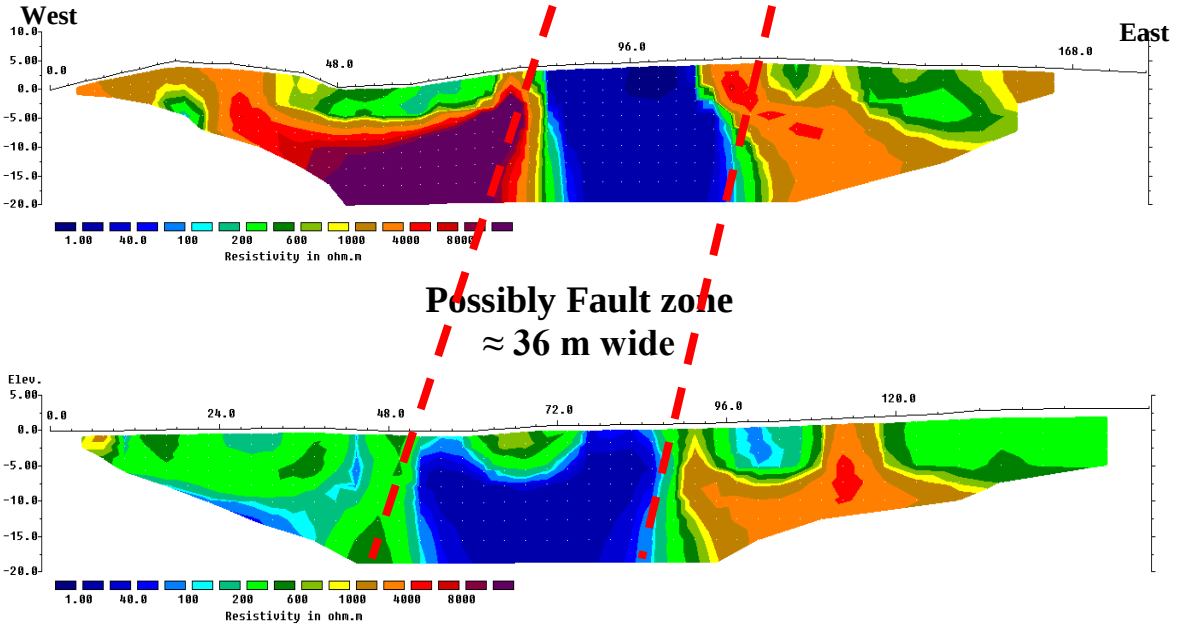

Fig. 8: Arrangement of all resistivity results based on site position (Top and bottom of the landslide).

4. Conclusions

The problematic subsurface profile in landslides was successfully being investigated using electrical resistivity tomography (ERT). The geometry and electrical resistivity distribution of localize landslides at Kenyir Lake area, Terengganu, Malaysia has determined by analyzing electrical resistivity data obtained and the result has generally shown a very good agreement with drilling data. This finding has proved that this method is able to predict the landslides features in order to assist the conventional borehole data. ERT was successfully mapped the subsurface profile which able to extend the surface information mapped by geodynamic mapping and other physical mapping. The mechanics and physical characteristics of the landslide can be easily recognized. The determination of shape and depth of the subsurface landslide which caused ground damage are easier and cheaper than with conventional borehole method. The information from the electrical resistivity results was useful for rehabilitation and mitigation purposes. This geophysical method is suitable for our sustainable ground investigation since it can reduce time, money and compliment others conventional method especially by its 2D surface technique of investigation. The application of electrical resistivity tomography in conjunction with geological and borehole information was effectively being applied for forensic assessment with particular reference of near surface landslides.

Peer-review under responsibility of the organizing committee of SCESCM 2016.

Acknowledgements

Thank are due to all research members for their tremendous work and cooperation. Many thanks go to Universiti Tun Hussein Onn Malaysia for the sponsor and financial support (IGSP from Vot U258) throughout this research activity.

References

[1] H.G Poulos, A Framework for Forensic Foundation Engineering, in: Proc. International Conference on Forensic Engineering: From Failure to Understanding, London, 2008, pp. 247.
[2] I. Anastasopoulos, Building damage during nearby construction: Forensic analysis, Engineering Failure Analysis. 34 (2013) 252–267.
[3] G. Russo, V. Abagnara, H. Poulos, J. Small, Re-assessment of foundation settlements for the Burj Khalifa, Dubai Acta Geotechnica. 8 (2013) 3–15.
[4] L. Pando, J. Pulgar, M. Gutiérrez-Claverol, A case of man-induced ground subsidence and building settlement related to karstified gypsum (Oviedo, NW Spain), Environmental Earth Sciences. 68 (2012) 507–519.
[5] M.H.Z. Abidin, F. Ahmad, D.C. Wijeyesekera, R. Saad, M.F.T. Baharuddin Soil Resistivity Measurements to Predict Moisture Content and Density in Loose and Dense Soil, Applied Mechanics and Materials. 353–356 (2013) 911-917.
[6] A. Godio, C. Strobbia, G. De Bacco, Geophysical Characterisation of a Rockslide in an Alpine Region, Engineering Geology. 83 (2006) 273–286.
[7] H. J. Mauritsch, W. Seiberl, R. Arndt, A. Römer, K. Schneiderbauer, G.P. Sendlhofer, Geophysical Investigations of Large Landslides in the Carnic Region of Southern Austria, Engineering Geology. 56 (2000) 373–388.
[8] R. Fragaszy, J. Santamarina, A. Amekudzi, D. Assimaki, R. Bachus, S. Burns, M. Cha, G. Cho, D. Cortes, S. Dai, D. Espinoza, L. Garrow, H. Huang, J. Jang, J. Jung, S. Kim, K. Kurtis, C. Lee, C. Pasten, H. Phadnis, G. Rix, H. Shin, M. Torres, C. Tsouris Sustainable development and energy geotechnology — Potential roles for geotechnical engineering, KSCE Journal of Civil Engineering. 15 (2011) 611–621.
[9] C.R.I. Clayton, M.C. Matthews, N.E. Simons, Site Investigation, Blackwell Science Ltd, UK, 1995.
[10] Z.A.M. Hazreek, S. Rosli, D.C. Chitral, A. Fauziah, A.T.S. Azhar, M. Aziman, B. Ismail, Soil Identification using Field Electrical Resistivity Method, Journal of Physics: Conference Series. 622 (2015) 1–7.
[11] R. Khatri, V.K. Shrivastava, R. Chandak, Correlation between vertical electric sounding and conventional methods of geotechnical site investigation, Int. Journal of Advanced Engineering Sciences and Technologies. 4 (2011) 042–053.
[12] C. Liu, J.B. Evett, Soils and Foundation, Pearson International, New Jersey, 2008.
[13] P. Cosenza, E. Marmet, F. Rejiba, Y. Jun Cui, A. Tabbagh, Y. Charlery, Correlations between geotechnical and electrical data: A case study at Garchy in France, Journal of Applied Geophysics. 60 (2006) 165–178.
[14] T. S. Lee: Slope Stability and Stabilization Methods, John Wiley & Sons, Inc. New York, 2002.
[15] M.H. Loke, J.E. Chambers, D.F. Rucker, O. Kuras, P.B. Wilkinson, Recent developments in the direct-current geoelectrical imaging method, Journal of Applied Geophysics. 95 (2013) 135–156.
[16] G. Grandjean, J.C. Gourry, O. Sanchez, A. Bitri, S Garambois, Structural study of the Ballandaz landslide (French Alps) using geophysical imagery, Journal of Applied Geophysics. 75 (2011) 531–542.
[17] M.I. Kim, J.S. Kim, N.W. Kim, G.C Jeong, Surface geophysical investigations of landslide at the Wiri area in southeastern Korea, Environmental Earth Sciences. 63 (2011) 999–1009.
[18] S. Friedel, A. Thielen, S.M. Springman, Investigation of a slope endangered by rainfall-induced landslides using 3D resistivity tomography and geotechnical testing, Journal of Applied Geophysics. 60 (2006) 100–114.
[19] A. Godio, G. Bottino, Electrical and electromagnetic investigation for landslide characterisation. Physics and Chemistry of the Earth, Part C: Solar, Terrestrial and amp, Planetary Science. 26 (2001) 705–710.
[20] R. Hack, Geophysics for Slope Stability, Surveys in Geophysics. 21 (2000) 423–448.
[21] H.J. Mauritsch, W. Seiberl, R. Arndt, A. Römer, K. Schneiderbauer, G.P. Sendlhofer, Geophysical investigations of large landslides in the Carnic Region of southern Austria, Engineering Geology. 56 (2000) 373–388.
[22] A. Perrone, V. Lapenna, S. Piscitelli, Electrical resistivity tomography technique for landslide investigation: A review, Earth-Science Reviews. 135 (2014) 65–82.
[23] G. Göktürkler, C. Balkaya, Z. Erhan, Geophysical investigation of a landslide: The Altindag landslide site, Izmir (western Turkey), Journal of Applied Geophysics. 65 (2008) 84–96.
[24] D.M. McCann, A. Forster, Reconnaissance geophysical methods in landslide investigations, Engineering Geology. 29 (1990) 59–78.

[25] V.A. Bogoslovsky. A.A Ogilvy, Geophysical methods for the investigation of landslides. International Journal of Rock Mechanics and Mining Sciences & amp, Geomechanics Abstracts. 15 (1978) 562–571.
[26] D.F. Palmer, S.L. Weisgarber, Geophysical survey of the Stump Basin Landslide, Ohio, Bulletin Association of Engineering Geologist. 3 (1988) 363–370.
[27] D.M. McCann, A. Forster, Reconnaissance geophysical methods in landslide investigations, Engineering Geology. 29 (1990) 59–78.
[28] S.G.C. Fraiha, J.B.C. Silva, Factor analysis of ambiguity in geophysics, Geophysics. 59 (1994) 1083–1091.
[29] R.C. Benson, L. Yuhr, R.D. Kaufmann, Some Considerations for Selection and Successful Application of Surface Geophysical Methods, in: Proc. The 3rd Int. Conf. on Applied Geophysics, Orlando, Florida, 2003.
[30] H. Almalki, A.K. El-Werr, K. Abdel-Rahman, Estimation of near-surface geotechnical parameters using seismic measurements at the proposed KACST expansion site, Riyadh, KSA, Arabian Journal of Geosciences. 4 (2011) 1131–1150.
[31] K. Sudha, M. Israil, S. Mittal, J. Rai, Soil characterization using electrical resistivity tomography and geotechnical investigations, Journal of Applied Geophysics. 67 (2009) 74–79.
[32] S. Oh, C.G. Sun, Combined analysis of electrical resistivity and geotechnical SPT blow counts for the safety assessment of fill dam, Environmental Geology. 54 (2008) 31–42.
[33] Minerals and Geoscience Department Malaysia, Geological Map of Peninsular Malaysia, 8th Ed. Ministry of Natural Resources and Environment, 1985.
[34] U. Hamzah, R. Yaacup, A.R. Samsudin, M.S Ayub, Electrical imaging of the Groundwater Aquifer at Banting, Selangor, Malaysia, Environmental Geology. 49 (2006) 1156–1162.
[35] M.H. Loke, I. Acworth, T. Dahlin, A comparison of smooth and blocky inversion methods 2-D electrical imaging surveys, Exploration Geophysics. 34 (2003) 182–187.
[36] M.H. Loke, R.D. Barker, Rapid least squares inversion of apparent resistivity pseudosection using a quasi-Newton method, Geophysical Prospecting. 44 (1996) 131–152.
[37] H.R. Burger, A.F. Sheehan, C.H. Jones, Introduction to Applied Geophysics, W.W. Norton & Company, New York, 2006.
[38] D.H. Griffiths, R.F. King, Applied Geophysics for Geologist and Engineers The Element of Geophysical Prospecting, Pergamon Press, Oxford, 1981.
[39] Y. Jung, Y. Lee and H. Ha, Application of electrical resistivity imaging techniques to civil and environmental problems, Use of Geophysical Methods in Construction, 2000.
[40] M.H.Z. Abidin, R. Saad, F. Ahmad, D.C. Wijeyesekera and M.F.T. Baharuddin, Correlation analysis between field electrical resistivity value (ERV) and basic geotechnical properties (BGP), Soil Mechanics and Foundation Engineering. 51 (2014) 117–125.
[41] M.H.Z. Abidin, F. Ahmad, D.C. Wijeyesekera and R. Saad , The influence of basic physical properties of soil on its electrical resistivity value under loose and dense condition, Journal of Physics: Conference Series. (2014) 1–13.
[42] M.H.Z. Abidin, F. Ahmad, D.C. Wijeyesekera and R. Saad, Small soil embankment electrical resistivity value on its array, moisture content and density influences. International Journal of Geology. 8 (2014) 9–18.
[43] M.H.Z. Abidin, D.C. Wijeyesekera, R. Saad and F. Ahmad, The influence of soil moisture content and grain size characteristics on its field electrical resistivity, Electronic Journal of Geotechnical Engineering. 18/D (2013) 699–705.
[44] V.A. Rinaldi, G. Cuestas, Ohmic Conductivity of a Compacted Silty Clay, Journal of Geotechnical and Geoenvironmental Engineering. 128 (2002) 824–835.
[45] D.F. McCarthy, Essentials of Soil Mechanics and Foundations Basic Geotechnics, Pearson International Edition, New Jersey, 2007.
[46] M.H.Z. Abidin, R. Saad, F. Ahmad, D.C. Wijeyesekera, M.F.T. Baharuddin, Integral analysis of geoelectrical (resistivity) and geotechnical (SPT) data in slope stability assessment, Academic Journal of Science. (2012) 305–316.
[47] D. Cummings, B.R. Clark, Use of seismic refraction and electrical resistivity surveys in landslides investigations, Bulletin Association of Engineering Geologists. 4 (1988) 459–464.

Available online at www.sciencedirect.com

ScienceDirect

Procedia Engineering00 (2017) 000–000

Procedia Engineering

www.elsevier.com/locate/procedia

Sustainable Civil Engineering Structures and Construction Materials, SCESCM 2016

The effect of bottom drainage channels type on seepage percentage

Sri Amini Yuni Astuti[a,]*, Munadhir[a], Dwi Astuti Wahyu Wulan Pratiwi[a]

[a]*Department of Civil Engineering, Islamic University of Indonesia, Yogyakarta 55584, Indonesia*

Abstract

Nowadays, a paradigm shift in the drainage system occurs due to lessons from the past experience that occurred and the scientific progress. This changes caused by the availability of groundwater in an area must be preserved, so that groundwater resources in the area can be sufficient for its residents (sustainable drainage system). In order to preserve the groundwater conservation, empirical research needs to be done in a laboratory on the effect of porosity of bottom drainage channels. The purpose of this study is to determine the type of bottom holes which gives the biggest percentage of seepage among 4 different types of channel's bottom. This laboratory research is aimed at observing the amount of seepage from different type of bottom material, i.e. ground channel, ground channel with few seepage holes, ground channel with many seepage holes, ground channel with PVC pipe and many seepage holes. The research is conducted on 11 m length of channel, width 40 cm, slope 0.0055, and permeability coefficient (K) 4.4261 x 10-4 m/s. Total discharge is measured by broad-crested weir. Seepage percentage is calculated based on the inflow and outflow of drainage channels discharge. The results is 19.56% as the largest percentage of seepage occurs in the 11 m length of ground channel with many seepage holes, without PVC pipe. Drainage channels design needs to consider the depth of shallow groundwater, soil type, soil permeability coefficient, slope, and the location of the drainage channel.

Peer-review under responsibility of the organizing committee of SCESCM 2016.

Keywords: paradigm shift; sustainable drainage system; porosity; seepage percentage; drainage channels.

1. Introduction

A paradigm shift in the drainage system due to scientific progress and lessons from the experiences that happened. Past paradigm state that drainage system denoted an effort to remove the excess water in an area as quickly as possible to the outside through a duct or a river to the sea. But this past paradigm has changed, because it

* Corresponding author. Tel.: +62-8132-878-3921; fax: +62-274-895-330.
E-mail address: amini_yuni@yahoo.co.id

1877-7058
Peer-review under responsibility ofthe organizing committee of SCESCM 2016.

is a necessity to preserve the availability of groundwater in the area. Moreover, groundwater resources in the area will be sufficient for its citizens (sustainable drainage system). In order to conserve soil water availability, a wide range of research has been carried out, i.e. research on infiltration wells, infiltration channels, garden infiltration, and catchment reservoir. These empirical research include experimental (laboratory) and mathematical analysis.

Sunjoto [1] since 1988 has been conducting research on infiltration wells or infiltration channels. This research proposes a mathematical formula for well or channel dimension based on water balance. The water balance includes rainfall potential and soil's ability to absorb water. Akhmad Aziz et.al. [2] conducted research on physical models of retarding basin. This research aimed to determine what type of retarding basin can absorb more water in a very low permeability area. Experiment and testing are conducted by measuring discharge through soil layer or sand column on physical model. Maximum effectiveness of sand column of 7.231% occurred in 12 of sand columns, 32.5 cm height and 10 cm depth. From this research, researcher conclude that shortage problems of groundwater can be solved in a very low permeability area. Ayu [3] studied and analyzed the effects of land use change in the District Kepanjen. The soil condition originally was an open area such as dry land or rice fields which have been converted to impermeable area just as office building and residential area. The result showed that ±80% permeable layer of land use changed into impermeable layer. The researcher applied porous channels to overcome puddles in this area, which it was based on a high permeability coefficient value of soil type (sand). This porous channels function as artificial recharge to ground water conservation by 0.0158 m^3/sec permeation.

Those researches was inspiring, what if we conduct a new study about seepage on several types of porous channels that can absorb water and provide benefits to the groundwater preservation in an area? The purpose of this study are knowing which type of drainage channel is more advantageous to soil water conservation or to move excess water as fast as possible to the outside system of drainage and also knowing the percentage of water that seeps into the soil through some type of drainage channel bottom.

This study conducted on the ground around Hydraulics Laboratory of Civil Engineering FTSP UII with 4 (four) different types of drainage channel bottom, i.e. ground channel; ground channel with few seepage holes; ground channel with many seepage holes; ground channel with PVC pipe and many seepage holes.

2. Theoretical Foundations

The drainage system based on present paradigm is a method or process to remove excess water - caused by rainfall - in an area as fast as possible by drained through channel, river, and end up to the sea while absorbing water into the ground along the way. According Sunjoto (2015), water amount wasted into the sea as wastewater on conventional drainage system (past paradigm) is nearly the same as a need for clean water in an area [4]. So it will be a very superfluous. Types of drainage systems have been known are based on:

- Formation: natural and artificial drainage systems.
- Building layout: surface and subsurface drainage.
- Functions: one function (single-purpose) and many functions (multi-purpose).
- Structure: open channels and closed conduits.
- Cross-section of the channel: square, trapezoid, ellipse and circle.
- Construction method: on site and prefabricated.

2.1. Groundwater

In the beginning, human civilization marked by the emergence of economic growth in a very fertile area such as rivers and springs. It shows that the water has a very important role for human existence. In hydrology terms, water can be divided into: rainwater, surface water, and groundwater. Of the whole types, groundwater has advantages with better quality, relatively small changes in water quality as a result of the time, large reserves, easy to obtain, distribution and extent of groundwater is greater than surface water (thus reducing distribution costs), and also the land on top of ground can be used for a variety of needs (Purnama, 2010) [5]. However, groundwater also has limitations such as contains chemical compounds in certain area (Ca, Mg, Na, K, CO_2, Cl, and SO_4), anaerobic decomposition of buried organic substance in the soil causing gas release (CH_4, NH_3 and H_2S), difficulty in

neutralizing contaminated groundwater, and excessive use of groundwater may cause intrusion of sea water in an area.

Groundwater is water under the subsurface in saturated zone. It comes from rainfall that seeps into the ground following hydrological cycle. Groundwater has largest percentage (96%) of all fresh water on earth (excluding ice poles). The remaining forms are rivers, lakes, reservoirs, and water vapor in the air. Groundwater is strongly related with civil engineering jobs (Sri Harto, 1988) [6], such as for:

- Construction of underground buildings: groundwater level should be lowered, so it does not interfere the construction.
- Meet a demand of raw water: amount of groundwater can be pumped.
- Irrigation: groundwater level must be controlled for plant growth.

Concept of artificial groundwater recharge is a new method to solve problem of groundwater shortage (e.g. artificial inundation from rivers, ponds around the house, and underground reservoirs). The benefits of this are (Suripin, 2004) [7] increasing groundwater level, storing excess of surface water in underground reservoirs, improving quality of local groundwater, preventing saltwater intrusion and increasing production of ground water (for drinking or other purposes). Nevertheless, prerequisites and appropriate conditions are needed for recharge, i.e. shallow groundwater level, potential for heavy rainfall, quality of rainfall (better than local groundwater), and moderate permeability land.

2.2. Groundwater Flow

Fluctuation denoted the change of groundwater level (rise and fall). Types of fluctuation are: annual fluctuations caused by abnormal drought and rainfall below/above annual average; seasonal fluctuations caused by rainy and dry seasons; daily fluctuations caused by evapotranspiration; and a moment fluctuation caused by pumping.

Permeability defined as properties of porous materials that allow fluids seeps through pore cavities which interconnected each other, so that water can flow from high to low elevation head. Soil permeability described as characteristic of water through soil pore cavities. Materials that have continuous pores named permeable [8].

2.3. Darcy Law

Darcy Law state water ability to flow through soil cavities (pores) and influenced characteristics. Darcy's experimental apparatus is shown in Fig. 1. Darcy's law says that the discharge rate (q) is proportional to the gradient in hydraulic head and the hydraulic conductivity. Hydraulic gradient given by:

$$i = \frac{\Delta H}{\Delta L} \tag{1}$$

$$q = \frac{Q}{A} \quad ; \quad Q = A \,.\, V \quad ; \quad V = k \,.\, i \,.\, A \tag{2}$$

whereas q is discharge rate, Q is discharge or the volume of water flow per unit of time (cm^3/sec), A is the cross-sectional area through soil water (cm^2), k is permeability coefficient (cm/sec), i is the hydraulic gradient, and V is the flow velocity (cm/sec).

2.4. Steady Flow of Free Aquifer with Infiltration

Steady flow implies that no change occurs with time. Water penetrates deep into the ground to form a subsurface water flow system (groundwater), which will be different in each region. Position ground water level on a free aquifer (as shown in Fig. 2) is important to note, because it reflects the equilibrium hydrodynamics of groundwater in an area.

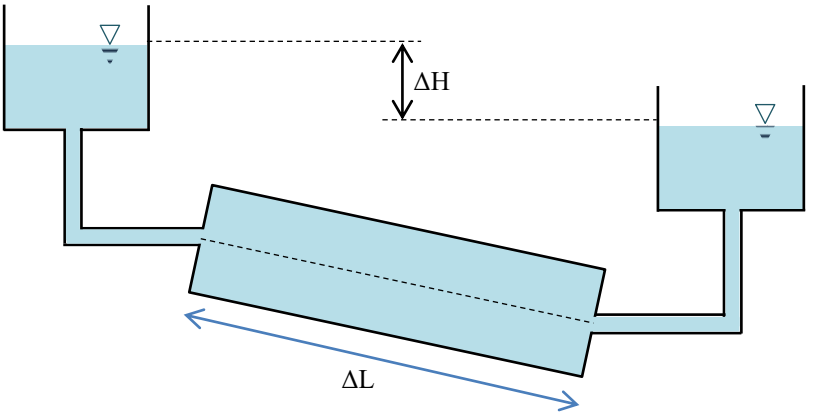

Fig. 1. Darcy Experiment (Freeze and Cherry, 1979) [9]

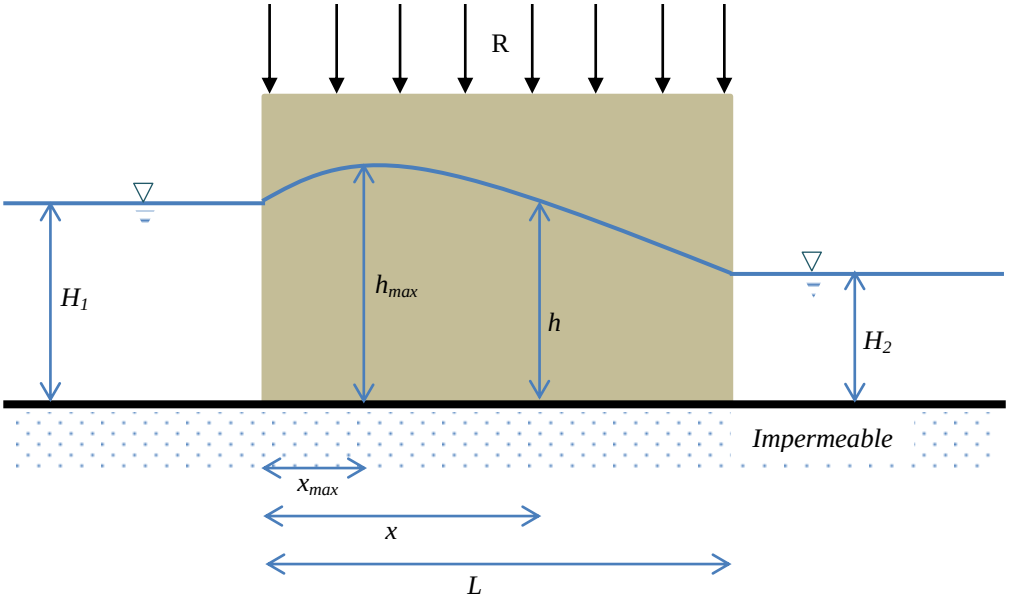

Fig. 2. Steady flow of free aquifer with infiltration

The formula remains in the aquifer flow freely with infiltration (Luknanto, 1998) [10]:

$$dQ = R\ b\ dx \tag{3}$$

⇨ $Q = R\ b\ x + C$ boundary condition $x = 0$ → $Q = Q_0$

⇨ $Q = R\ b\ 0 + C$ → $C = Q_0$

entered into $Q = R\ b\ x + Q_0$ whereas

⇨ $Q = -K\frac{dh}{dx}\ b\ h$

⇨ $-K\frac{dh}{dx}\ b\ h = R\ b\ x + Q_0$ ⇨ $K\ b\ h\ dh = (R\ b\ x + Q_0)dx$

$\Rightarrow \quad -K\,b\frac{1}{2}[h^2]_{H_1}^{H_2} = R\,b\frac{1}{2}[x^2]_0^L + Q_0\,[x]_0^L$ $\Rightarrow \quad -K\,b\frac{1}{2}(H_2^2 - H_1^2) = R\,b\frac{1}{2}L^2 + Q_0\,L$

$\Rightarrow \quad Q_0 = \frac{Kb}{2L}(H_1^2 - H_2^2) - \frac{R\,b\,L}{2}$ (4)

parabolic groundwater level:

$-K\frac{dh}{dx}\,b\,h = R\,b\,x + Q_0$

$\Rightarrow \quad -K\,b\int h\,dh = \int(R\,b\,x + Q_0)dx$

$\Rightarrow \quad -K\,b\frac{1}{2}h^2 = R\,b\frac{1}{2}x^2 + Q_0\,x + C$ boundary condition $x = 0 \rightarrow h = H_1$

$\Rightarrow \quad -K\,b\frac{1}{2}{H_1}^2 = R\,b\frac{1}{2}.0^2 + Q_0\,.0 + C$ $\Rightarrow \quad C = -K\,b\frac{1}{2}{H_1}^2$

entered into equation:

$-K\,b\frac{1}{2}h^2 = R\,b\frac{1}{2}x^2 + Q_0\,x + \left(-K\,b\frac{1}{2}{H_1}^2\right)$

$\Rightarrow \quad h^2 = -\frac{Rx^2}{K} - 2\frac{Q_0 x}{K\,b} + {H_1}^2$ $\Rightarrow \quad h^2 = {H_1}^2 - \frac{Rx^2}{K} - 2\frac{Q_0 x}{K\,b}$

maximum value occurred on:

$\frac{dh}{dx} = 0$

$\frac{1}{2}\left[{H_1}^2 - \frac{Rx^2}{K} - 2\frac{Q_0 x}{K\,b}\right]^{-\frac{1}{2}}\left(-\frac{2\,R\,x}{K} - \frac{2\,Q_0}{K\,b}\right) = 0$

$\Rightarrow \quad \left(-\frac{2\,R\,x}{K} - \frac{2\,Q_0}{K\,b}\right) = 0$ $\Rightarrow \quad x = -\frac{Q_0}{R\,b}$

$\Rightarrow \quad x = -\frac{\frac{Kb}{2L}(H_1^2 - H_2^2) - \frac{R\,b\,L}{2}}{R\,b}$ $\Rightarrow \quad x = \frac{L}{2} - \frac{K}{2LR}(H_1^2 - H_2^2)$

Seepage water percentage (p) stated with following formula:

$$p = \left(1 - \frac{Q_o}{Q_{in}}\right)100\% \quad (7)$$

whereas Q_{in} is inflow and Q_o is outflow discharge.

3. Research Methods

The method used are observation experiments in the laboratory, data processing, discussion, conclusion and recommendation. Primary data derived from experiments conducted at Hydraulics Laboratory of Islamic University of Indonesia. The data used to analyze the effect of bottom drainage channels are: channel length (L), channel width (b), characteristic (type) of bottom materials, dimension of broad crest weir, head (H), reservoir volume (Volume), time (t), and reservoir mass (m). For more details can be seen in Fig. 3.

Channel characteristics in research mechanism: (i.e. uniform slope 0.0055)

- Quadrilateral Channel Type I where b = 40 cm, L = 11 m, original soil used for bottom material (permeability coefficient – K = $4.4261x10^{-4}$ m/s).

- Quadrilateral Channel Type II where b = 40 cm, L = 11 m, original soil used for bottom material with 6 holes (diameter of hole – D = 10 cm) filled materials husks.
- Quadrilateral Channel Type III where b = 40 cm, L = 11 m, original soil used for bottom material with 11 holes (diameter of hole – D = 10 cm) filled materials husks.
- Quadrilateral Channel Type IV where b = 40 cm, L = 11 m, original soil used for bottom material with 11 holes with PVC pipe (diameter of hole – D = 10 cm) filled materials husks.

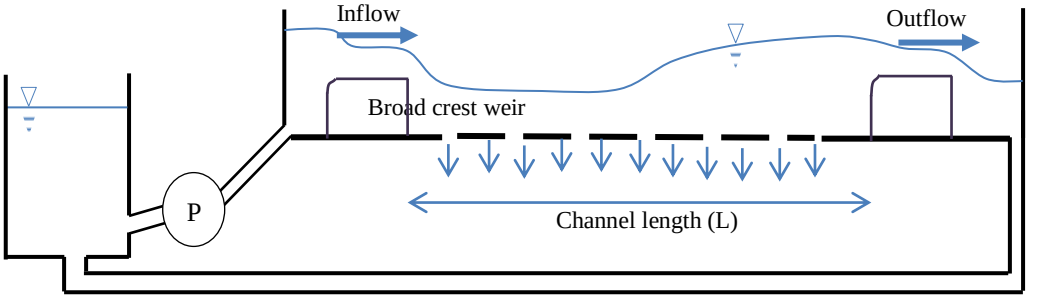

Fig. 3. Research mechanism

Tools and materials used to achieve purposes of this study i.e. broad crest weir with dimension of height 10 cm, width 20 cm, thick 40 cm; a water pump is used to fill a channel a tank using water from a tank (reservoir); a stopwatch is used to calculate the length of water flow; a meter is used to measure dimensions and distances on research tools; and scales is used to weigh the reservoir.

4. Results and Discussion

4.1. Results

Results of the study are presented in Table 1 and for comparison, seepage percentage of channel types can be seen in Fig. 4

Table 1. Seepage Percentage of Bottom Drainage Channels

No	Type	Channel characteristic	Seepage Percentage
1	I	Quadrilateral Channel where b = 40 cm, L = 11 m, original soil used for bottom material	15,41 %
2	II	Quadrilateral Channel where b = 40 cm, L = 11 m, original soil used for bottom material with 6 holes (diameter of hole – D = 10 cm) filled materials husks	17,45 %
3	III	Quadrilateral Channel where b = 40 cm, L = 11 m, original soil used for bottom material with 11 holes (diameter of hole – D = 10 cm) filled materials husks	19,56 %
4	IV	Quadrilateral Channel where b = 40 cm, L = 11 m, original soil used for bottom material with 11 holes with PVC pipe (diameter of hole – D = 10 cm) filled materials husks	15,82 %

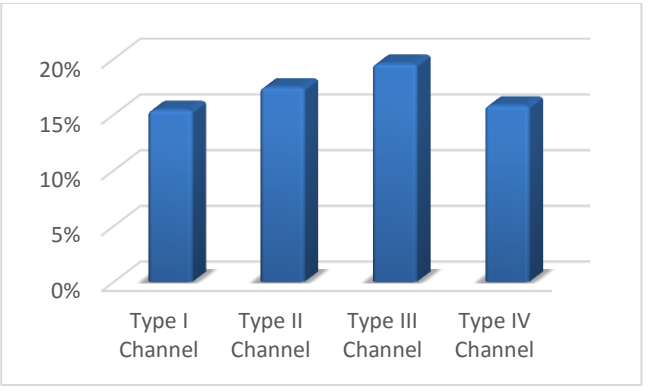

Fig. 4. Results of seepage percentage

4.2. Discussion

From Table 1 and Fig. 4 shows that largest seepage percentage occurred from Type III Channel, which is a channel with a lot of seepage holes without PVC pipe. Seepage hole is an absorption hole with certain diameter, which is the contents of certain low permeability soil materials replaced by high permeability materials (sand, gravel, husks, etc.).

Channel with seepage holes which contained high permeability material can absorb water much more, it is because infiltration velocity will be faster (shown in Fig.5). From the calculation results, the more seepage holes will cause bigger percentage of permeated water.

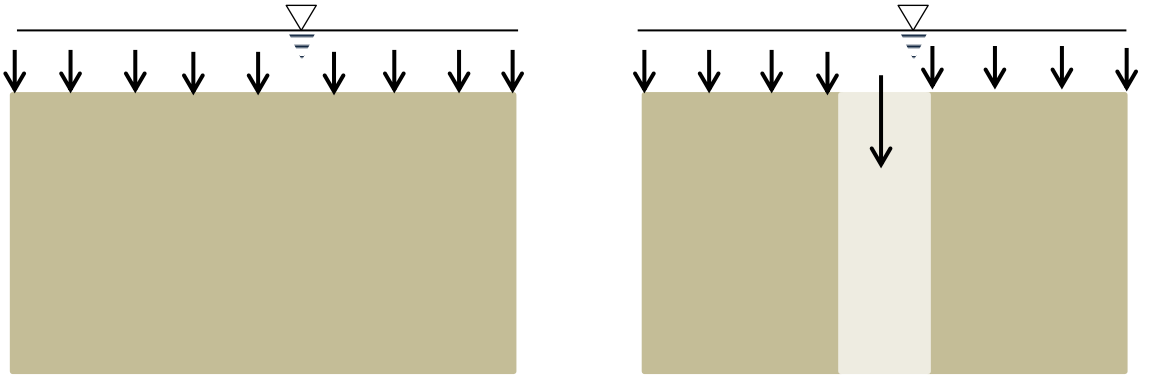

Fig. 5. Comparison of absorption mechanism in line with and without seepage hole based on research

In channel with seepage holes with PVC pipe, water will be absorbed under the pipe but cannot seep into the sideways because it was detained by pipe. Compared with no PVC pipe, water can seep down or sideways/round, so that the percentage of absorption will be greater in channel with seepage holes without PVC pipe. Comparison of seepage holes with and without PVC pipe shown in Fig. 6. The amount of water flow through drainage channels with seepage holes will increase groundwater level (based on theory of groundwater flow in free aquifer). Some of the water will seep downward following groundwater flow, so that water table will be increase also. Comparison of the groundwater level in permeable and impermeable channel due to seepage sketched in Fig. 7.

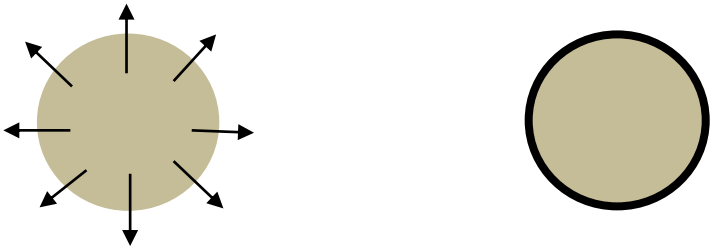

Fig. 6. Comparison of seepage holes with and without PVC pipe.

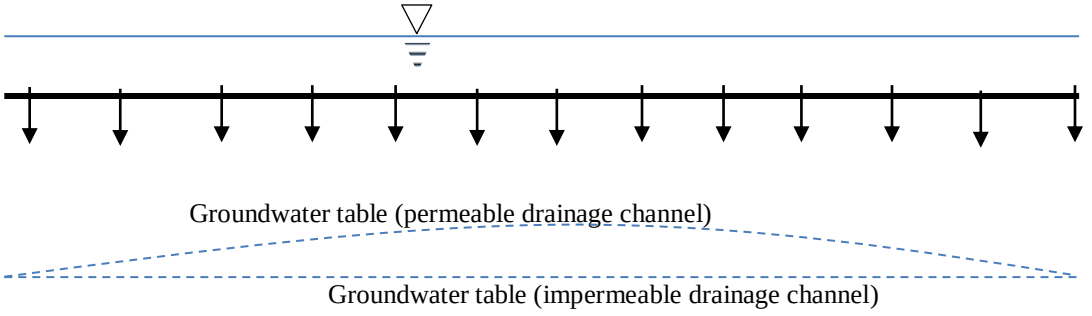

Fig. 7. Comparison of permeable and impermeable groundwater level in channel

The layout of proposed drainage channels should also be reviewed. If the channel designed along the highway, then groundwater level rising will destabilize construction of it. Means that, the proposed channel is not appropriate and will be more suitable for drainage system in villages or alongside small road.

5. Conclusion and Recommendations

5.1. Conclusion

From the research, can be concluded that Type III Channel (11 m length, 40 cm width, slope of 0.0055, has 11 seepage holes with D = 10 cm (containing husk material), without PVC pipe) has the highest percentage of seepage for 19.56% along 11 m channel length, in other word seepage percentage is 1.78% for each meter. The more seepage holes, the bigger percentage of seepage. Holes with PVC pipe have a lower seepage percentage value than without it. Drainage channel with permeable bottom materials will absorb more water, increase groundwater level, and raise the water table, which will be a very agreeable recommendation for water conservation.

5.2. Recommendations

Based on the above study, some suggestions that could be addressed are on the construction of sustainable drainage channel, it is a necessary to consider depth of groundwater level, soil permeability condition, slope, soil characteristics, and channel layout, so that soil water conservation can be preserved. Further research on the original soil and varied channel bottom materials needs to be done.

References

[1] Sunjoto, Infiltration Wells Analysis and Development, Scientific Summit, Public Works Department: board of Research and Development Public Works, Center of Research and Development Settlement, Bandung, 1991.
[2] Akhmad Azis, M.Saleh Pallu, A.M. Arsyad Thaha, and Ahmad Bakri Muhiddin, Study Effectiveness of Sand Pond At Reservoir Absorption Column With Various Parameters. Proceeding HATHI 29th, Bandung, 2012.

[3] Eka Ayu I.L, Setyawan, Rainwater Infiltration Wells Draft as One of Soil Water Conservation Effort in Dayubaru Housing Sleman, Special Region of Yogyakarta, accessed by March 2nd, 2014 http://lib.geo.ugm.ac.id/.
[4] Sunjoto, Drainage Technic Pro-Water as Settlement Conservation, Civil Engineering and Environmental, FT, UGM, Yogyakarta, 2015.
[5] Setyawan Purnama, Groundwater Hydrology, Publisher Kanisius, Yogyakarta, 2010.
[6] Sri Harto, Applied Hydrology, BP – KMTS – FT – UGM, Yogyakarta, 1985.
[7] Suripin, Sustainable Urban Drainage System, Publisher Andi, Yogyakarta, 2004.
[8]Ussy Andawayanti, Linda Prasetyorini, Analysis of Inundation Volume on Land Use Change and Its Remedies Based on Environmental Conservation, Journal of Irrigation, Universitas Brawijaya, Vol. I, no 1. Malang, 2010
[9] Freeze, R.A. and Cherry, Groundwater. Prentice Hall, 604, 1979.
[10]Djoko Luknanto, Water Flow in the Porous Media, Regional Training: Drainage, Filtration, and Geotechnical, HEDS/JICA-UNLAM, Banjarmasin, 1998.

Available online at www.sciencedirect.com

ScienceDirect

Procedia Engineering 00 (2017) 000–000

Procedia Engineering

www.elsevier.com/locate/procedia

Sustainable Civil Engineering Structures and Construction Materials, SCESCM 2016

Settlement of residential houses supported by piled foundation embeded in expansive soil

Gogot Setyo Budi[a,*]

[a]*Civil Engineering Department, Petra Christian University, Surabaya 60236, Indonesia*

Abstract

The damage has occurred on residential houses built on expansive soils. The weight of the walls and roof of the houses is transferred onto pile foundations through suspended tie beams and columns, respectively. The typical pile used to support the house was 30 cm in diameter and it was penetrated into the depth of 600 cm. The slabs or floors were rested on the fills.This study was conducted to determine all potential sources that initiated the settlement and damages to the houses. Site investigation to each and every houses that experienced settlement and damages was conducted to gather and inventory the pattern of the cracks or damages. The result of site invesgation showed that there were no damages induced by swelling, but the settlements and cracks were triggered by settlement, instead. It was also noticed that the settlement of piled foundations located on the area that susceptible to the water infiltration relatively larger than those piled foundation in the covered area. Therefore, it was concluded that, based on the analysis, the damages which occurred on the residential ordinary houses were mainly caused by the settlement of the piled foundations and the fills due to the soil softening.

Peer-review under responsibility of the organizing committee of SCESCM 2016.

Keywords: expansive soils, settlement, crack, soil softening, residential houses

1. Introduction

The demand of housing in urban area has been increasing in the last few decades. Accordingly, it requires large area of land for residentials and infrastructures. Several Real estates in Surabaya, the second largest city in Indonesia, have been expanding to the areas that consist of expansive soil formation.

The ordinary low rise housing, which is built on expansive soils require better and more comprehensive design

* Gogot Setyo Budi. Tel.: +62-31-2983397; fax: +62-31-2983392.
E-mail address: gogot@petra.ac.id

Peer-review under responsibility of the organizing committee of SCESCM 2016.

due to its swell and shrink behavior. The expansive soil will swell when contact with water, and shrink when lose its moisture content. Due to seasonal climate change, the moisture content of soil at the upper layer changes. The depth of expansive soil to which its moisture content changes periodically by the seasonal climate change, is called active zone [1]. Based on the soil investigation in Surabaya – Indonesia reported by Testana Engineering, the thickness of active zone is about 5 m [2]. When the weight of a structure rested on the active zone is less than the swelling pressure of soil, the structure will heave and may experience differential deformation.

The consistency of expansive soil will soften when its moisture content increases and harden with losing its water content. In their research focusing on expansive soil in Surabaya – Indonesia, Tjandra et al. [3] stated that the seasonal wetting and drying cycles affects the undrained shear strength of soils, and furthermore it has an impact to the friction capacity and adhesion factor of pile foundation.

2. Wetting Behavior of Unsaturated Soils

The wetting-induced softening behavior of the unsaturated expansive clay is crucial to understanding the rain-induced settlement of foundation and progressive slope failure in unsaturated of expansive soils.

Zhan et al. [4] investigated the softening characteristics of unsaturated recompacted and natural soils using suction-controlled triaxial tests. It was found that the wetting process for recompacted specimen generally showed ductile failure, while for the natural specimens exhibited a brittle failure similar to a heavily over consolidated soils, which is caused by the cementation effect of iron and manganese oxides. It was also stated that dilative behavior developed only for the natural specimen during wetting process.

Upon wetting, the failure of soil specimen was indicated by development of rapid shear strain in soil when the suction was reduced to certain threshold value. Along the wetting path, an increase in degree of saturation is related to the decreasing suction is associated with the flooding of soil voids with water. As a result, the normal forces at interparticle contacts decrease, thereby reducing the overall stability of soil skeleton. From the macroscopic viewpoint, both yield stress and shear strength of the soil specimen decrease Wheleer et al. [5].

According to Melinda et al. [6], at the beginning of the infiltration process, the soil deformation was small but matric suction decreased rapidly. When failure approaches, soil deformation increases sharply (Melinda et al. 2004).

3. Typical Ordinary Houses

The typical low rise houses, which were studied, consisted of brick walls confined by reinforced concrete columns and beams. The weight of the walls was transferred onto pile foundations through suspended beam, which was supported by the piles. The floor was laid on the approximately 80 cm thick fill material. The schematic of cross section of the house is presented on Fig. 1. Typical diameter of pile foundation was 30 cm in diameter and it was penetrated into the depth of 600 cm (Fig. 2)

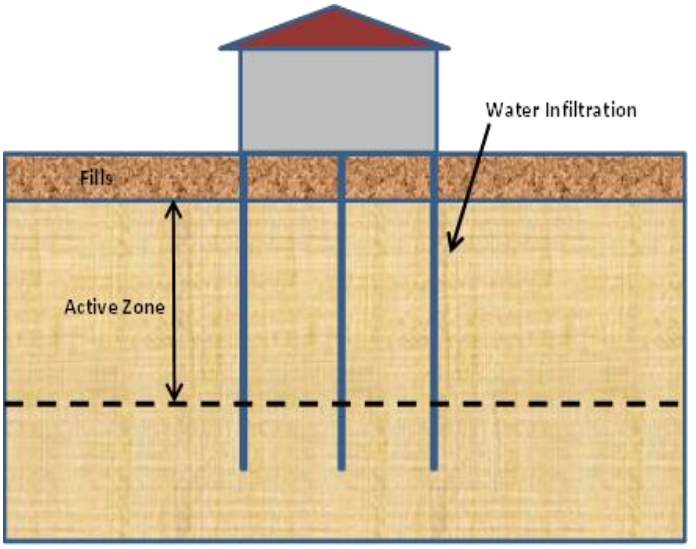

Fig. 1 Schematic of cross section

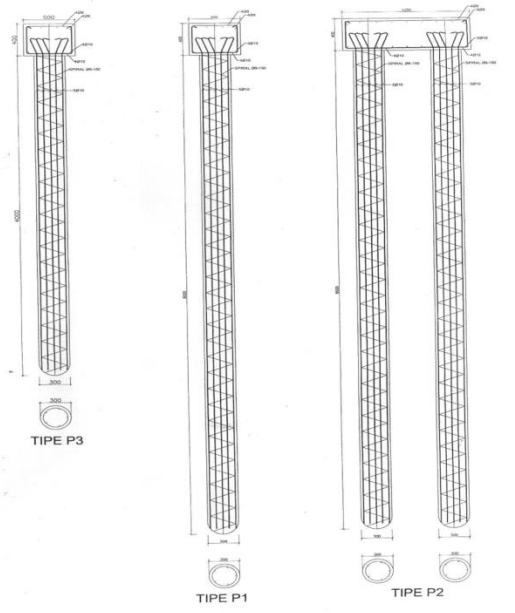

Fig. 2 Typical piled foundation

4. Soil Data

Soil profile of the housing area is presented on Fig. 3. The soil formation is dominated by unsaturated clay layer. Based on the soil investigation report conducted by Testana Engineering, the existing soil layer consists of expansive soil with the active zone of 5 m (Fig. 4). The properties of soil is presented in Tabel 1.

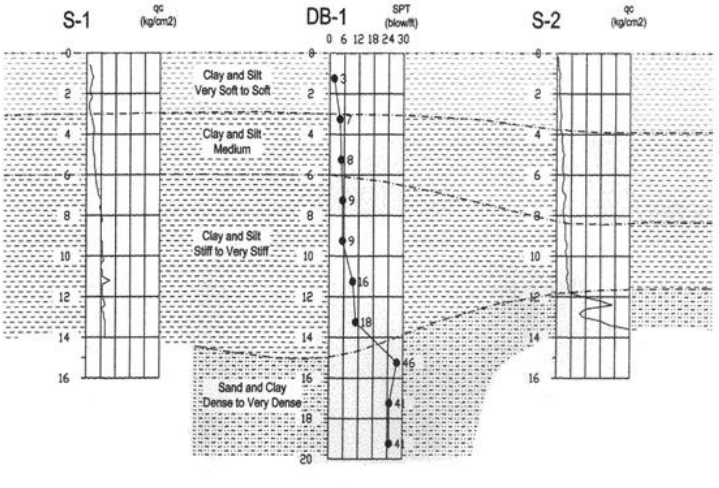

Fig. 3 Soil profile

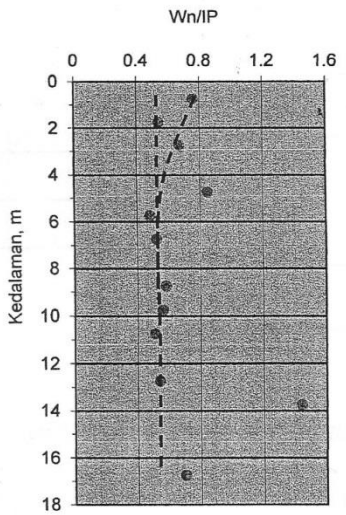

Fig. 4 Active zone

Tabel 1 Soil Properties

Depth (m)	Classification	Wc (%)	Gs	γ_t (t/m^3)	Deg. of saturation S (%)	e_o	LL	PL	Cohesion (kg/cm^2)
2.5 – 3.0	CH	35	2.60	1.63	79	1.15	76	24	0.24
6.5 – 7.0	CH	32	2.60	1.68	80	1.04	87	26	0.55
10.5 – 11.0	CH	29	2.56	1.74	83	0.90	82	25	0.76
16.5 – 17.0	CH	30	2.60	1.74	83	0.94	66	23	0.78

Fig. 5 Differential settlement of floor

Fig. 6 Gap between floor and wall

Fig. 7 Differential settlement of carport slab

Fig. 8 Crack and differential settlement of unreinforced carport slab

Fig. 9 Diagonal crack on the wall and ceiling

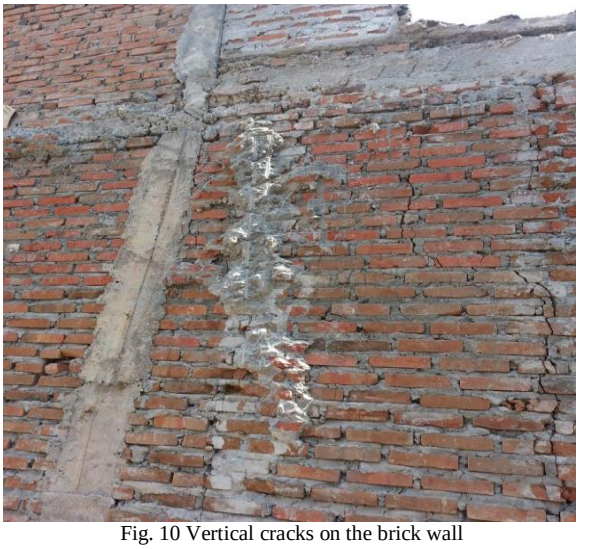

Fig. 10 Vertical cracks on the brick wall

Fig. 11 Poor detailing at beam-column joint

Fig. 12 Poor detailing of beam-column joint and horizontal cracks on the brick wall

5. Reseach Method

Site investigation was conducted to identify, take documentation of cracks, and gather additional information from the owners. The observation was focused on the condition of the floors, pattern of cracks on the walls, detailing of joints, and source of water infiltration that potentially triggers heaving or softening of soils.

It was observed visually that settlement of the floor occurred in several areas, such as presented in Fig. 5 and Fig. 6, and the differential settlement of carport slabs as presented in Fig. 7 and Fig. 8. In addition, there were gaps between ceramic floor and the fill. It was indicated by echo on several areas of ceramic floor when the floor was knocked. In general, there were no indication of damage that initiated by heaving on the floors.

The diagonal cracks on the walls caused by the differential settlement between adjacent columns, where the settlement of one column relatively larger than that of another column. In several locations, wider cracks were noticed on the upper part of the wall and continue to the ceiling, as presented in Fig. 9. Crack was also observed on the neighbouring wall after the house was demolished, as presented in Fig. 10.

Poor detailing of beam-column joints was noticed on the neighbouring wall as presented in Fig. 11. Horizontal crack was also noticed on the wall due to the absence of column to support beam as presented in Fig. 12. These poor joints definitely reduced the stiffness of the walls when it experiences differential settlement

Important information was noted during site investigation. It was found that the perimeter walls, which located in the borderline with open ground experienced relatively larger settlement than those bordered by covered ground

(neighboring house)

6. Analysis

By combining all available data that were collected during site observation such as pttern of craks, construction drawing, and as built drawing of the damage houses, potential factors that contribute to the damage of the houses can be summarized as follows.

Site observation data showed that there was no indication of damage on the houses, whic was triggered by swelling of soil. All data indicated that the damage was initiated by settlement (or differential settlement) of foundation and filling material. The expansive soil located in the active zone might experience swelling or heaving due to the presence of infiltration water, but it was relatively small compared to the settlement of the fill material. Therefore, there were no indication of cracks due to heaving or swelling of soil.

The thickness of the fill was ranging from 0.5 m to 1 m. Meanwhile, the length of the piled foundation was about 6 m. In other words, almost the entire length of the pile foundation is penetrated into the active zone. It means that bearing capacity of the piled foundation is vulnerable to the changing of shear strength of soil due to wetting-drying of soil layer in the active zone. The softening of soil in the active zone due to infiltration of water definitely will reduce bearing capacity of the piled foundation. Consequently, the piled foundation will experience settlement during wetting.

Infiltration of the water into the active zone is the main factor affecting the change of moisture of the expansive soil. Therefore, permeability of the fill and the potential source of infiltration water play the very important role in triggering the damage of the houses.

The damage of the houses was also contributed by poor detailing of joints between beam and column. The rigidity of the brick wall would decrease significantly when the quality of the connection between beam and column that encased the wall is poor. As a results, cracks on will easily develop on brick wall when it experiences differential settlement.

Based on the aforementioned facts, it is safe to state that the damage of the houses mainly caused by soil softening rather than swelling of soil.

7. Conclusion

Based on the available data and analysis, it can be concluded that the damage of the houses is initiated by the following factors:

The fills were not compacted properly and less impermeable so it experienced relatively large settlement when flooded with water.

The length of the piled foundation was not adequate so that almost the entire length of the pile embeded in the active zone

The infiltration of water initiated softening of soil in the active zone at which the pile foundation was implanted. This softening process reduced the bearing capacity of the piled foundation that mainly rested on this layer. The reduction of bearing capacity of this piled foundation has generated settlement

Improper detailing of beam-column joints and joints between walls reduced the stiffness of the brick walls, so that several diagonal cracks developed on the walls due to differential settlement

References

[1] B.M. Das, Principles of Geotechnical Engineering, California, PWS Publishing, 1999
[2] Testana Engineering, Soil Investigation Report, January 2015
[3] D. Tjandra, Indarto, and R.A.A. Soemitro, Effect of drying-wetting process on friction capacity and adhesion factor of pile foundation in clayey soils. Jurnal Teknologi, 77:11 (2015) 145-150.
[4] T.L.T. Zhan, R. Chen, and C.W.W. Ng, Wetting-induced softening behavior of an unsaturated expansive clay. Landslides 11 (2014) 1051-1061
[5] S.J. Wheleer, S.J. Sharma, M.S.R. Buisson, Coupling of hydraulic hysteresis and stress-strain bahaviour in unsaturated soils. Geotechnique 53:1 (2003) 41-54

[6] F. Melinda, H. Rahardjo, K.K. Han, and E.C. Leong, Shear strength of compacted soil under infiltration condition. Journal of Geotechnical and Geoenvironmental Engineering, 130:8 (2004) 807-817,
[7] W.M. Ye, Y.W. Zhang, B. Chen, S.F. Zhang, Characteristics of Shear Strength of Unsaturated Weak Expansive Soil. Proc. Of International Symp. On Geoenvironmental Eng. ISGE 2009. September 8-9 2009, Hangzhou, China.

Available online at www.sciencedirect.com

ScienceDirect

Procedia Engineering 00 (2017) 000–000

Procedia Engineering

www.elsevier.com/locate/procedia

Sustainable Civil Engineering Structures and Construction Materials, SCESCM 2016

Evaluation of frost heave pressure characteristics in transverse direction to heat flow

Chikako Amanuma[a]*, Takashi Kanauchi[a], Satoshi Akagawa[b], Zheng Hao[c], Shunji Kanie[c]

[a]*Guraduate Scool of Engineering, Hokkaido University, Sapporo, Japan*
[b] *Cryosphere Engineering Laboratory, Tokyo, Japan*
[c]*Faculty of Engineering, Hokkaido University, Sapporo, Japan*

Abstract

The freezing method for underground construction has been attracting attention owing to its non-polluting characteristics. This method requires precise forecasting of freezing behavior and countermeasure technology against frost expansion. To improve this method, it is necessary to know the expansion characteristics in a transverse direction to heat flow as well as in the heat flow direction. In this study, we developed a new apparatus for frost heave experiments that can measure the pressure due to expansion in the transverse direction. As a conclusion, we successfully evaluated the characteristics of frost heave pressure in the transverse direction to heat flow through experiments.

Peer-review under responsibility of the organizing committee of SCESCM 2016.

Keywords: frost heave; measuring method; frozen soil

1. Background and Object

Nowadays, the freezing method is a promising application for underground constructions owing to its non-polluting characteristics. However, during the process of ground freezing, frost heave would seriously affect the ambient infrastructure. Frost heave is a phenomenon that is caused by not only the volume expansion of phase-change, but also the migration of water from the non-frozen side to the freezing fringe. In this phenomenon, a one-dimensional experimental formula, derived from indoor frost heave experiments, is widely applied for the evaluation of volume expansion and pressure confinement. However, the study of expansion in a transverse direction to heat flow is very limited. In the future, the forecasting of expansion in complicated underground spaces and the evaluation of frost heave pressure characteristics in the heat flow direction and in the transverse direction to heat flow becomes more important. In this study, we designed an innovative apparatus for frost heave testing to measure expansion in transverse direction, and evaluate frost heave pressure characteristics in the transverse direction to heat flow by using an open system with a water supply.

* Corresponding author. Tel.: +81-11-706-6176; fax: +81-11-706-6176.
E-mail address: tcaco.ama@gmail.com

Peer-review under responsibility of the organizing committee of SCESCM 2016.

2. Development of the Apparatus

2.1. The apparatus to measure stress in transverse direction to heat flow

We selected a strain gauge and a small-sized water pressure gauge as instruments to measure the stress in the transverse direction to heat flow. We adopted sensors that are frequently used in frost heave experiments for the measurement of frost heave displacement in the vertical direction. Small-sized water pressure gauges with a diameter of 6 mm were buried in the frost heave test cell in order to measure the transverse pressure Fig. 1. The strain gauge had a length of 10 mm, was placed in the heat flow direction, and had the same thermal expansion coefficient as the acrylic material that was used in the frost heave test cell. We placed this instrument over the outer part of the frost heave test cell and calculated the inner radial stress by the outer strain based on the thick layer shell theory (Fig. 2).

Fig. 1 Installation of small-sized water pressure gauge

Fig. 2 Installation of strain gauge

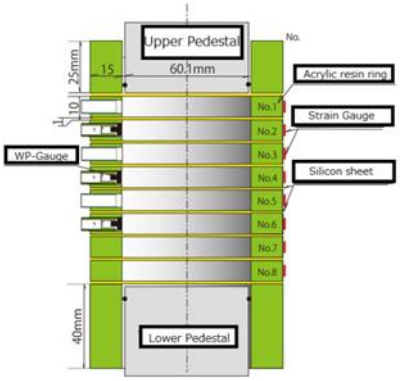

Fig. 3 Schematic diagram of frost heave test cell

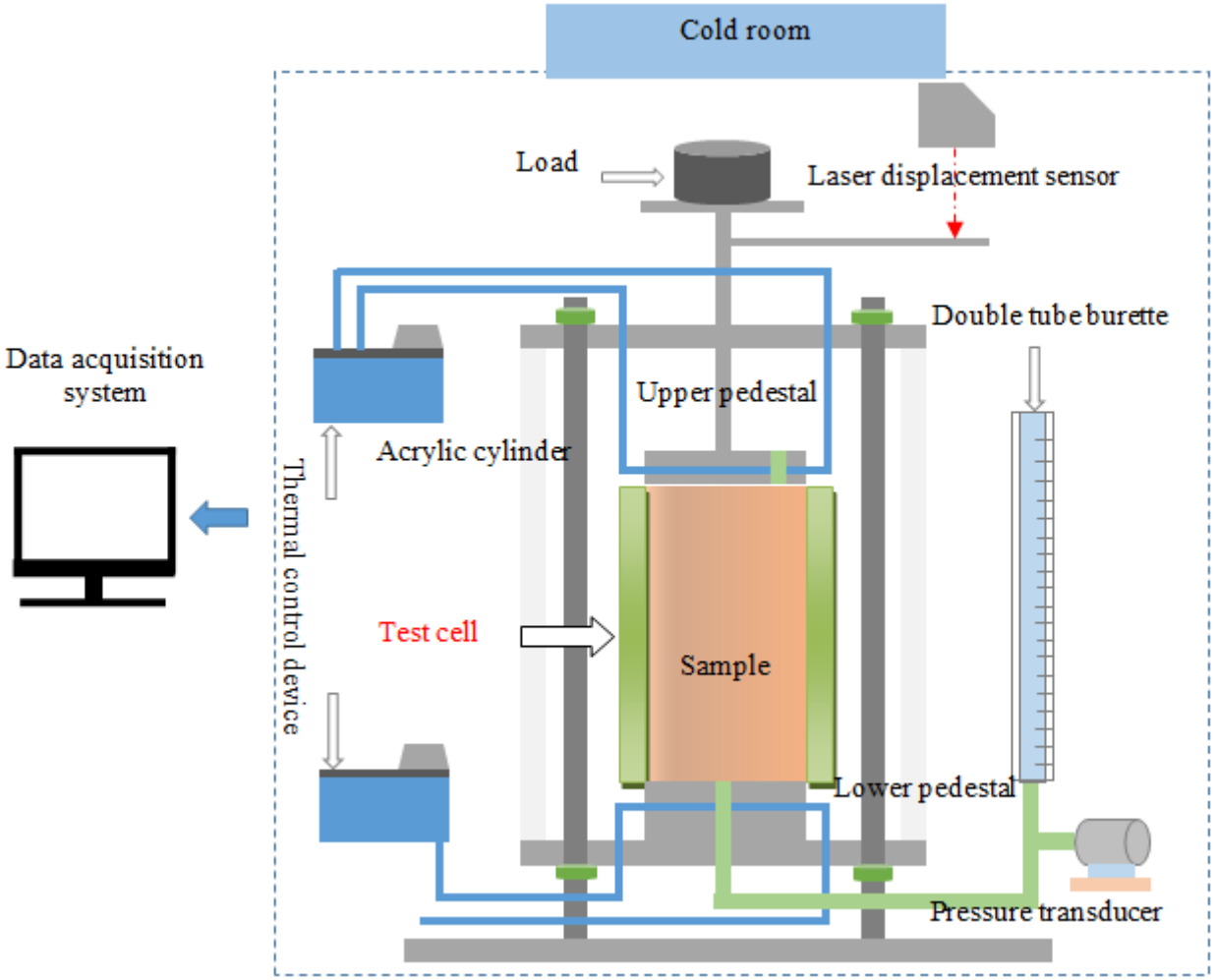

Fig. 4 Schematic diagram of the frost heave test apparatus

2.2. Frost heave cell

Fig. 3 shows the schematic diagram of the frost heave test cell. The cell was made of an acrylic material, which had a similar thermal conductivity to Dotan, a Neogene silty soft rock. We piled up eight acrylic rings to form the frost heave test cell. The height of each acrylic ring was 10 mm with a thickness of 15 mm. We set strain gauges and thermometers in all of these eight rings in order to obtain the thermal distribution. The small-sized water pressure gauges were set in ring numbers 2, 4, and 6. We set a 1-mm silicon sheet between each ring to prevent water from leaking.

2.3. Performance test of measuring instruments

As the temperature of the specimen during the frost heave test changes from a positive to a negative value (°C), we have to pay attention to the thermal expansion, and remove the effect of temperature change from the observed values. Before performing the frost heave test, we conducted two performance tests in order to verify measuring accuracy.

First, we carried out a pressure test to confirm the accuracy of pressure gauges. We filled the acrylic cells with fresh water and applied various water pressures by overburdening. In the loading process, the water pressure was increased from 0 to 500 kPa in increments of 100 kPa. Similarly, in the unloading process, the water pressure was decreased in five steps. The measured water pressures are shown in Fig. 5 by comparing the values obtained by the water pressure gauges to those obtained by the strain gauges. In this Fig., it is clearly observed that the pressures measured by both the gauges are identical to each other; therefore, we concluded that the measuring instruments are reliable and sufficiently accurate for the measurement.

Second, we conducted a thermal expansion test to confirm the effect of the thermal expansion coefficient of the acrylic material on the strain gauges. Similar to the pressure test, we filled the acrylic cells with fresh water and gradually decreased the temperature of the water. In the frost heave experiment, the freezing rate of the specimen was carefully controlled at approximately 1 mm/h with a thermal gradient of 0.1 ℃/mm. This implies that the specimen, having a height of 100 mm, is gradually frozen for 100 h. Then, we spent 20 h to decrease the water temperature from 1°C to -1 °C and compared the temperatures obtained by the strain gauges with those obtained by the water pressure gauges. Fig. 6 illustrates the temperatures measured by the pressure gauges. As the water pressure gauge measures the pressure of liquid directly, the observed values are never influenced by the change in temperature of the water. On the contrary, the pressure measured by the strain gauge is calculated from the strain and includes the effect of the material's thermal expansion coefficient. The pressures that were estimated by the strain gauges are shown in Fig. 6(a), and it can be seen that the estimated values slightly drift with an increase in temperature. Assuming that the relationship between the temperature and pressure measured by the strain gauge is linear, we decided to introduce a correction coefficient derived from a regression formula based on Fig. 6(b).

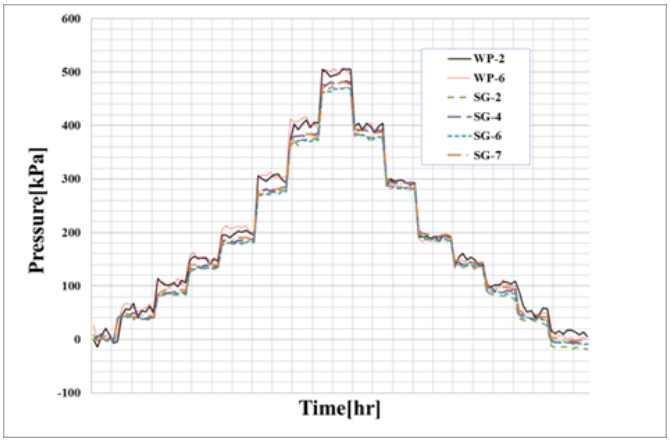

Fig. 5 Pressure verification results

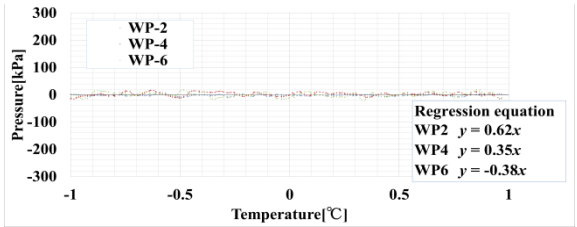

(a)Water pressure gauge

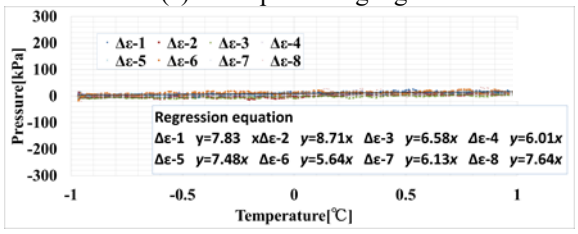

(b) Strain gauge

Fig. 6 Temperature verification results

2.4. Measuring accuracy in the frost heave test

After confirming the performance of this new apparatus, as described in the previous section, we executed a frost heave test with a typical Neogene silty soft rock known as Dotan. The purpose of this experiment was to approve that every measuring instrument works well with sufficient accuracy. Fig 7 and Fig 8 show the pressures at rings 4 and 6 measured by the water pressure and strain gauges, respectively. As shown in these Fig.s, the pressures measured by both the measuring instruments are similar, thus successfully establishing the validity of this experimental device. Then, we used the pressures estimated by the strain gauges as the horizontal pressures in transverse direction to heat flow, which is described in the following sections.

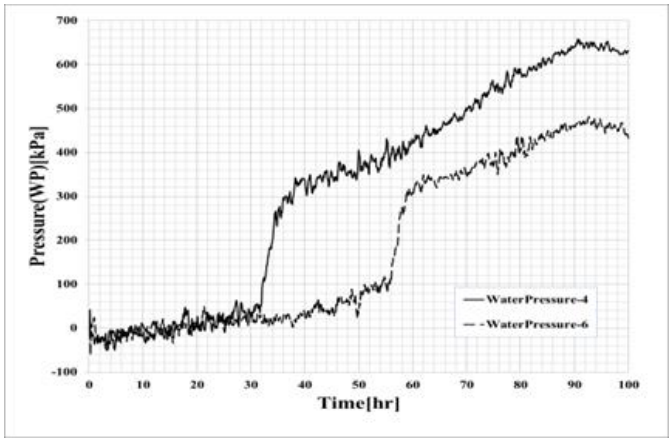

Fig. 7 Horizontal stress (water pressure gauge)

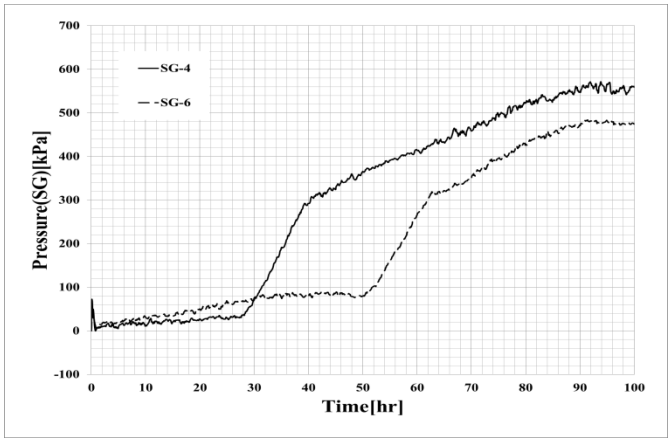

Fig. 8 Horizontal stress (strain gauge)

3. Triaxial frost heave experiments

3.1. Procedure and experimental conditions

We adopted Dotan, a Neogene silty soft rock, for the triaxial frost heave experiment along with Toyoura standard sand for comparison. Dotan is known as a soil that is susceptible to frost and its use is spreading in Tokyo and its vicinities. On the other hand, sand never heaves except for in-situ freezing. The confining pressures were set at 50 kPa, 100 kPa, and 200 kPa in the heat flow direction. Before starting the experiment, we put specimens in a cold room with a temperature of 1°C to keep the original temperature of the specimens constant. During the experiments, the temperatures at the top and bottom pedestals were gradually and carefully decreased by keeping the freezing rate of 1.0 mm/hr. The experimental conditions are tabulated in Table 1 and Table 2.

Table 1 Experimental conditions

Soil	1) Dotan 2) Toyoura standard sand
Height of the specimen	92 mm
Confining Pressure σ_1 (Overburden pressure)	50 kPa・100 kPa・200 kPa
Freezing rate	1.0 mm/h
Distribution of temperature	0.1°C/mm

Table 2 Measured values

Displacement in heat flow direction
Content of absorbed water
Temperature of upper and lower pedestal
Temperature of each ring
Pressure in the transverse direction to heat flow(By WPG and SG)

3.2. Frost heave test result of Dotan

Fig. 9 shows the results of pressure in the transverse direction to heat flow for each ring under the confining pressure of 100 kPa. The specimen starts to freeze from top to bottom according to the order of ring numbers such as Ring 1 to Ring 8. The pressures in the transverse direction to heat flow increase drastically at each level for the first 10 h of freezing. After these drastic changes in pressure, the transverse pressure increases gradually and linearly with time. The pressure in the transverse direction becomes constant at the end of the experiment. Fig. 10 shows the relationship between the pressure and temperature. From these results, we found that the pressure in transverse direction to heat flow drastically increases at a temperature between 0 and -1°C. However, even after freezing at each level, the pressure increases gradually with the decrease in temperature.

Fig. 11 illustrates the changes in frost heave displacement as well as the amount of absorbed water with time. The larger the confining pressure becomes, the smaller the frost heave displacement. The amount of absorbed water is proportional to the frost heave displacement, and this can be fully explained by the formula known as the Takashi's equation. Fig. 12 shows the change in transverse pressure of ring 4 with time under different confining pressures. As already described, the pressure drastically increased in all cases of freezing at a temperature between 0 to -1°C. However, the increments in transverse pressure depend on the confining pressures. The most interesting finding is that the pressures in the transverse direction to heat flow finally converge to an almost same value after nearly the same number of hours regardless of the difference in the confining pressure.

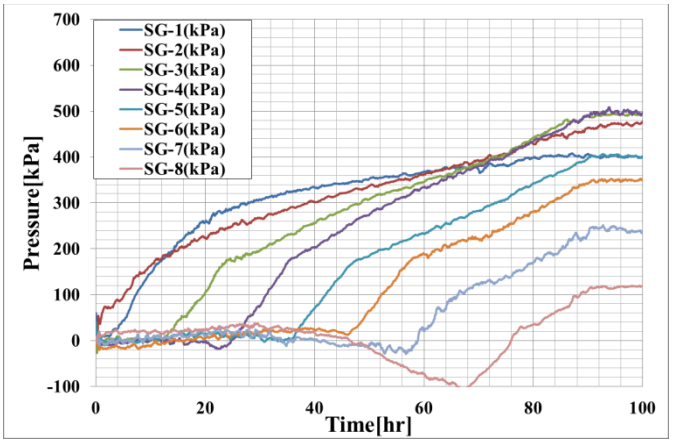

Fig. 9 Change in transverse pressure with time when the confining pressure is 100 kPa in the Dotan test

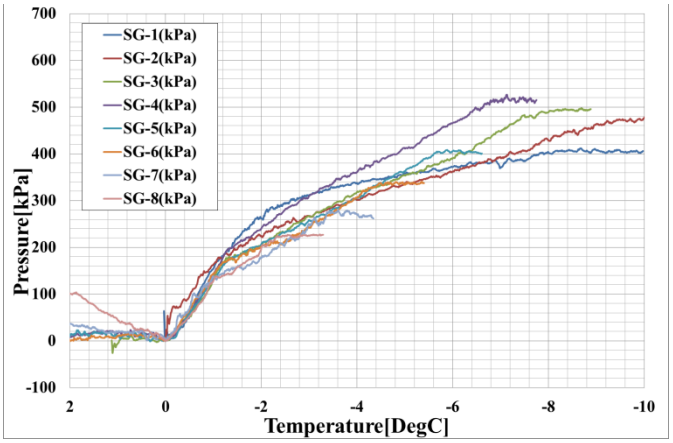

Fig. 10 Change in transverse pressure with temperature when the confining pressure is 100 kPa in the Dotan test

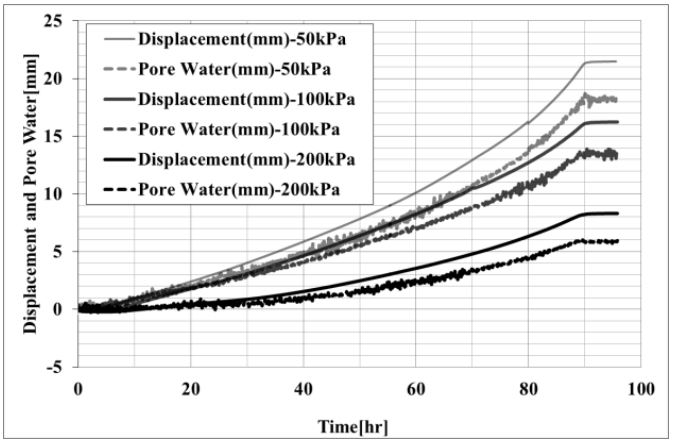

Fig. 11 Frost heave displacement and absorbed water (Dotan)

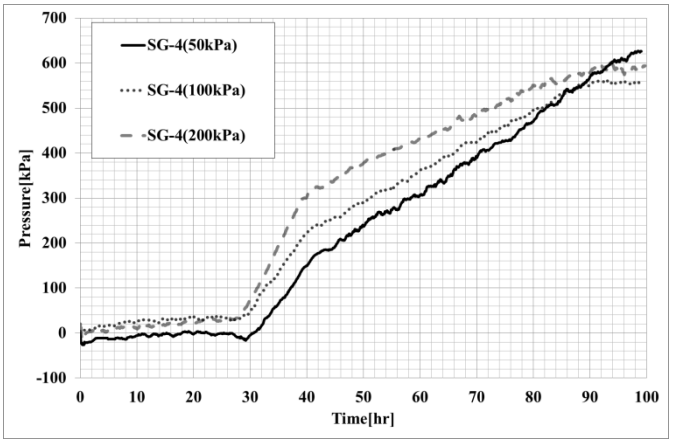

Fig. 12 Increase in transverse pressure at ring 4 (Dotan)

3.3. Frost heave test result of sand

Fig 13 and Fig 14 show the transverse pressures of each ring under a confining pressure of 100 kPa. The characteristics of pressure increase of sand are similar to those of Dotan as described in the previous section. The transverse pressures increase drastically while freezing and keep increasing with time and temperature.

The frost heave displacement and the amount of absorbed water, however, show completely different behaviors compared to those of Dotan as shown in Fig. 15. The sand specimen is never deformed with freezing and the frost heave displacements remain almost 0 under all confining pressures. The reason why the amount of absorbed water becomes negative can be explained by the fact that unfrozen water, within the specimen, was drained by the inflation of saturated sand. It should be noted that the amount of water drained from the specimen is equal to the volumetric change of water owing to in-situ freezing. In addition, the behavior of the transverse pressure of sand seems to be different from that of Dotan. The transverse pressures drastically increase with time, as shown in Fig. 16, owing to freezing but the increments are almost the same regardless of the confining pressure. The final pressures also converge to an almost equal value irrespective of the confining pressure.

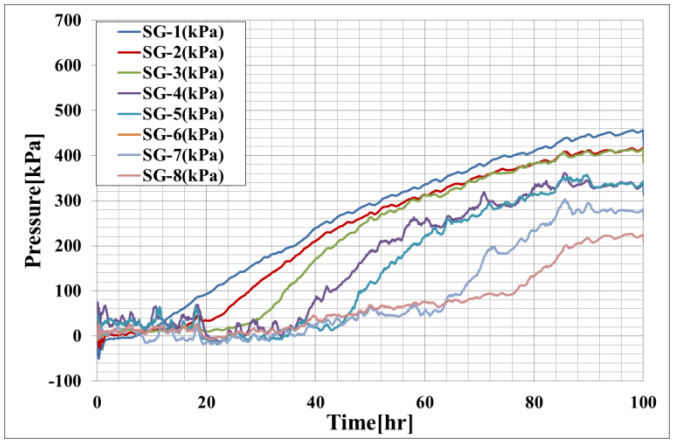

Fig. 13 Change in transverse pressure with time when the confining pressure is 100 kPa in the sand test

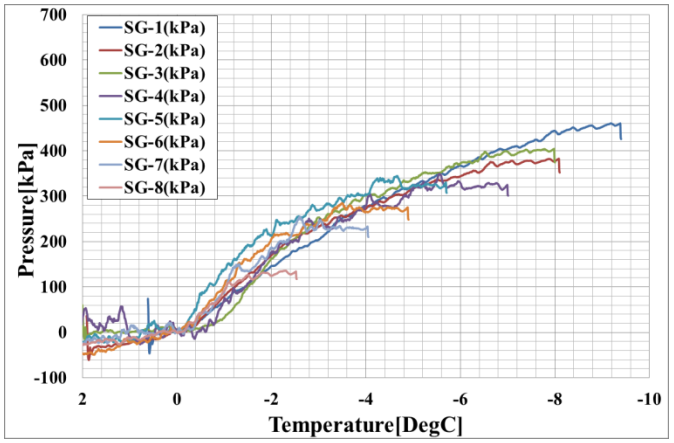

Fig. 14 Change in transverse pressure with temperature when the confining pressure is 100 kPa in the sand test

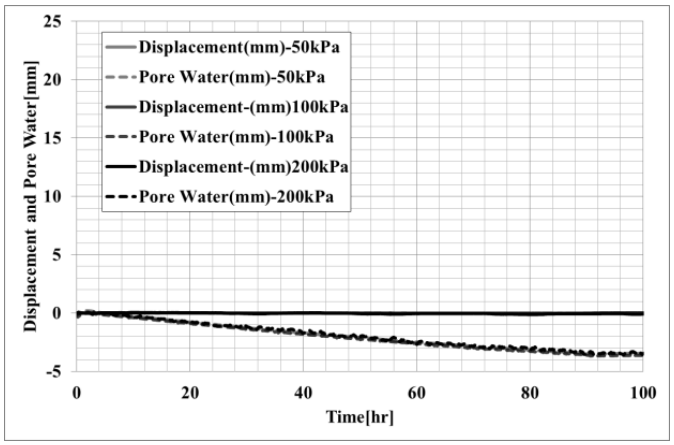

Fig. 15 Frost heave displacement and absorbed water (Sand)

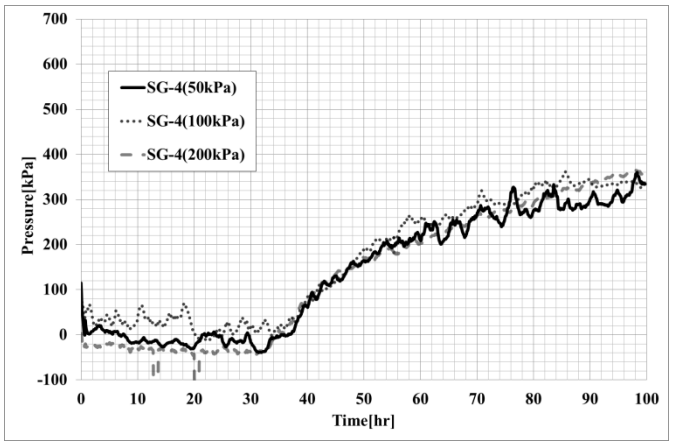

Fig. 16 Increase in transverse pressure at ring 4 (Sand)

4. Conclusion

We developed a new triaxial frost heave apparatus in order to observe the change in lateral pressure which is transverse to the heat flow direction. The applicability and measuring accuracy have been successfully evaluated through verification tests. The frost heave tests were carried out with soil and sand specimens in order to understand the mechanism of frost heaving and we obtained some interesting findings. In the case of Dotan test, which is a frost-susceptible material, a drastic increment of transverse pressure was observed in the first 10 h of freezing. And we found that the increasing amount of transverse pressure depended on the confining pressure. In addition, as the temperature of the specimen decreased, the transverse pressure increased continuously and gradually as well. However, the final pressure in transverse direction converges to the similar value regardless of confining pressure. On the contrary, in the case of sand, where no frost heave occurred, the transverse pressure is never influenced by the confining pressure even though the increasing trend of transverse pressure is similar to that of Dotan.

We are convinced that the evaluation of the stress condition in three-dimensional frost heave should be seriously discussed before applying freezing skills to large construction projects located in urban areas. Therefore, it is necessary to conduct triaxial frost heave experiments under many different conditions to clarify the mechanism of multi-dimensional frost heave behaviour. This innovative triaxial frost heave apparatus developed by us is just designed for this purpose and we will improve this system continuously to enlarge its applicability to various soil materials and freezing conditions.

5. References

[1] Tsutomu Takashi, Takahiro Orai, Hideo Yamamoto, Jun Okamoto, Experimental study about unconfined compressive strength of the frozen sand, Journal of JSCE. No.203, 1980, pp. 79- 88.

[2]Teruyuki Yumisogi, S. B. Tamrakar, Satoshi Akagawa, Evaluation of friction in horizontal direction on frost heave experiment, Journal of JGS, No.37, 2002, pp.1191-1192

[3]Seiichi Kinoshita, Physical science of frozen soil, Morikita Publishing, 1982

[4]Library of basic soil engineering, Freezing of soil-control and application-, Japanese Soc, of Soil Mechanics and Foundation Engineering, 1982

[5]Hokkaido branch of JGS, Soil engineering for cold district-frost heave damages and its measures-, Nakanishi Publishing, 2009

Available online at www.sciencedirect.com

ScienceDirect

Procedia Engineering 00 (2017) 000–000

Procedia Engineering

www.elsevier.com/locate/procedia

Sustainable Civil Engineering Structures and Construction Materials, SCESCM 2016

Analysis of the seepage due to the thawing of permafrost, considering the gradient of the impermeable layer

Masaya Ogawa [a,*], Shunji Kanie[b]

[a]*Graduate School of Engineering, Hokkaido University, Sapporo, Japan*
[b]*Faculty of Engineering, Hokkaido University, Sapporo, Japan*

Abstract

Topographical deformation due to global warming has become a serious problem. However, scientific studies have not been sufficiently conducted to understand the mechanisms. Solifluction, a gradual mass movement related to freeze-thaw processes, is known as a typical topographical deformation. The purpose of this study is to simulate the solifluction process considering the seepage influence, and then establish a predictive numerical model. The authors adopted the Finite Volume Method (FVM) and Dupuit's assumption in order to precisely simulate the seepage flow. Consequently, according to this study, the authors suggested to adopt a non-linear assumption for appropriate estimation of seepage flow velocity.

Peer-review under responsibility of the organizing committee of SCESCM 2016.

Keywords: FVM; solifluction; seepage; permafrost;thermal erosion.

1. Introduction

In recent years, it has been frequently reported that global warming causes various environmental issues, including topographical deformation such as solifluction and thermal erosion in permafrost regions. Permafrost is defined as a soil layer that remains frozen for a minimum of two consecutive years, and it is distributed over a wide area in the northern hemisphere of the earth. If permafrost starts to thaw, the soil layer is likely to deform and deteriorate in strength. When the thawing is accelerated, it allows water to flow underground. The water runs down

* Corresponding author. Tel.: +81-90-6630-2874.
E-mail address: taichik2@ec.hokudai.ac.jp

Peer-review under responsibility of the organizing committee of SCESCM 2016.

along the gradient of the permafrost table, taking with it soil particles in the vicinity. These phenomena are known as solifluction and thermal erosion. Fig. 1 shows the deformation of and damage to structures due to thawing. The effects of this damage are not limited to topographical or geographical deformation, but also affect the decline in plant life and vegetation, as hydrological circulation through the surface is seriously affected. Finally, these mechanisms may limit ability of the earth to absorb carbon dioxide.

In this study, we aimed to elucidate the mechanism behind the land deformation caused by underground seepage through both experimental and numerical approaches. In order to simulate the phenomenon, many factors must be taken into account, such as thawing processes, water flow dynamics, the interaction between water and soil particles, etc. First, we focused on the underground seepage flow and attempted to confirm the applicability of the numerical method used, which includes the Finite Volume Method based on Dupuit's assumption.

(a) solifluction (b) thermal erosion (c) collapse of structure

Fig. 1. Damage caused by the thawing of permafrost

2. Analytical model and boundary conditions

Initially, we prepared an indoor experimental device in order to reproduce the underground water flow and corresponding soil deformation. The box-shaped device is 50 cm in the length, with a rectangular cross-section of 15× 10 cm. We then filled the device with fully saturated fine sand. By inclining the device, after removing the wall at the downstream end, water started to flow within the sand layer. We discretized into small elements along the stream-line and Fig. 2 shows the numerical model for the calculation.

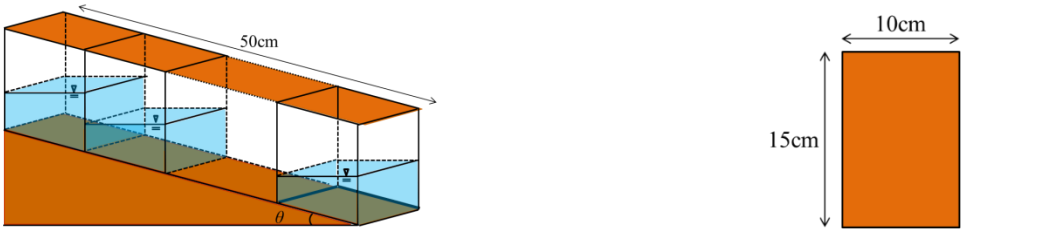

(a) Complete view of the analytical model (b) Cross-section of the model

Fig. 2. Analytical model

3. Method and Equations

Underground water gradually flows according to the hydraulic pressure gradient within the foundation. Since the coefficient of permeability of sand is sufficiently small, at 0.025 cm/s, we assumed that the quasi-uniform flow proposed by Dupuit can be adopted. It says that the flow velocity along the stream-line can be assumed to be constant, regardless of the height from the bottom, and the velocity in the transverse direction to the stream-line is negligible. Fig. 3 illustrates a schematic diagram of the quasi-uniform flow and the distribution of hydrostatic pressure. Even though the water table, as a free surface, decreases continuously along the stream line, the difference in hydrostatic pressures between two points along the stream-line can be assumed to be approximately equal and constant, irrespective of the height.

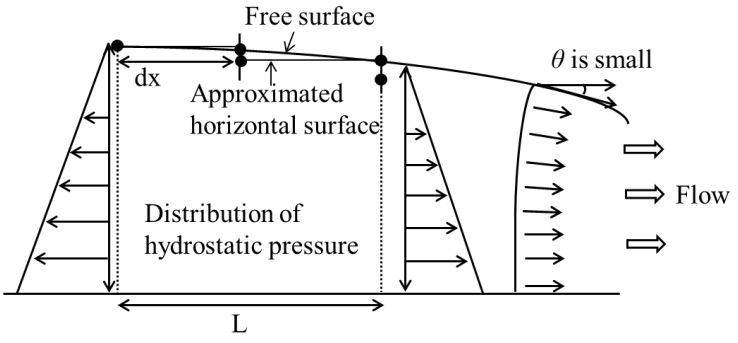

Fig. 3. Quasi- uniform flow of unconfined groundwater

As a numerical method for the evaluation of underground flow, the Finite Element Method (FEM) may be one of the well-known techniques. The model is divided into small elements along a stream-line, and the hydraulic pressure, as an objective function, is assigned at the boundary of each element. In the FEM, the flow velocity within each element is evaluated by the gradient calculated from the pressures at the boundaries of each element. As a result, the estimated velocity is continuous within each element, but the velocities on the boundaries become discontinuous. An alternative method to this is the Finite Volume Method (FVM). In this method, the water height within each element, rather than at the element boundary, is used as the objective function, therefore, the flow velocity is continuous at the boundary. In the numerical evaluation of the underground water flow, we applied the FVM in order to obtain a unique and continuous flow velocity at the boundary of each element. This makes it possible to manage the amount of water contained within each element more precisely and more adequately than when using the FEM.

Here, we derive the equations based on the FVM. First, we name the element where we consider the equilibrium of material balance. If this element is located at the *j*-th position in the order, from the upstream end, the element is named ‘el.j’, as shown in Fig. 4. Similarly, the element located at the upstream side of ‘el.j’ is named ‘el.j-1’, and the element at the downstream side is ‘el.j+1’. The volume of water flowing from ‘el.j’ to ‘el. j-1’ within a unit time is given as $q_{j,j-1}$. The water height of ‘el.j’ varies with time due to the water flow through the boundaries. By introducing the projected bottom area of ‘el.j’ as A_j, we derive Equation (1), as shown below.

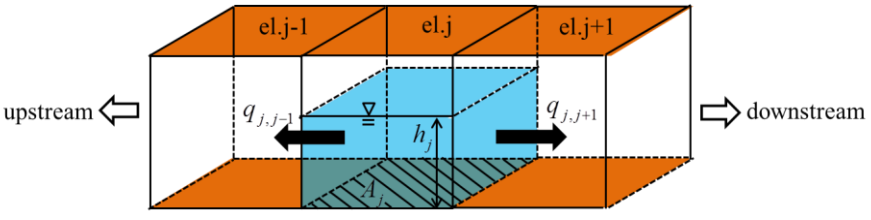

Fig. 4. Modelling in FVM

$$A_j \frac{\partial h_j}{\partial t} = -(q_{j,j-1} + q_{j,j+1}) \tag{1}$$

The water flow, given by $q_{j,j-1}$ and $q_{j,j+1}$ in Equation (1), is calculated by the cross-sectional flow area multiplied by the flow velocity. Assuming Darcy’s law, which states that the flow velocity is proportional to the hydraulic gradient multiplied by a coefficient of permeability, the right-hand-side term of Equation (1) can be decomposed, like Equation (2), by applying the forward difference method to the time dependent term. The superscript, *m*, in Equation (2) denotes a time-step in the calculation.

$$A_j \frac{{h_j}^{m+1} - {h_j}^{m}}{\Delta t} = -(\Gamma_{j,j-1} \times k \times i_{j,j-1} + \Gamma_{j,j+1} \times k \times i_{j,j+1}) \tag{2}$$

Where, $\Gamma_{j,j-1}$ and $\Gamma_{j,j+1}$ are the cross-sectional areas of flow at the boundaries, k is the permeability of sand, and $i_{j,j-1}$ and $i_{j,j+1}$ are the hydraulic gradients at the boundaries.

Here, we consider the cross-sectional area of flow at a boundary. We assume that the height of the cross-sectional area is equal to the water height, h_j, of 'el.j'. The cross-sectional area, $\Gamma_{j,j+1}$, is calculated by Equation (3). Another possibility is to take an interpolated value for the water height, as shown by Equation (4). In both cases shown in Fig. 5, the width of the channel is denoted as l and the combined length of all the elements along the stream-line is denoted as d.

$$\Gamma_{j,j+1} = h \times l \tag{3}$$

$$\Gamma_{j,j+1} = \frac{h_j \times d + h_{j+1} \times d}{d + d} \times l = \frac{h_j + h_{j+1}}{2} l \tag{4}$$

If we use Equation (3) and introduce it into Equation (2), the time domain calculation becomes very simple because all the terms in Equation (2) are linear. In the case of Equation (4), however, Equation (2) includes non-linear terms expressed as a quadratic function of height, h. Fig. 5 shows the difference in the cross-sectional area of flow between these models.

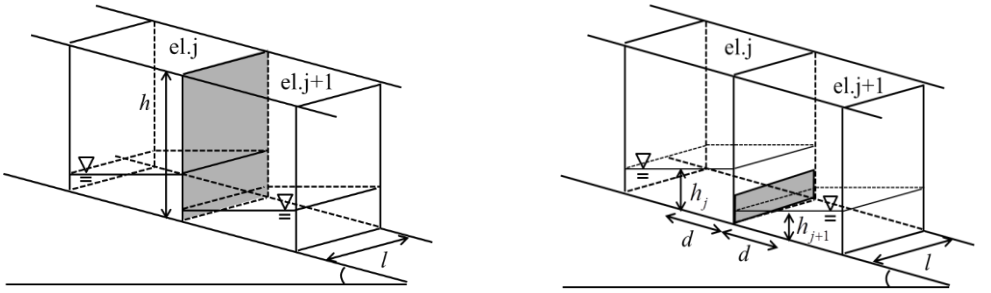

(a) Model for Equation (3) (b) Model for Equation (4)

Fig. 5. Definition of flowing sections

In the next step, we define the hydraulic gradient from a reference plane (in following sections, referred to r.p). This is because we are assuming that the bottom layer is inclined to r.p by an impermeable layer, as shown in Fig. 6. The inclined angle of the bottom layer from r.p is given as θ, and the vertical distance from the reference plane to the bottom of each element is expressed as z with a subscript, such as z_j. The hydraulic gradient, i, can be described by Equation (5).

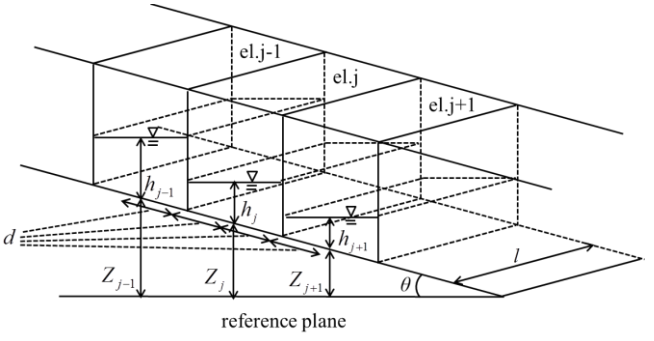

Fig. 6. Water height from the reference plane

$$i_{j,j-1} = \frac{(h_j + Z_j) - (h_{j-1} + Z_{j-1})}{2d\cos\theta} = \frac{h_j - h_{j-1}}{2d\cos\theta} + \frac{Z_j - Z_{j-1}}{2d\cos\theta} = \frac{h_j - h_{j-1}}{2d\cos\theta} - \tan\theta \tag{5}$$

$$i_{j,j+1} = \frac{(h_j + Z_j) - (h_{j+1} + Z_{j+1})}{2d\cos\theta} = \frac{h_j - h_{j+1}}{2d\cos\theta} + \frac{Z_j - Z_{j+1}}{2d\cos\theta} = \frac{h_j - h_{j+1}}{2d\cos\theta} + \tan\theta$$

Combining all the equations above, we derived Equations (6) and (7) for the time domain analysis. Equation (6) is used for the linear model by assuming that the height of the flow cross-section is equal to the depth of each element. Conversely, Equation (7) is adopted for the non-linear model, based on Equation (4). The coefficients included in Equation (6) and (7) are described by Equation (8). The aim is then to evaluate the effect of the non-linear term, given by Equation (7), on the flow simulation. In addition, the authors discuss the validity of the forward difference method, depending on the time interval.

$$h_j^{m+1} = C_1 h_{j-1}^{m} + (1 - 2C_1) h_j^{m} + C_1 h_{j+1}^{m} \tag{6}$$

$$h_j^{m+1} = C_2 h_{j-1}^{m} + h_j^{m} - C_2 h_{j+1}^{m} - C_3 \left\{ -(h_{j-1}^{m})^2 + 2(h_j^{m})^2 - (h_{j+1}^{m})^2 \right\} \tag{7}$$

$$C_1 = \frac{\Delta t}{A_j} \cdot hkl\tan\theta,\ C_2 = \frac{\Delta t}{A_j} \times \frac{kl}{2}\tan\theta,\ C_3 = \frac{\Delta t}{A_j} \times \frac{kl}{4d\cos\theta} \tag{8}$$

4. Result of analysis

In a numerical calculation, fine discretization is generally preferable in order to gain accurate approximations. However, too much discretization increases the computational load on the CPU as well as the computing time. In order to fix an appropriate number of elements along the stream-line, the authors carried out a simulation by introducing 50 discrete elements as the finest level of discretization in the model. This results in the length of each element being 1 cm. We then applied different numbers of discretized elements, such as 5, 10, 15, 20, and 25, in order to compare the calculation results with those generated by the finest model. Fig. 7 shows the calculation errors of each of these models at 10, 30, and 50 cm from the upstream side. The error ratios shown in Fig. 7 were calculated as the difference in the estimated water height compared to those estimated by the finest, 50 element model. From Fig. 7, it can be said that the error ratio becomes larger towards the middle of the stream-line at around 30 cm. If we allow for a 5 % error in the estimation, the minimum number of discretized elements should be 15 or more. As a result, in the following discussion, we adopted a model consisting of 15 elements. Where, n, in Fig. 7 denotes the number of discretized elements.

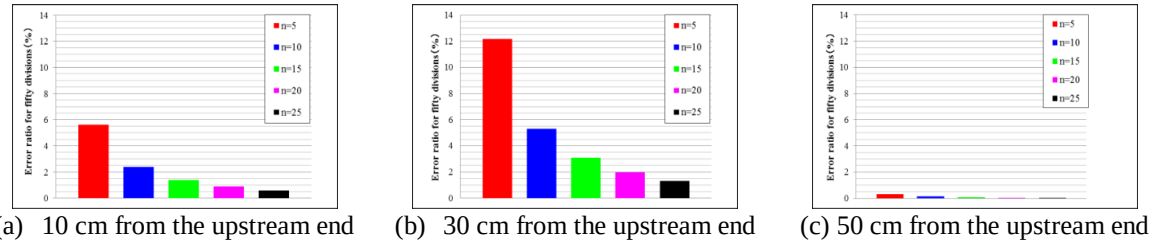

(a) 10 cm from the upstream end (b) 30 cm from the upstream end (c) 50 cm from the upstream end

Fig. 7. Calculation error compared with the solutions produced by the finest model

The authors conducted numerical simulations under two different conditions. In Case-1, the four boundaries consisting of side-walls never allow water to flow in or out through them. As an initial condition, we assumed that the element located at the most upstream end is fully saturated with water, and the other elements in the downstream side are dry. In other words, the water level of ‘el.1’, which is located at the upstream end, is greater than 18 cm above the r.p, but the water levels in the other elements are equal to the height between the bottom impermeable layer and the r.p. Fig. 8 shows the numerical results. As was described earlier, we adopted two assumptions for the cross-sectional area of flow; (a) a linear model using Equation (6), and, (b) a non-linear model using Equation (7). After the calculation is started, water gradually moves in the downstream direction and the water levels in the downstream elements converge to an equal value of less than 4 cm. Some water levels in the upstream elements have values larger than 4 cm, but those levels are expressed as the height from the r.p, and they are equal to the

heights of the bottom layer. By comparing Fig.s 8 (a) and 8 (b), we find that the water levels after convergence are the same for both models, but their behaviors leading towards convergence look very different. When we adopt the linear model, the water levels converge in a very short time, less than 1,000 s as shown in Fig. 8 (a). Conversely, for the non-linear model, the necessary time for convergence is much greater, close to 15,000 s, as shown in Fig. 8 (b). The same trend can be noted by Fig. 9. Fig. 9 shows the water level result at fixed time. Similar to Fig. 8, (a) shows a linear model using Equation (6), and, (b) presents a non-linear model using Equation (7). By comparison with Fig. 9 (b), we find that Fig. 9 (a) converges faster.

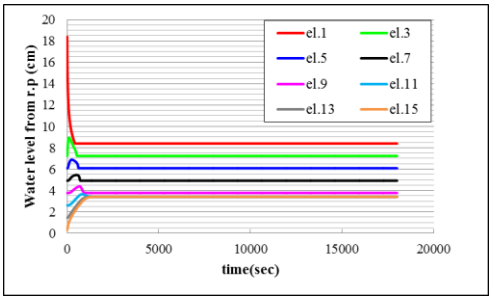

(a) Calculation using Equation (6)

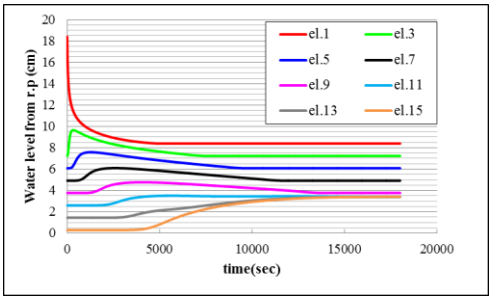

(b) Calculation using Equation (7)

Fig. 8. Numerical Results of Case-1

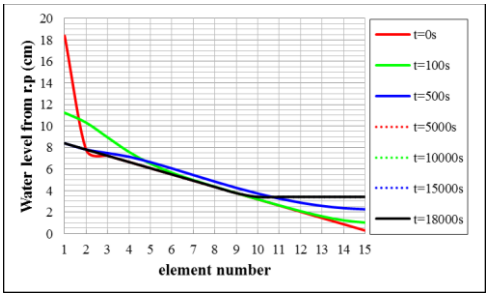

(c) Calculation using Equation (6)

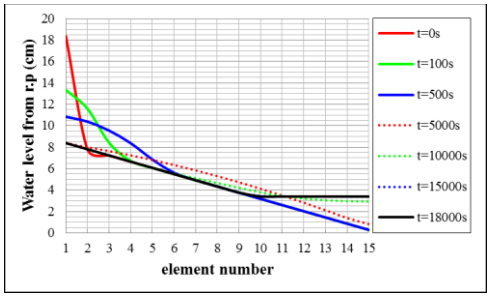

(d) Calculation using Equation (7)

Fig. 9. Water Level Results at fixed time of Case-1

In Case-2, we include a further calculation condition. We assume that all of the elements are fully saturated with water as an initial condition, and we allow water to flow out through the downstream end-wall. As water gradually migrates from upstream to downstream, the water levels of all the elements decrease. After a certain amount of time, all the elements dry up and the water level heights of each element decrease to their respective heights of the bottom layer above the r.p, as shown in Fig. 10. Fig.s 10 (a) and 10 (b) illustrate the linear model using Equation (6) and the non-linear model using Equation (7), respectively. As shown in these Fig.s, it can be confirmed that the two models converge to the same values, however, the processes that take place resulting in this convergence are very different. Such a large difference in convergence time may lead to an overestimation of the flow velocity, as well as an overestimation of the erosion caused by underground water. Fig. 11 (a) and 11 (b) show the water level result at fixed time similar to Fig. 9. As can be seen from these Fig.s, the water level converge immediately in the linear model, on the contrary, the water level converge gradually in non-linear model.

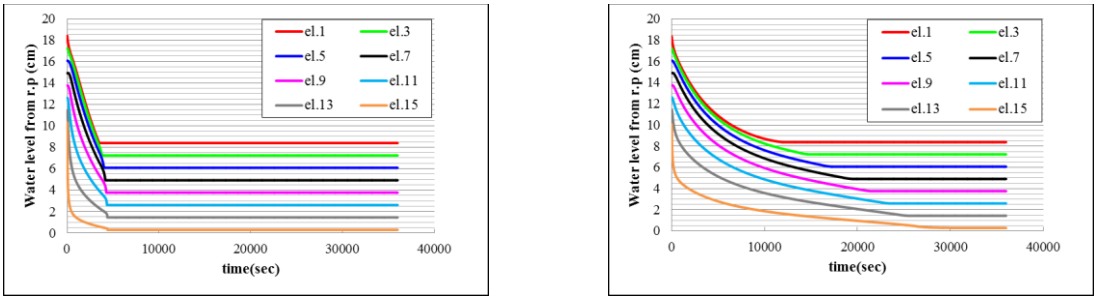

(a) Calculation using Equation (6) (b) Calculation using Equation (7)

Fig. 10. Numerical Results of Case-2

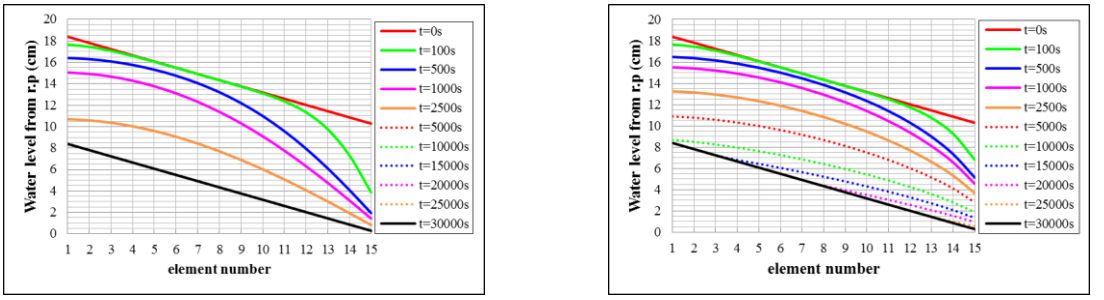

(a) Calculation using Equation (6) (b) Calculation using Equation (7)

Fig. 11. Water Level Results at fixed time of Case-2

5. Conclusion

In this study, the authors established a simulation model using the FVM in order to evaluate the foundation water flow. Since the permeability of soils such as sand is as low as 0.025 cm/s, it can be said that the quasi-uniform flow advocated by Dupuit is applicable in this case, and would make the time domain analysis simpler. According to our calculation results, we note that linear model has a faster convergence speed compared with non-linear model. Therefore, in order to avoid the overestimation of the foundation flow velocity, we recommend to adopt a non-linear assumption for the cross-sectional area of flow. Based on the knowledge obtained through this study, the authors are planning to develop a simulation model in order to evaluate the topographical erosion due to underground water flow, and then verify the simulation results by indoor experiments.

References

[1] M. Nishigaki, Y. Futami, I. Kohno, An Integrared Finite Difference Method for Seepage Analysis in Anisotropic Aquifer, Vol.26, No.3, 169-179, The Japanese Geotechnical Society, Japan, Sept. 1986

[2] N. Yasuda, M. Kawasaki, K. Murase, Y. Tomizawa, M. Amakata, Research on Groundwater Model, No.322, Technical Note of NILIM, Japam, March 2006

Available online at www.sciencedirect.com

ScienceDirect

Procedia Engineering 00 (2017) 000–000

Procedia Engineering

www.elsevier.com/locate/procedia

Sustainable Civil Engineering Structures and Construction Materials, SCESCM 2016

Shear behavior of calcium carbide residue- bagasse ash stabilized expansive soil

John Tri Hatmoko[a,*], Hendra Suryadharma[a]

[a]*Department of Civil Engineering Universitas Atma Jaya Yogyakarta, Jln. Babarsari No.44 Yogyakarta, Indonesia*

Abstract

Expansive soil is widespread all over the world, also in Indonesia. Its existence results on damage of building structures due to its low strength and high expansion. As a result, improvement of this soil is extensively investigated and continually in progress. Calcium carbide residue (CCR) is a hazardous waste produced from burning acetylene. It contains high CaO, then it is considered to be an admixture to reduce the plasticity index, expansion potential as well as to increase shear and compressive strength of expansive soil. Whereas bagasse ash (BA) is a fine residue collected from the burning of bagasse in sugar factory. This research was undertaken to improve the physical and mechanical behavior of expansive soil stabilized with CCR and BA, and it was done in two steps. The first step was the improvement of the physical and mechanical behavior of expansive clay by adding calcium carbide residue (CCR) to the original soil. The result indicates that at 8% CCR, plasticity index and potential pressure of expansive clay was significantly reduced, and unconfined compressive strength of stabilized soil increased. Then, standard compaction, unconfined compression and direct shear tests were carried out on soil + 8% CCR + bagasse ash (BA). The variation in BA was 0, 3, 6, 9, and 12%, and each specimen was cured on 7, 14, 21, 28 and 36 days of curing time. The study indicates that at 9% of BA and on 28 day-curing time, the MDD and unconfined compressive strength were significantly increased. Moreover, addition of bagasse ash on CCR soil mixture improves soil ductility.

Peer-review under responsibility of the organizing committee of SCESCM 2016.

Keywords: expansive soil; calcium carbide residue; bagasse ash; shear behavior.

* Corresponding author. Tel.: +62-0274-882326; fax: +62-0274-487748.
E-mail address: john@mail.uajy.ac.id

Peer-review under responsibility of the organizing committee of SCESCM 2016.

1. Background

Expansive soil is found in many locations in Indonesia, especially in arid areas such as Wonogiri Regency, Gunung Kidul, Purwadadi Regency, and Cikampek. It covers more than 20% of Indonesian area [1]. Its existence results in damage to building, road and bridge structures due to its low shear strength and high volume changing. Therefore, improvement of engineering characteristics of this soil is extensively investigated and continuously in progress. Cement stabilized expansive clay, for example, has been already done by some researchers [2−6]. The results indicated that addition of cement on expansive soil improves shear strength and reduces volume changing. Moreover, stabilization of expansive clay with cement mixed with fly ash, rice husk ash, and bagasse ash was done by [7−9]. The results are similar to the previous research, that is, plasticity index and volume changing decrease, and shear strength of stabilized soil improves. Even though much research about admixtures to stabilized expansive clay has been done, the finding of new materials for admixture is always in progress.

Bagasse ash is a fine residue collected from the burning of bagasse in sugar factory. The production of bagasse ash is growing according to production of sugar. Research about using of bagasse ash is continually performed. Bagasse ash is a non-cohesive material having a low specific gravity that is relatively smaller than that of normal soil. When burned, bagasse ash behaves as pozolanic material, and therefore its engineering behavior can be improved by addition of calcium carbide residue (CCR). It is hazardous waste produced from burning acetylene. It contains high CaO, then it is considered to be an admixture to reduce the plasticity index, expansion potential as well as increase shear and compressive strength of expansive soil.

Studies about the shear strength behaviour of calcium carbide residue bagasse ash stabilized soil, so far, have not been found yet. This research was then undertaken to improve the physical and mechanical behavior of expansive soil stabilized with CCR and BA, and it was done in two steps. The first step was the improvement of the physical and mechanical behaviour of expansive clay by adding calcium carbide residue (CCR) to the original soil. Then, standard compaction and unconfined compression tests were carried out on soil + 8% CCR + bagasse ash (BA). The variation in BA was 0, 3, 6, 9, and 12%, and each specimen was cured on 7, 14, 21, 28 and 36 days of curing time.

2. Literature Review

Chemical stabilization by calcium carbide residue (CCR), cement, fly ash (FA), rice husk ash (RHA), and bagasse ash, or a combination of them, is a proven technique to improve soil performance. Research on undrained compression triaxial test to study the effect of calcium carbide residue on shear strength of expansive clay was carried out by [10]. Observation about the addition of bagasse ash alone to expansive clay was done by [11]. The result indicated that both the compressive and shear strength of expansive clay did not significantly increase. The use of CCR and rice husk ash (RHA) was investigated by [12,13]. A ratio of 50% CCR: 50% RHA resulted in unconfined compressive strength of 15.6 MPa on 28-days curing time and of 19.1 MPa on 180-days curing time. Based on the research, cementation material CCR and RHA was potentially used for high strength concrete. Research of micro structure of CCR and ground fly ash (GFA) by using SEM, XRD and FTIR was done by [14]. CCR-GFA resulted from calcium silicate hydrate (C-S-H) is in the form of $Ca_5(SiO4)_2(OH)_2$, that is also found on FTIR analysis. The C-S-H was obtained from a reaction of SiO2 and Ca(OH)2 from CCR with chemical reaction similar to pozzolanic reaction. The presence of C-S-H improved the compressive strength of pasta. In general, the compressive strength of all specimens improved with the addition of curing time, and it was almost constant at 42 days. The use of CCR and fly ash (FA) as concrete admixture was done by [15]. The ratio of CCR and ground fly ash (GFA) that was used as an admixture for cement replacement was 30 : 70. The result of the research indicated that without cement, the new admixture (the mix of CCR and GFA) resulted in 28.4 and 33.5 mPa on 28 days and 90 days of curing time respectively. Concrete with CCR-GFA admixture has a longer initial and final setting time compared to that of normal concrete. In addition, CCR and fly ash can be used as a new admixture for concrete, and decreases the production of cement and environmental pollution. Investigation about the possibility of using CCR and FA to improve shear strength of silty-clay was done by [16]. Micro-mineral structure examination was done through SEM whereas shear strength was examined by performing an unconfined compression test. The result showed that the addition of CCR decreases the specific gravity, plasticity-index, MDD and OMC. The changes of shear strength was separated on three zones, namely the active, inert and deteoration zone. On the active zone, shear

strength improves due to increase of CCR for all ratio of CCR : FA. The addition of FA, however, did not significantly improve the shear strength of stabilized soil.

Research about the engineering properties of CCR stabilized silty clay was done by [17]. In the research, the CCR content required to stabilize was determined by CCR fixation point that indicates the clay's capacity to absorb Ca++ and react with $Ca(OH)_2$. Pozzolanic reaction needs the optimum moisture content because moisture contents lower than OMC are not enough to perform the reaction. The results indicate that CCR stabilized soil has a higher shear strength compared to the shear strength of lime stabilized soil. This is due to the higher content of pozzolanic material on CCR, which is around 12.3%. Moreover, the use of CCR as an admixture is better from an engineering, economic and environmental point of view. The use of RHA and CCR to improve unconfined compression strength of clay was done by [18]. Similar research was done by [19, 20]. Ratio of CCR : RHA were 30:70; 50:50, and 70:30%; however, the proposed parameter was splitting tensile strength. The results indicated that composition of 50 (CCR) : 50 (RHA) resulted in splitting tensile strength 84% higher than that of unstabilized soil.

3. Research Methods

3.1. Property Index

The property index experiment used ASTM Standard D 423-66, D 424-74, and D 427-74. In this experiment, soil stabilized samples were prepared as follows: original soil (CCR 0%), soil + CCR 2%, soil + CCR 4%, soil + CCR 6%, soil + CCR 8%, and soil + CCR 10%. Those samples were cured for 7 and 14 days to examine the change of property indices. Table 1 summarizes the samples that were examined.

Table 1. Summary of samples for property indices experiment

CCR content	Curing time (day)		
(%)	0	7	14
0	C0W0	C0W7	C0W14
2	C2W0	C2W7	C2W14
4	C4W0	C4W7	C4W14
6	C6W0	C6W7	C6W14
8	C8W0	C8W7	C8W14
10	C10W0	C10W7	C10W14

CxWy = sample with CCR content of x%, and y days curing time

3.2. Compaction Test

The compaction test was undertaken under two conditions. The first was for soil + x% CCR alone with 7, 14, 21, 28 and 36 days curing time, and the second for soil + x% CCR + bagasse ash (3, 6, 9 an 12%) with the same curing time as the previous one. A summary of samples can be seen in Table 2.

Table 2. Summary of Compaction samples (CCR = x%)

Curing time	Bagasse Content (%)				
(days)	0	3	6	9	12
0	W0T0	W0T3	W0T6	W0T9	W0T12
7	W7T0	W7T3	W7T6	W7T9	W7T12
14	W14T0	W14T3	W14T6	W14T9	W14T12
21	W21T0	W21T3	W21T6	W21T9	W21T12
28	W28T0	W28T3	W28T6	W28T9	W28T12
36	W36T0	W36T3	W36T6	W36T9	W36T12

x: CCR content resulting maximum decease of : plasticity index, potential and swelling pressure

WaTb: sample with a day curing time, bagasse ash content b% and X% of CCR

3.3. Unconfined Compression Test

The standard used in this experiment was ASTM D2850-70 and AASHTO T234-70. The purpose of this experiment was to find unconfined compression strength of original and stabilized soil. The CCR content used in this experiment was the one that resulted in the maximum decrease of plasicity index, potential and swelling pressures, as well as activity of original soil (x%). Whereas the content of bagasse ash was 0, 3, 6, 9, and 12% with 7, 14, 21, 28 and 36 days curing time. The summary of samples tested on unconfined compression is the same as that of the compaction test (Table 2).

3.4. Direct Shear Test

The specimens of direct shear test were circular with a diameter of d = 6.30 cm and a thickness of t = 2.55 cm. Two combinations were tested: soil + CCR with 28 days curing time (CxWz), and soil + CCR + bagasse ash (CxAyWz), in which x is the CCR content resulting on maximum decrease of plasticity index, potential and swelling pressure of original soil, y is the bagasse ash content resulting on maximum unconfined compression strength, and z is the curing time of 28 days. The normal stress was 28.4 ; 41.2 and 54 kPa.

4. Results and Discussion

4.1. Plasticity Index and Swelling Potential

The results of plasticity index and swelling potential experiment can be seen in Table 3. A maximum decrease of those parameters occured on 8% CCR content and 7 days curring time (C8C7) due to optimum ion reaction, i.e. Ca+2 and Mg+2 in CCR replace Na+ and K+ on expansive clay. Because of this fenomenon, the soil is siffer. Therefore the plasticity index swelling potential as well as the swelling pressure decrease. The result is in good agreement with the previous study by [21].

Table 3. Result of Plasticity Index and Swelling Potential

		Swelling Potential (%)		Swelling pressure (kPa)	
CCR(%)	I P(%)	[21]	Lab	[21]	Lab
C0W7	47.5	11.2	12.11	298	301
C2W7	41	7.8	10.4	278	286
C4W7	35	4.9	5.3	209	217
C6W7	27.4	3.6	3.9	172	181
C8W7	16.7	1.9	2.3	129	136
C10W7	16.9	0.82	2.4	98	137

4.2. Compaction Test

CCR stabilized soil compaction test was done on 8% CCR content and 0, 7, 14, 21, 28 and 36 days curing time. Table 4 is the result of this experiment. Maximum dry density (MDD) improved proportionally to the increase of curing time. On 28 days curing time, the maximum improvement of MDD occured. This is due to an ion transfer reaction that resulted in flocculation-agglomeration, causing the change of physical and mechanical properties. In addition, on 28 days curing time, pozzolanic reaction, i.e. formation of C-S-H and C-A-H, start to happen then MDD improves significantly.

Table 4. Result of CCR stabilized soil compaction

Curing time (days)	0	7	14	21	28	36
MDD (gr/cc)	14.3	15.2	16.8	17.8	18.5	18.3
OMC (%)	36	34,5	33,5	33	32	31

The CRR- Bagasse ash stabilized soil was done with 8% CCR content, and bagasse ash variation was 0, 3, 6, 9, and 12% with 7, 14, 21, 28 dan 36 days curing time. Table 5 summarizes the result of the experiment. When bagasse ash content increased, OMC decreased proprtionally to the improvement of bagasse ash. This is due to bagasse ash being not water absorbing. The MDD, however, improves due to increase of the bagasse ash content. At 6% bagasse ash content, there is significant improvement in MDD, in particular at 28 days curing time. Previous research [6] stated that the optimum ratio of bagasse ash : cement optimum is 3:4, therefore this research which result on ratio 6% bagasse ash : 8% CCR is in good agreement with the previous one.

Table 5.Summary of CCR-bagasse ash stabilized soil compaction

Curing time(days)	Content of bagasse ash (%)									
	0		3		6		9		12	
	γ (kN/m3)	wopt (%)	γ (kN/m3)	wopt (%)	γ (kN/m3)	wopt (%)	γ (kN/m3)	wopt (%)	γ (kN/m3)	wopt (%)
0	14.3	36	14.8	35	15	34	15.4	33	15.5	36
7	15.2	34.5	15.9	34	15.6	33.5	15.9	32	15.9	34.5
14	16.8	33.5	16.9	33	17.1	33	17.3	31.5	17.3	33.5
21	17.8	33	18.1	32	17.9	32.5	17.8	31	17.9	33
28	18.5	32	18.9	31	18.8	31	18.7	30	18.4	32
36	18.6	31	18.9	30	18.8	30.5	19.2	29	19.3	31

4.3. Unconfined Compression of CCR- bagasse ash Stabilized Soil

Unconfined compression experiment of CCR-bagasse ash stabilized soil was performed on MDD and OMC, 8% CCR, and various content of bagasse ash (0, 3, 6, 9 and 12%). The speciment was cylindrical, with a diameter of 6.6 cm and height of 13.7 cm. The soil sample was then statically compacted. To obtain the proposed compaction, the stabilized soil was filled in the cylinder then compacted on three layers. Table 5 shows the result of the experiment.

Table 6. Result of UCS of CCR-bagasse ash stabilized soil

Curing time (days)	Containt of Bagasse Ash (%)				
	0	3	6	9	12
0	40.2	40.9	41	41.8	42.1
7	41.2	58.5	65.3	75.1	76
14	45.3	98.2	108.8	125.9	129.6
21	52.6	156.1	170.4	227.8	235.2
28	72.1	245.6	304.5	337.9	345.9
36	74.2	250	310.8	354.7	368

Improvement of unconfined compression strength with respect to curing time occures on 0% baggase ash content; however, it is not significant. It happens significantly on 9% bagasse ash content in which unconfined compression strength without curing time is 41.8 kPa, and it improves markedly on 36 days curing time, that is 354.7 kPa. Smililarly, improvement happens on 12% bagasse ash content. However, an improvement of unconfined

compression strength from 9% to 12% bagasse ash content is not significant. With respect to curing time, a significant improvement of unconfined compression strength is shown on 21 to 28 days. After 28 days curing time, there is no significant improvement (Fig. 1).

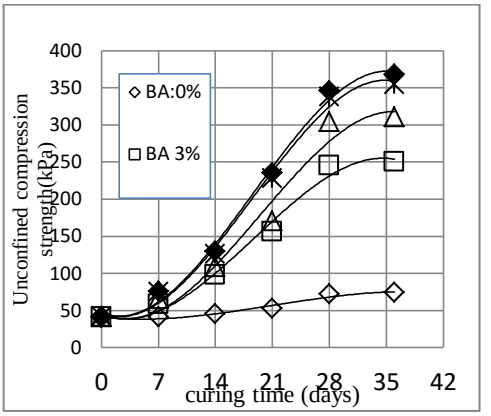

Fig. 1. UCS of CCR- bagasse ash stabilized soil

4.4. Direct Shear Test

The result of direct shear experiment of CCR-bagasse ash stabilized soil with respect to curing time is given on Table 6. When curing time increases, cohesion improves and internal friction angle decreases. However, there is still improvement of shear stress. Those penomena occur due to the the first pozzolanic reaction in which generates calcium slicate hydrate (C-S-H) and aluminum silicate hydrate (C-A-H) was totally completed, and the second pozzolanic reaction which generates calcium aluminum silicate hydrate C-S-A-H starts to happen.

Table 6. Result of Direct Shear Test

Shear Stress Parameter	C8A9W21	C8A9W28	C8A9W36
Cohesion, c (kPa)	32.15	35.5	36.4
Int. friction angle ,φ(O)	21.20	25.90	27.80

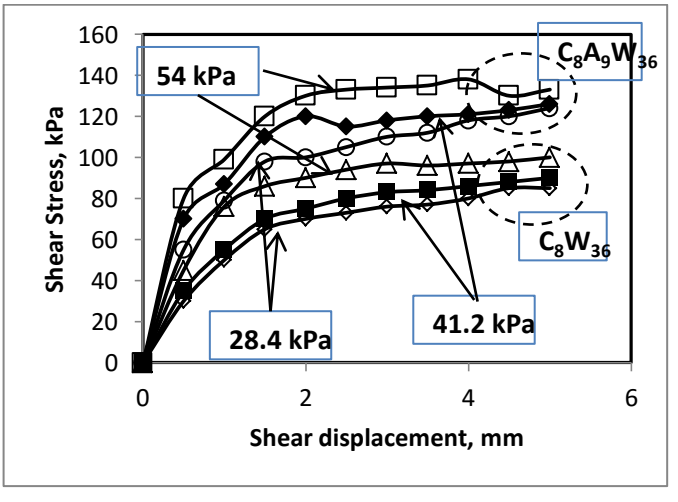

Fig. 2. Shear stress-Shear displacement of C_8W_{36} and $C8A9W_{36}$

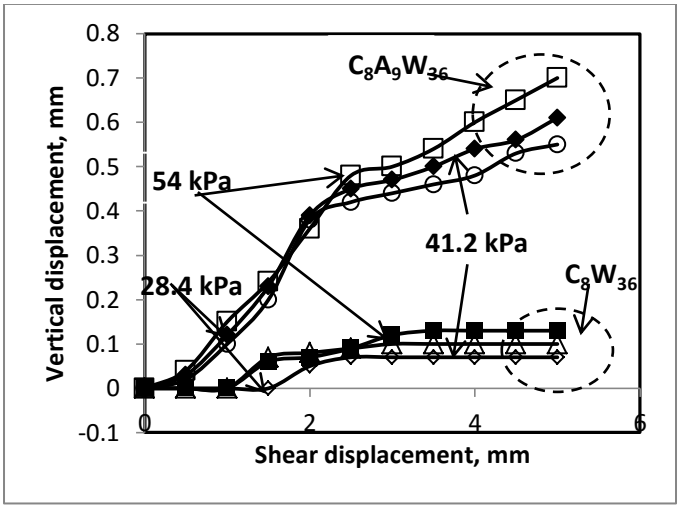

Fig. 3. Vertical displacement-Shear displacement of C_8W_{36} and $C_8A_9W_{36}$

Fig.s 2 and 3 show the variation of shear stress and vertical displacement with shear displacement of CCR stabilized and CCR bagasse ash stabilized soil specimens. The shear stress displacement behavior was influenced markedly by bagasse ash admixture. While soil specimens without bagasse ash reached their failure shear stress at displacement around 2 mm, the corresponding displacement on CCR-bagasse ash stabilized soil specimens were generaly greater than 3.5 mm. This is evidence that the addition of bagasse ash improves the ductility.

5. Conclusion

An experimental program was performed to investigate the effect of calcium carbide residue (CCR) and bagasse ash on shear strength and other geotechnical characteristics of expansive soil. The experiment was conducted on soil + CCR and soil + CCR + bagasse ash with 7, 14, 21, 28 and 36 days curing time. Conducted experiment were index properties, compaction test, unconfined compression test and direct shear test. The following conclusions are drawn from the study.

- The addition of 8% calcium carbide residue (CCR) significantly decreases the plasticity index, swelling and pressure potential of CCR stabilized soil.
- The CCR stabilized soil compaction test indicates that maximum dry density (MDD) improves proportionally to the increase of curing time, and maximum improvement occurred on 28 days.
- The addition of 6% bagasse ash to CCR-bagasse ash stabilized soil significantly improved MDD, especially on 28 days curing time.
- Significant improvement of unconfined compression strength of CCR-nagasse ash stabilized soil specimens occured on 9% bagasse ash and 28 days curing time. An increase of unconfined compression strength still occured on 36 days curing time; however, it was not significant.
- In direct shear tests, the bagasse ash increase the failure displacement and the vertical displacement of CCR stabilized soil compacted on MDD – OMC state. In addition, it increases ductility the behavior of CCR-soil specimens.

Acknowledgement

The writers are grateful for the financial support from Ministry of Research and Higher Education Republic of Indonesia for this research through Competitive Research Grant. They are also thankful to Madukismo Sugar Factory for providing the bagasse ash to complete this research.

References

[1] Wibowo , S.Y., (2011): " Perilaku Sifat Fisik dan Keteknikan Tanah Ekspansif di daerah Majalengka, Jawa Barat" *Jurnal Riset Geologi dan Pertambangan* Vol. 21 No 2 (2011), 1131-1139.

[2] Idrus (1991): " Stabilisasi pada lempung Losari dengan kapur dan semen" *Master Tesis*, Institut Teknologi Bandung

[3] Keshawarz, M.S., and Dutta, U. (1998):" Stabilization of South Texas soils with cement" *Cement for Soil Improvemen*t, ASCE, New York, pp. 33 – 42

[4] Transportation Research Board (1996):" State of the Art : Cement Stabilization, reaction, properties design and construction" *Transportation Research Circular*, Washington

[5] Hatmoko, John., T. & Lulie, Y. (2005) : "*UCS* Tanah Lempung Ekspansif yang di stabilisasi dengan Abu Ampas Tebu dan Semenr". Laporan Penelitian Universitas Atma Jaya Yogyakarta

[6] Hatmoko, J, T. & Lulie, Y. (2007) : "Perilaku Tanah Lempung Ekspansif yang di stabilisasi dengan Abu Ampas tebu & Semen di dalam alat uji Triaksial". Laporan Penelitian Universitas Atma Jaya Yogyakarta

[7] Consoli, N.C., (2001):" Behavior of *expansive soil- fly ash-cement mixture" Journal* of Geotechnical and Geo environmental Engineering, Vol. 127, No.9

[8] Mitzchell, J.K. (1996) :" The properties Cement-fly ash – stabilized soil " *Proceeding of Residential Workshop on Material and Methods for Low Cost Road, Rail and Reclamation Works*, Leura, Australia, September 1996

[9] Diane, Ch. (2001): " Stabilisasi tanah ekspansif dengan Semen dan Abu Sekam Padi" *Skripsi Sarjana*, Universitas Atma Jaya Yogyakarta.

[10] Hatmoko, J.T., dan Lulie, Y. (2006):" Perilaku geser tanah ekspansif yang distabilisasi dengan limbah karbid" *Laporan Studi* Lembaga Penelitian dan Pengabdian Masyarakat Universitas Atma Jaya Yogyakarta

[11] Hatmoko, J.T. , (2003):" Stabilisasi tanah ekspansif dengan abu ampas tebu" *Laporan penelitian hibah dosen muda* Departemen Pendidikan Tinggi Kemendikbud RI

[12] Horpibulsuk, S., and Miura, N., (2001) : A new approach for studying of behavior of cement stabilized clay: *Proceeding the 15th International Conference on soil mechanics and geotechnical engineering, vol. 3., Istanbul, Turkey, pp.1759-1762*.

[13] Horpibulsuk, S., Phetchuay, C., Chinkulkijniwat, A., (2012). "Soil Stabilization by Calcium Carbide Residue and Fly Ash". Journal of materials in Civil Engineering @ASCE, Vol.24 No.2., 184-193.

[14] Somna, K., Jaturapitakkul, C., Kajivichyanukul, P., (2011)., "Microstructure of Calcium Carbide Residue-Ground Fly Ash Paste**"**., *Journal of materials in Civil Engineering* @ASCE, Vol.23 No.3., 298-302

[15] Makaratat, N., Jaturapitakkul, C., Laosamathikul, T., (2010).,"Effect of Calcium Carbide Residue -Fly ash Binder on Mechanical Properties of Concrete". Journal of materials in Civil Engineering @ASCE, Vol.22 No.11., 1164-1170.

[16] Horpibulsuk (2013) :"Engineering properties of silty clay stabilized with calcium carbide residue ", *Journal of materials in Civil Engineering, ASCE*, Vol. 125, No.5, 470 -475.

[17] Kampala, A., Horpibulsuk, S., (2013)." Engineering Properties of Silty Clay Stabilized with Calcium Carbide Residue". *Journal of materials in Civil Engineering @ASCE*, Vol.25 No.5., 632-644.

[18] Diana, W, dkk (2012): "Kuat tekan bebas tanah lempung yang distabilissi dengan limbah karbit dan abu sekam padi", *Prosiding Konferensi Nasional Teknik Sipil ke 6*, Universitas Trisakti , Jakarta 1- 2 Nopember 2012risk husk , hal. 33-37.

[19] Diana, W, dkk (2013): "Kuat geser dan kuat tarik belah tanah lempung yang distabilisasi dengan limbah karbit dan abu sekam padi", *Prosiding Konferensi Nasional Teknik Sipil ke 7*, Universitas Sebelas Maret , Surakarta 24 – 26 Oktober 2013, hal. 69 – 75.

[20] Jaturapitakkul, C., Roongreung, B., (2003)." Cementing Material from Calsium Carbide Residu-Rice Husk Ash".*Journal of materials in Civil Engineering @ASCE*, Vol.15 No.5., 470-475.

[21] Yhalib, M., and Bankole, G,M., (2011)."Improvement of index properties and compaction characteristic of lime stabilized clays with risk husk ash admixture" Journal of Geotechnical and Geoenvironmental Engineering, Vol 16, No.8 983-996

Available online at www.sciencedirect.com

ScienceDirect

Procedia Engineering 00 (2017) 000–000

Procedia Engineering

www.elsevier.com/locate/procedia

Sustainable Civil Engineering Structures and Construction Materials, SCESCM 2016

A Study of The Effectiveness of The Use of Cement and Bottom Ash towards The Stability of Clay in terms of UCT Value

Ika Puji Hastuty[a,*], Roesyanto[b] and Jeriko B.S[c]

[a]*Department of Civil Engineering, University of Sumatera Utara, Medan, Indonesia*
[b,c]*Department of Civil Engineering, University of Sumatera Utara, Medan, Indonesia*

Abstract

Stabilisation is one of efforts in improving the condition of soil which has less good index of properties. One example of stabilisation is by adding chemicals into the soil. The chemicals commonly used are cement, lime, and asphalt. This research used the addition of cement and Bottom Ash which was waste material of the combustion of coal that was not used and harmful if disposed carelessly.This research was performed on clay without Bottom Ash mixture, and clay that has been mixed with 1% cement, 2% cement, and Bottom Ash with several percentages of variation levels of mixed materials. This research included preparatory work, laboratory testing, and analysis of the results of laboratory testing. Results that would be achieved is the effect of adding cement and Bottom Ash against Unconfined Compression Test (UCT) value on clay. The results showed that the addition of 2% cement and 9% Bottom Ash with a curing time of 14 days had the largest compressive strength of soil which was 2.69 kg/cm². The addition of 1% cement and 10% Bottom Ash with a curing time of 14 days had the largest compressive strength of soil which was 2.02 kg/cm².The use of 2% cement on clay had a compressive strength of 1.77 kg/cm², while the use of 1% cement on clay had a compressive strength of 1.61 kg/cm^2. It showed an increase in the compressive strength value with the mixture of 2% cement which was 9.62%, compared to compressive strength value with the mixture of 1% cement.

Peer-review under responsibility of the organizing committee of SCESCM 2016.

Keywords: clay, cement, Bottom Ash, soil stabilising material, UCT.

1. Introduction

In terms of engineering in general, soil is a material which consists of solid mineral granular that are not chemically bonded to each other and consists of solid particles accompanied by liquids and gases that fill the empty spaces between the solid particles. Soil is composed of grains of soil itself as well as the pore spaces filled with water and air.

* Corresponding author. Tel.: +0-000-000-0000 ; fax: +0-000-000-0000 .
E-mail address: ikapuji@gmail.com

1877-7058
Peer-review under responsibility of the organizing committee of SCESCM 2016.

Clay is very hard in dry conditions and is plastic in the medium content of water. However, at a higher level of water, clay will be cohesive and very lenient. Cohesive indicates the fact that the particles are attached to each other while plasticity is a nature which allows the form of material to be modified without changing the content or without returning to its original form and without any cracks or fragmentation.

Soil stabilisation is an attempt which is used to repair or even change the nature of basic soil with the aim that the basic soil can increase its quality and its ability of supporting capacity so it becomes safe for building constructions that will be built above it.

Clay stabilisation is conducted by using a mixture of cement and Bottom Ash in order to increase the supporting capacity of clay by improving the physical and mechanical nature of the sample of less good soil so it fulfills the technical requirement.

Bottom Ash is coal waste that is widely available in the area of Sibuluan, Tapanuli Tengah, North Sumatera. Through this research, it is expected that unused waste can be utilised as possible, thereby reducing the impact of waste on the surrounding environment. The use of cement in this research is because cement is a material that is relatively affordable and very easy to obtain. In addition, soil stabilisation using cement materials mixing ingredients is very often used in the stabilisation process (Bowles, 1993). However, the cement also has shortcomings, namely prone to cracking at high temperatures, brittle, and corrosive. Other than that, the cement production process also produces high carbon emissions waste so it is not friendly to the environment. To overcome the shortcomings and take the advantages of cement, it requires the addition of an alternative mixing ingredient. One way is to mix Bottom Ash.

Bottom Ash is solid waste which is a result of coal combustion and the numbers will continue to grow as long as the industry continues to produce. Bottom Ash is known as one of the alternative filler which is used in making concrete asphalt. From this study, it can be seen that Bottom Ash contains silica and oxide levels which are the basic mineral of cement making, so it has the nature of pozzolan. From this, it is expected that mixing cement and Bottom Ash can bind clay minerals and increase the value of supporting capacity of the clay

2. Research Methods

2.1 Research Materials

a. Soil used in the test was clay from a small town called Sipahoras, Sibuluan.
b. Mixing materials used was Bottom Ash which was obtained from PT. ASAHI Sibolga.
c. Cement used was the kind of Portland cement type I, with trademark ‘Semen Padang’ (PPC / Portland Pozzolan Cement).

2.2 Stages of Research

Methods used in this final report research were literature study, field observation, laboratory analysis at Research Institution of University of Sumatera Utara and laboratory analysis in the Laboratory of Soil Mechanic, Department of Civil Engineering, Faculty of Engineering, University of Sumatera Utara.

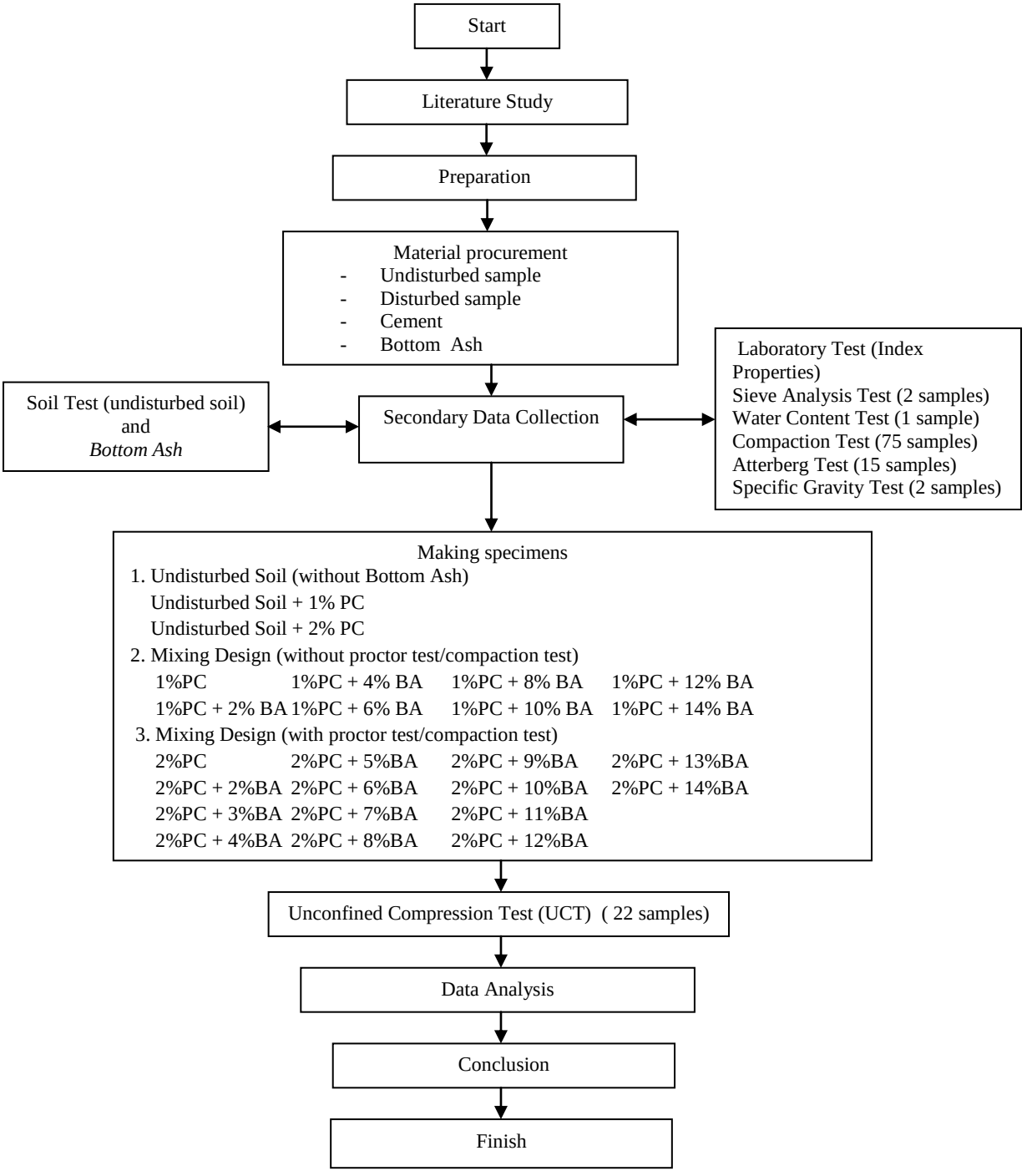

Picture 1 Research Flow Chart

3. Research Results

According to the classification system of AASHTO, data was obtained in the form of percentage of sieve analysis soil no. 200 amounted to 58.90% and the value of Liquid Limit amounted to 48.15%, then the soil sample met the requirements of >35% passing the sieve no. 200 with the minimum passing the sieve no. 200 amounted to 36%, had Liquid Limit ≥41 and Plasticity Index >11, so the sample of soil could be classified as type of soil A-7-6.

According to the classification system of USCS, the data was obtained in the form of percentage of sieve analysis soil no. 200 amounted to 58.90% and the value of Liquid Limit amounted to 48.15%. The physical test data of soil can be seen in Table 1. From this table , soil is included in the group of CL which is inorganic clay with low to medium plasticity.

Table 1. Data of Physical Nature of Soil

No.	Testing	Result
1.	Water Content	14.68 %
2.	Specific Gravity	2.66
3.	Liquid Limit, LL	48.15 %
4.	Plastic Limit, PL	13.54 %
5.	Plasticity Index, PI	34.61 %
6.	Percentage of sieve analysis soil no. 200	58.90 %

According to the classification system of USCS, the data was obtained in the form of percentage of sieve analysis soil no. 200 amounted to 58.90% and the value of Liquid Limit amounted to 48.15%, so the plot is carried out on the determination of soil classification graph which is shown in Figure 1. From the plot results, it is obtained that soil is included in the CL group which is inorganic clay with low to middle plasticity.

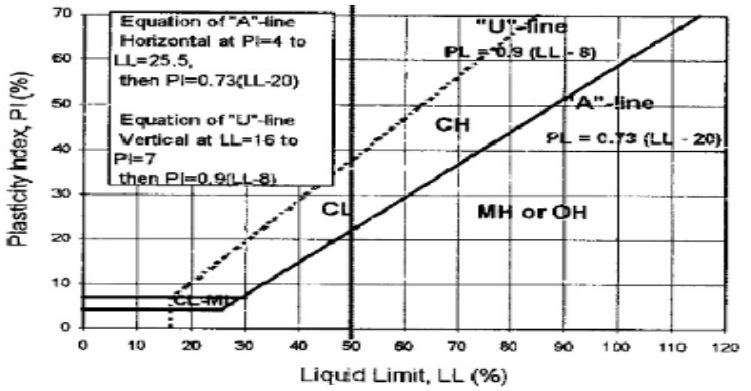

Figure 1. USCS Classification Graph Plot

3.1. The Value results of Liquid Limit (LL, Plastic Limit (PL), and Plastic Index (PI)

Following is the results of Atterberg testing where the value of Liquid Limit is shown in graph 1.A. The test results for the disturbed clay with a mixture of 2% cement without the addition of Bottom Ash resulted in a decrease of the liquid limit amounted to 46.09% against the liquid limit test results of undisturbed soil samples.

For disturbed soil samples with a mixture of 2% cement and the addition of content variation of Bottom Ash mixture, the result obtained showed that the value of liquid limit in addition of Bottom Ash declined gradually.

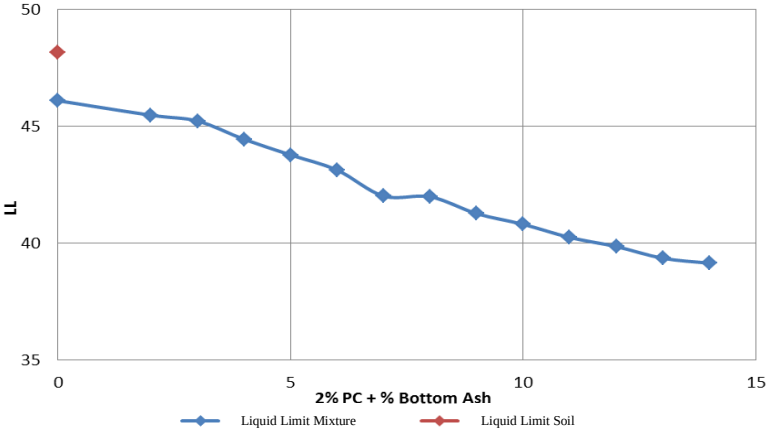

1.A

The value of Plastic Limit in graph 1.B showed that the test results for the disturbed clay with a mixture of 2% cement without the addition of Bottom Ash rose in terms of plastic limit amounted to 15.04% against the liquid limit test results of undisturbed soil samples. For disturbed soil samples with a mixture of 2% cement and the addition of content variation of Bottom Ash mixture (2%, 3%, 4%, 5%, 6%, 7%, 8%, 9%, 10%, 11% , 12%, 13%, 14%), the result obtained showed that the value of plastic limit has also increased significantly.

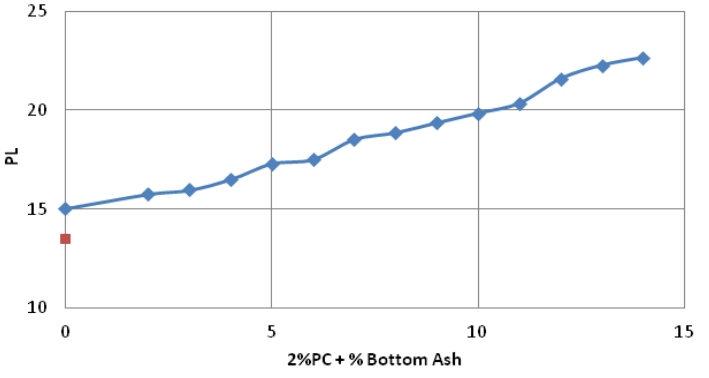

1.B

The value of Plastic Index in graph 1.C showed that the test results for disturbed clay with a mixture of 2% cement without the addition of Bottom Ash resulted in a decrease of the plasticity index value on undisturbed soil samples. For disturbed soil samples with a mixture of 2% cement and the addition of content variation of Bottom Ash mixture showed that the plasticity index value in the addition of 2% Bottom Ash decreased with value amounted to 31.05%, as well as plasticity index value of % mixture variation of Bottom Ash also decreased.

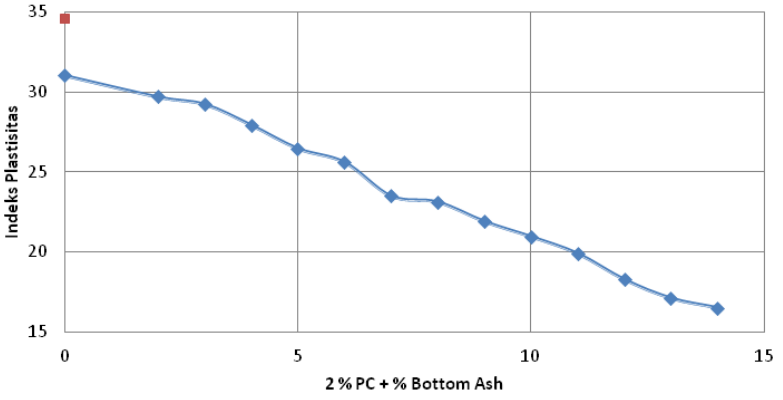

1.C

3.2 Graphs of Compaction Testing Result

From the test results of soil compaction on original soil, the optimum value of water content of soil was obtained amounted to 20.00%. Graph 2.A showed that the optimum value of water content in the soil with a mixture of 2% cement and % variations of Bottom Ash decreased until it reached the minimum water content in the mixture of 9% Bottom Ash, but then increased started from 10% Bottom Ash to 14% Bottom Ash.

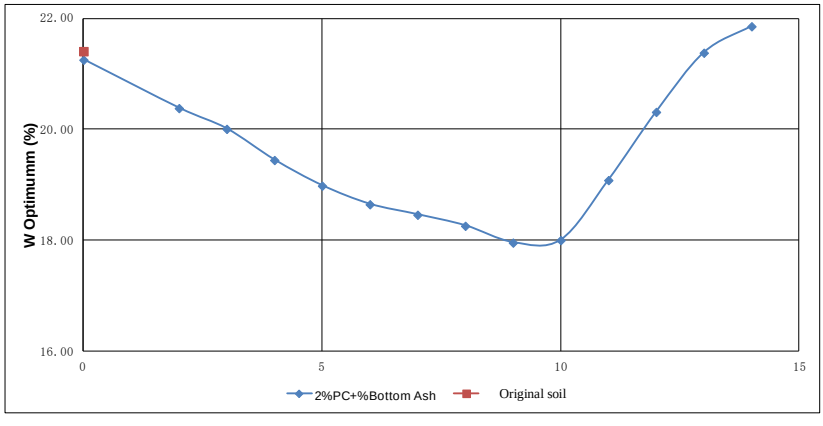

Graph 2A.The Graph of Relationship Between Optimum Water Content in Soil (Wopt) and % Variations of Bottom Ash

From the test results of soil compaction on original soil, dry bulk density values of soil was obtained amounted to 1.299 g/cm³. Graph 2.B showed the maximum value of dry bulk density of the soil which was mixed with 2% cement without Bottom Ash mixture increased to 1.322 g/cm³. And for mixture sample of 2% cement and the variation of 2% Bottom Ash had an increase in term of dry bulk density until it reached a maximum in a mixture of 9% Bottom Ash, then the dry bulk density decreased starting from a mixture of 10% Bottom Ash to 14% Bottom Ash.

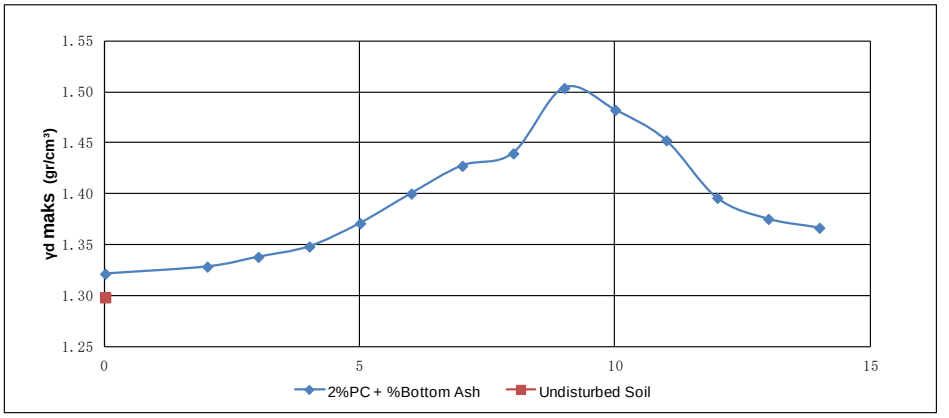

Graph 2.B. The Graph of Relationship between Maximum Dry Weight volume (γd maks) of Original Soil and Mixed Variation % Bottom Ash

Graph 2.C showed that the highest value of free compressive strength test was in the mixture of 9% Bottom Ash. For the testing of 1% PC + % variation of Bottom Ash, the optimum water content was used from the compaction testing results in 9% Bottom Ash.

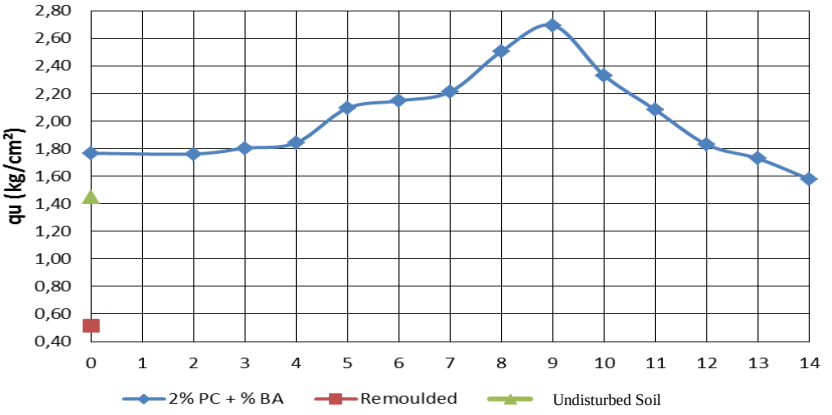

Graph 2.C. The Graph of Relationship between Soil Compressive Strength Value (q_u) and Mixed Variations of Bottom Ash

3.3 The Graph of Unconfined Compressive Strength Testing Result

From the testing result, it was obtained that the value of unconfined compressive strength of the original soil amounted to 1.45 kg/cm², while the remoulded soil amounted to 0.51 kg/cm². Graph 3.A shows a comparison between soil compressive strength (qu) with the addition of 2% PC and 1% PC with content variation of the addition of Bottom Ash. Soil compressive strength which used 2% PC had maximum value of 9% ash content which was 2.69 kg/cm², while the use of 1% PC had the highest compressive strength value when added with 10% Bottom Ash which was 2.02 kg/cm². From these trials, it was also obtained a comparison of compressive strength between original soil with 2% PC and original soil with 1% PC, the result was original soil with 2% PC had 1.77 kg/cm² compressive strength value, 9.62% higher than 1% PC which was 1.61 kg/cm.

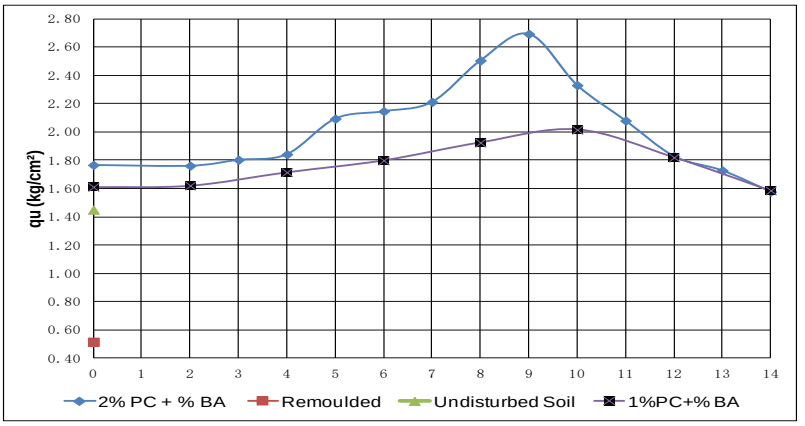

Graph 3.A. The Graph of Relationship Between Soil Compressive Strength Value (qu) 1% PC and 2% PC Variations in Bottom Ash Mixture

4. Acknowledgements

Financial support for the research was provided by University of Sumatera Utara, Medan.

References

[1] Bowles, J. E. 1984. Physical and Geotechnical Properties of Soil. United States of America: McGraw-Hill, Inc
[2] Fadilla, N. 2013**.** The Stability of Clay in Terms of UCT Value Used the Addition of Cement and Fly Ash. Civil Engineering, University of Sumatera Utara, Medan.
[3] Coal Bottom ash /Boiler Slag-Material Description, 2000.
[4] David, M.W. 1990.Soil Behaviour and Sritical State Soil Mechanics, Cambridge University Press.

Available online at www.sciencedirect.com

ScienceDirect

Procedia Engineering 00 (2017) 000–000

Procedia Engineering

www.elsevier.com/locate/procedia

Sustainable Civil Engineering Structures and Construction Materials, SCESCM 2016

Effect of clay core configuration of the rock fill dams against hydraulic fracturing

Didiek Djarwadi[a]*, Kabul Basah Suryolelono[b], Bambang Suhendro[b], Hari Christady Hardiyatmo[b]

[a]*Engineering Division, PT Pamapersada Nusantara, Jakarta 13930, Indonesia*
[b]*Professor, Civil and Environmental Department, Engineering Faculty, Gadjah Mada University, Yogyakarta 55281, Indonesia*

Abstract

Hydraulic fracturing occurred in Hyttejuvet dam in Norway during its first impounding. The water containing soil particle was emerging from the downstream toe of the dam. The water level on the reservoir was then lowered in order to reduce the potential of failure. Further investigation indicated that the clay core configuration was the main caused of the hydraulic fracturing to occur. The clay core material was moraine till soils. Due to the pore water pressure dissipation in the core was very slow, the upstream slope was steepened. This practice increased the arching effect and load transfer between embankment zones.

This paper studies the effect of clay core configuration on the rock fill dams against hydraulic fracturing using numerical analysis. The configuration of the Hyttejuvet dam was analyzed using finite element method. Couple analyses between stress & deformation and seepage analyses were used. The stress and deformation during construction was then used as initial stress in the couple analysis with increasing water in the reservoir. When the effective vertical stresses in the upstream face of the clay core was less than the water pressure in the reservoir, hydraulic fracturing will occur. In order to investigate the effects of clay core materials in the analyses, the clay core material was replaced by clay core materials used in 5 major dams in Indonesia The variation of the clay materials were made in the 6 different fine contents. There were 30 variations of the clay core materials were analyzed.The results indicated that hydraulic fracturing was still occurred in the relatively same locations, event the clay core materials were replaced by 30 variations. The analyses results indicated that the configuration of clay core of the rock fill dam strongly influence to the hydraulic fracturing.

Peer-review under responsibility of the organizing committee of SCESCM 2016.

Keywords: hydraulic fracturing; clay core configuration; arching effect; numerical analysis

* Corresponding author. Tel.: +62-811-289602; fax: +62-21-4601916.
E-mail address: d.djarwadi@yahoo.com

Peer-review under responsibility of the organizing committee of SCESCM 2016.

1. Introduction

Hydraulic fracturing may occur in the upstream face clay core of the rock fill dam in case the vertical effective stress in the core is reduced to levels that are small enough to allow tension fracture to occur. Pore water pressure in the core will also increase during impounding, and this will further reduce the effective stresses in the core. Wedging due to water pressure may crack the upstream face of the clay core. The arching effects may reduce the vertical effective stresses in the clay core to smaller than the overburden pressure. Arching effect on the clay core of the dam occurs due to the slope of the abutment foundations, stiffness of the embankment materials, and configuration of the clay core. Abutment with slope of 1V: 0.5H reduced the total stress measured to only 52% of its overburden pressure, while on the abutment slope of 1V: 0.85H, the total stress reduced to only 74% [1]. Holle and Harspranget dams in Norwegia were reported that the total stress only 50% of their overburden pressure [2]. The possibility of hydraulic fracturing on the rock fill dams due to load transfer between embankment zones has been analyzed and reported [3]. Widening of base of the upstream filter may reduce the arching effect and reduce the risk of hydraulic fracturing on the rock fill dams [4]. Statistical analysis on rock fill dams with central core which experience hydraulic fracturing has been studied [5], they concluded that the dams with ratio of height of the dam (H) against base width of the clay core (W) at (H/W >2) were much more likely will experiencing with hydraulic fracturing, while if (1 < H/W < 2) were more likely will experiencing with hydraulic fracturing. Hydraulic fracturing on rock fill dams did not influenced by longer time in construction period which allow the greater consolidation, and slower in impounding rate which allow the wetting and development of the flow-net [6]. The influence of arching effect to the hydraulic fracturing of rock fill dams were analyzed [7], and found that the increasing of the stiffness in the filter or clay core and widening the base width of the clay core will reduce the arching effect. All the studies mentioned above lead to the conclusion that the cause of hydraulic fracturing in the rock fill dams mainly due to the arching effect.

Crack developed in upstream face of the clay core due to hydraulic fracturing may create seepage and then piping in the clay core. The incident in Hyttejuvet dam in Norway when an unexpected leakage occurred during the first filling of the reservoir was due to hydraulic fracturing [8]. Similar incidents for the unusual leakage occurred just before the reservoir became full during the initial filling of Balderhead dam in England [9]. The failure of Stockton and Wister dams in USA were suspected due to hydraulic fracturing [10]. An investigation to the leakage that occurred at Viddalsvatn dam in Norway indicated that hydraulic fracturing might be the cause [11].

This paper study the effect of the clay core configuration against hydraulic fracturing. The case of Hyttejuvet dam which experiencing hydraulic fracturing was adopted, since the configuration of the clay core was unusual. The slope of the upstream and downstream of the clay core was not same. The typical cross section of the Hyttejuvet dam is shown in Figure 1 [8].

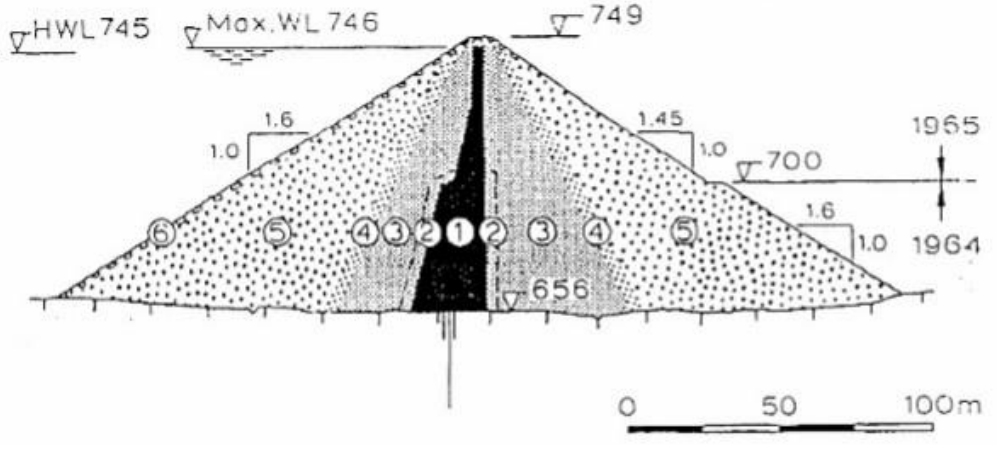

Fig. 1. Typical cross section of the Hyttejuvet dam [8].

The clay core of the Hyttejuvet dam was moraine till. The downstream slope of the clay core was vertical, while in the upstream the slope approximately was 2V : 1H. Hyttejuvet dam was constructed within 2 consecutive years. In the first year construction had reached elevation +700 m, and it's found that the pore water pressure dissipation in the clay was very slow. In order to accelerate the pore water pressure dissipation, the configuration of the upstream slope clay core was revised to be thinner and steeper. Hydraulic fracturing occurred in the first reservoir filling, when the water level of the reservoir has reached its normal elevation. The investigation by boring confirmed that the erosion had occurred in the clay core at the elevation between +717m up to +740m at the point where hydraulic fracturing occurred.

In this paper, the focus is drawn in the investigation of the clay core configuration. In case the clay core of the Hyttejuvet dam replaced by soil materials which have different engineering properties but in the similar configuration, did the hydraulic fracturing will still occurred. In case the hydraulic fracturing was not occurred, it can be concluded that the clay core configuration was not sensitive to the hydraulic fracturing. But if the hydraulic fracturing still occurred even the engineering properties of the clay core were changed, the clay core configuration was sensitive to the hydraulic fracturing.

2. Analyses method

Analyses of hydraulic fracturing were carried out using finite element method. Couple analysis between deformation & stress, and seepage was adopted [12, 13, 14, and 15]. The final stresses obtained from construction period were used as initial stresses during impounding period. This method was adopted considering that the hydraulic fracturing recorded mostly occurred on the first reservoir filling.

The selection of soil model on the stress and deformation analyses is very important. The soil model shall represent the actual condition and control the accuracy of calculation result's. In the dam construction, the embankment materials were compacted layer by layer to form the final dam configuration. In this case the non linear elastic hyperbolic soil model suits the embankment process. In the non linear elastic hyperbolic soil model, the elastic modulus was formulated as function of the confining pressure, so at every loading step the magnitude of the elastic modulus will be increased accordingly. The high order elements which consist of 8 nodal points of quadrilateral and 6 nodal points of triangular were used in the element discretization. The embankment dam modeled in 14 step loadings to represent the construction time of Hyttejuvet dam which reported in 520 days within 2 consecutive years. Figure 2 shows the element discretization of the Hyttejuvet dam.

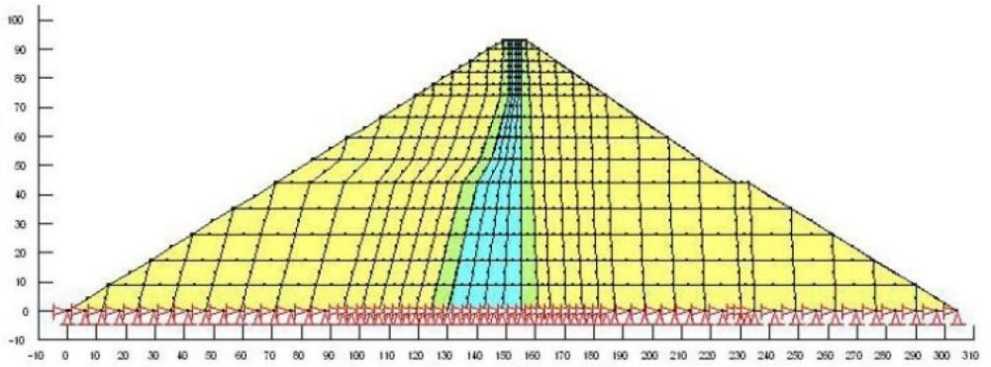

Fig.2. Element Discretization of Hyttejuvet dam.

The numerical analysis of hydraulic fracturing using finite element method was carried out in two steps. The first step, stress and deformation analysis was carried out to model the dam in the embankment process. The second step, using the final stresses obtained in the first step as an initial stresses in the couple analyses between deformation & stress, and seepage was carried out. The vertical effective stresses on the upstream face of the clay core from couple analyses comparing with the tensile stress at failure of the clay core material from hydraulic fracturing test in the laboratory. The evaluation of hydraulic fracturing on the upstream face of the clay core described as follows;

- The vertical effective stresses along upstream face of the clay core obtained from couple analysis (σ_y') compared to the hydraulic pressure due to the maximum water level in the reservoir (σ_w),
- In case the vertical effective stresses at certain points less than the hydraulic pressure ($\sigma_y' < \sigma_w$), the tension stress were occurred at those points,
- In the case the tension stresses at certain points less than the tensile stress at failure obtained from the hydraulic fracturing test at the laboratory, there were no hydraulic fracturing may occurred,
- In the case the tension stresses at certain points greater than tensile stress at failure obtained from the hydraulic fracturing test at the laboratory, the hydraulic fracturing may occurred at those points [16].

3. Materials

The materials used in the preliminary attempt of hydraulic fracturing analyses of the Hyttejuvet dam model were developed from the gradation of the Hyttejuvet dam for clay core and filter. Figure 3 shows the gradation of the embankment materials of the Hyttejuvet dam [8].

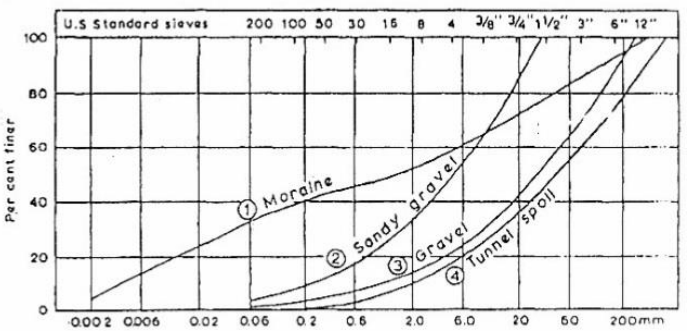

Fig. 3. The gradation of the embankment materials of Hyttejuvet dam [8].

In the preliminary attempt, the clay core material was obtained from borrow pit of Batubulan dam, and filter was river sand, both from Indonesia. The gradations were modeled based on original gradation of Hyttejuvet dam. The shear strength parameters of the clay core and filter were obtained from triaxial unconsolidated-undrained test results, while hyperbolic parameters were calculated using method developed by Duncan et al [17]. The clay core material and filter were compacted at their optimum moisture contents. The soil model for rock fill embankment materials was linear-elastic [18]. Table 1 shows the hyperbolic and shear strength parameters for clay core and filter, while Table 2 shows the parameters of the rock fill materials.

Table 1. Hyperbolic and shear strength parameters of clay core and filter.

Material	Hyperbolic parameters						Shear strength		Unit Weight
	K	n	K_{ur}	K_b	m	R_f	ϕ (°)	C (kPa)	γ_b (kN/m^3)
Clay Core	316.87	-0.116	380.44	181.74	-0.07	0.828	20.91	74.60	18.38
Filter	659.32	0.519	727.09	377.62	0.282	0.712	43.30	0	19.63

Notation: K was loading modulus number, n & m were modulus exponent, K_{ur} was unloading modulus number, K_b was bulk modulus number, R_f was failure ratio, ϕ was internal angle of friction, c was cohesion, and γ_b was bulk density.

Table 2. Parameters for rock fill

Material	Elastic Modulus (kPa)	Poisson Ratio	Unit Weight (kN/m^3)
Rock Fill	50.000	0.30	22.00

The hydraulic fracturing analysis on the Hyttejuvet dam indicated that the location of arching effects which leads to hydraulic fracturing was similar to the actual location of hydraulic fracturing [8], there was at elevation +718 to +740 m. Figure 4 show the plotting of the vertical effective stress and hydraulic pressure from the reservoir along the upstream face of clay core.

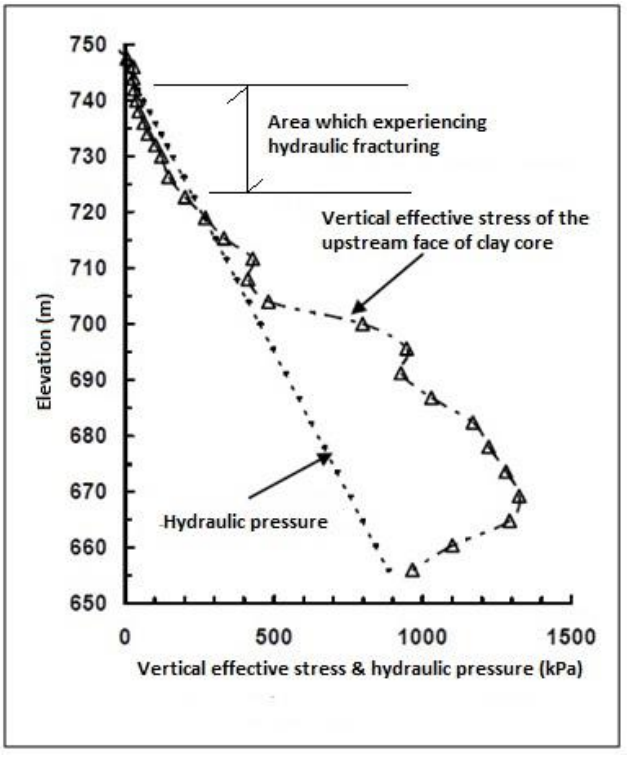

Fig. 4. Position of the hydraulic fracturing occurred on the Hyttejuvet dam.

Since in the preliminary attempt give a good accuracy in the analysis, the similar method then was used in the analysis with various geotechnical properties of the clay core. The clay core materials used in the next analysis were obtained from the borrow pits of five major dams in Indonesia, they are; Batubulan, Batutegi, Pelaparado, Sermo and Wonorejo dam. The clay core materials were tropical residual soils, and have different engineering properties with moraine which used in Hyttejuvet dam. In order to obtain the variety of the clay core properties, a variation in the percentage of fine contents (ϕ < 0.074mm) at around 30%, 40%, 50%, 60%, 70% and 80% were made. The hyperbolic and shear strength of the clay core materials used in the hydraulic fracturing analyses on the modeled Hyttejuvet dam were summarized in Table 3.

Table 3. Hyperbolic and shear strength parameters of the clay core materials at their variations.

	Fine Content	Hyperbolic parameters						Shear strength		Unit weight
	(%)	K	N	K_{ur}	K_b	m	R_f	ϕ (°)	C (kPa)	γ_b (kN/m^3)
Batubulan	30.14	357.02	-0.116	428.43	229.56	-0.089	0.92	18.15	78.20	18.38
	40.12	332.95	-0.033	399.54	185.03	-0.036	0.97	17.71	85.10	18.48
	50.24	329.93	0.072	395.92	180.00	0.064	0.95	16.21	88.30	18.55
	60.21	277.24	0.182	332.69	173.00	0.086	0.96	14.31	90.10	18.73
	70.27	261.65	0.245	313.26	145.17	0.145	0.91	13.35	95.50	18.80
	81.30	212.41	0.329	254.89	112.29	0.163	0.94	11.46	103.70	18.89
Batutegi	30.59	428.16	-0.231	513.79	318.21	-0.255	0.83	24.49	62.40	20.16
	40.31	389.15	-0.120	466.98	256.62	-0.160	0.87	23.51	72.40	20.28
	50.25	364.64	0.054	437.57	244.63	-0.091	0.88	21.87	76.00	20.10
	59.24	308.48	0.133	370.17	181.92	0.045	0.90	19.31	80.10	19.50
	72.37	273.07	0.242	327.68	163.58	0.081	0.88	18.29	84.30	19.35
	79.60	231.28	0.356	277.54	124.68	0.168	0.94	17.55	88.80	18.84

Table 3 continued

	30.84	369.96	-0.160	433.95	278.23	-0.247	0.94	22.22	72.00	19.80
Pelaparado	40.71	332.43	-0.081	398.95	242.05	-0.188	0.93	20.63	74.70	19.77
	50.60	280.64	0.095	330.77	190.81	-0.081	0.93	18.64	83.50	19.47
	60.28	268.21	0.256	321.85	170.89	-0.037	0.93	15.29	89.70	19.25
	70.40	235.59	0.281	282.71	135.07	0.066	0.92	14.70	90.30	18.95
	79.44	227.11	0.305	272.53	129.80	0.123	0.95	13.21	98.20	19.19
Sermo	30.17	289.17	-0.143	347.80	243.60	-0.215	0.88	18.74	76.00	18.43
	40.17	265.53	-0.046	318.64	218.20	-0.161	0.90	17.26	79.00	18.18
	47.68	238.13	0.028	285.76	165.46	-0.053	0.87	17.31	86.30	17.86
	60.38	222.49	0.073	266.99	156.82	-0.033	0.93	14.32	93.50	18.08
	69.95	180.03	0.164	216.04	136.26	0.068	0.93	12.51	94.80	17.89
	80.15	160.15	0.236	192.18	121.38	0.133	0.90	10.62	108.70	18.15
Wonorejo	30.26	348.02	-0.129	417.12	283.81	-0.238	0.92	19.20	72.70	19.22
	40.23	331.99	-0.069	398.39	274.23	-0.182	0.96	17.91	74.70	19.14
	50.14	278.22	0.011	333.86	235.96	-0.120	0.90	15.70	81.00	18.91
	61.68	264.20	0.067	317.04	219.74	-0.077	0.94	18.04	90.40	18.91
	70.26	189.35	0.229	227.22	142.85	0.068	0.95	14.10	97.40	18.46
	80.50	132.46	0.383	158.95	107.36	0.169	0.90	13.98	100.50	18.29

The total number of analyses was 30 samples, obtained from 5 clay core materials used in major rock fill dams in Indonesia, and 6 variations of fine contents at around 30%, 40%, 50%, 60%, 70% and 80%. The variations engineering properties in hyperbolic, shear strength parameters and unit weight enhanced the interpretation of the analyses results. Hyttejuvet dam's core configuration was unusual, since the slope at the upstream face of the clay core change 4 times from the bottom to the top of the dam, while on the downstream the clay core was vertical. Steeper slope of the core will create greater arching effect in the core. The greater arching effect will increase the possibility of the hydraulic fracturing in the clay core.

The analyses results from Hyttejuvet dam model with clay core materials from Batubulan, and Batutegi dams are shown in Figure 5, the analyses results for Pelaparado and Sermo dams are shown in Figure 6, while the analyses results from Wonorejo dam is shown in Figure 7.

All the analyses results whether from Batubulan, Batutegi, Pelaparado, Sermo and Wonorejo dams with their variations in fine contents indicated the similar results. Hydraulic fracturing occurs at mostly same locations, there are from elevation +718m up to +740m.

The analyses results indicated that the clay core configuration of the rock fill dams was sensitive to the hydraulic fracturing. These analyses results also conform to the statistical analyses [5], that the dams with ratio of height of the dam (H) against base width of the clay core (W) more than 2 (H/W >2) were much more likely experiencing hydraulic fracturing.

4. Conclusion

The numerical analyses of hydraulic fracturing using finite element method by coupling the stress & deformation and seepage analysis to investigate the effects of the slope of the upstream clay core and the height of the rock fill dam has been presented. The conclusions are summarized as follows;

- The clay core configuration of the rock fill dams are sensitive to the hydraulic fracturing due to the arching,
- The steeper upstream slope of the clay core tends to create greater arching on the upstream face of the clay core,
- It was confirmed that the dam which have ratio of height of dam (H), against base width of the clay core (B) at the ratio (H/B > 2) was much more likely experiencing hydraulic fracturing.

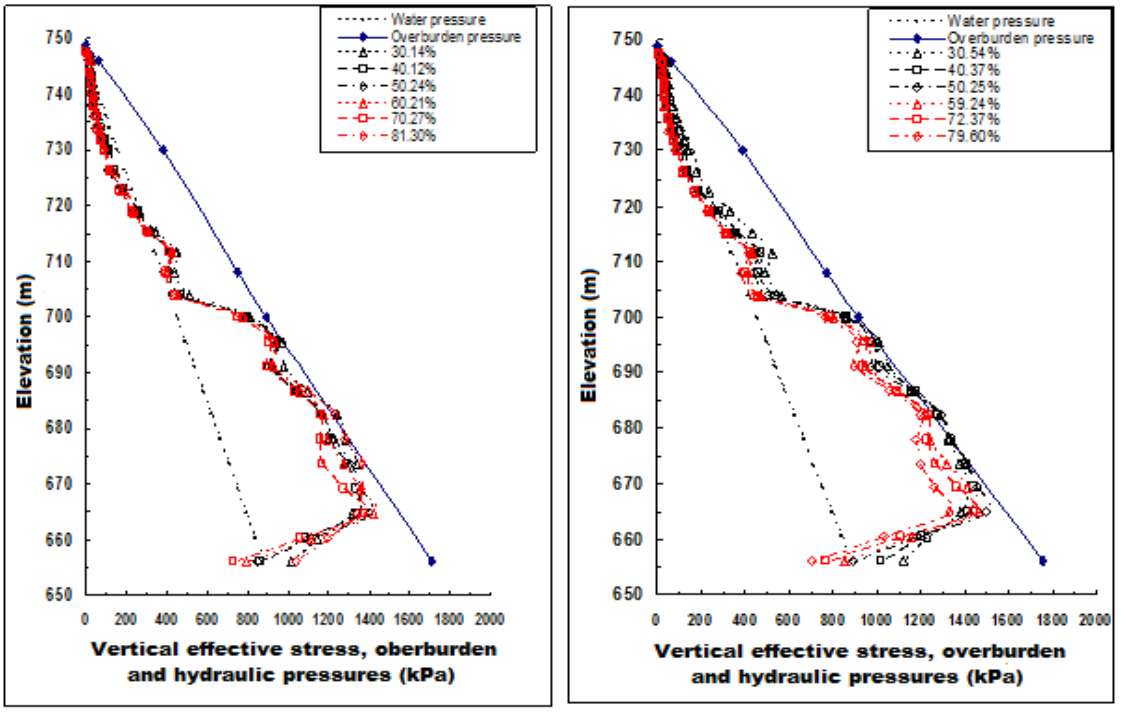

Batubulan dam Batutegi dam

Fig. 5. Position of hydraulic fracturing on Hyttejuvet model dam with clay core materials from Batubulan andBatutegi dam.

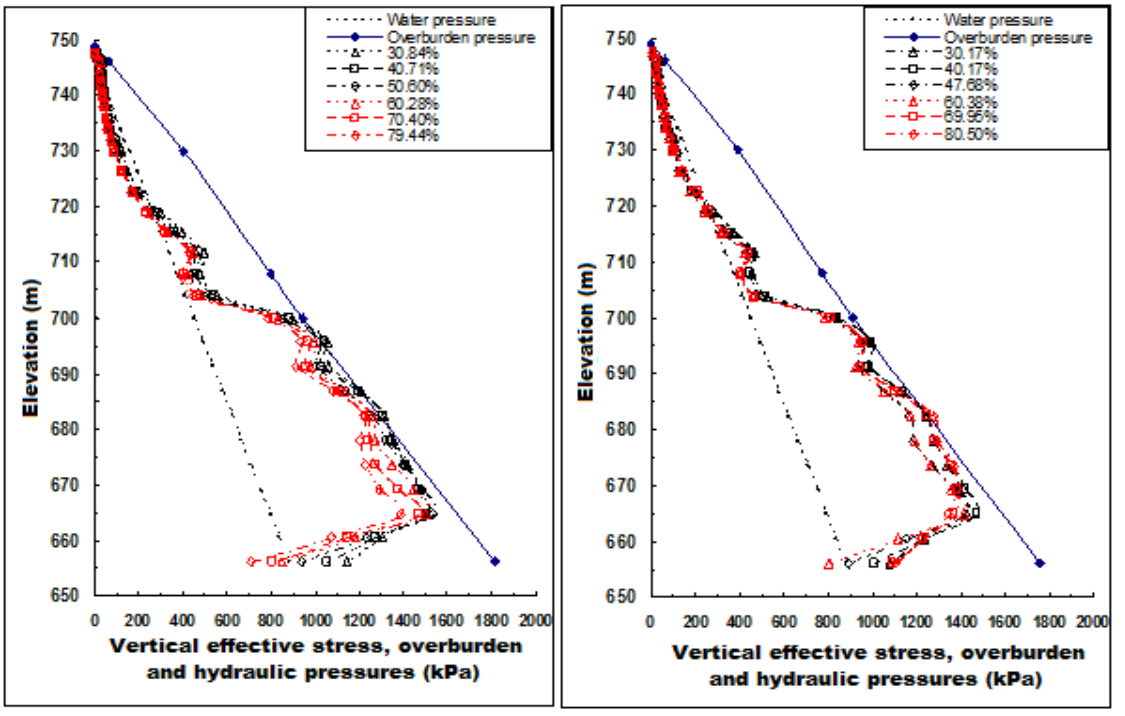

Pelaparado dam Sermo dam

Fig. 6. Position of hydraulic fracturing on Hyttejuvet model dam with clay core materials from Pelaparado and Sermo dam.

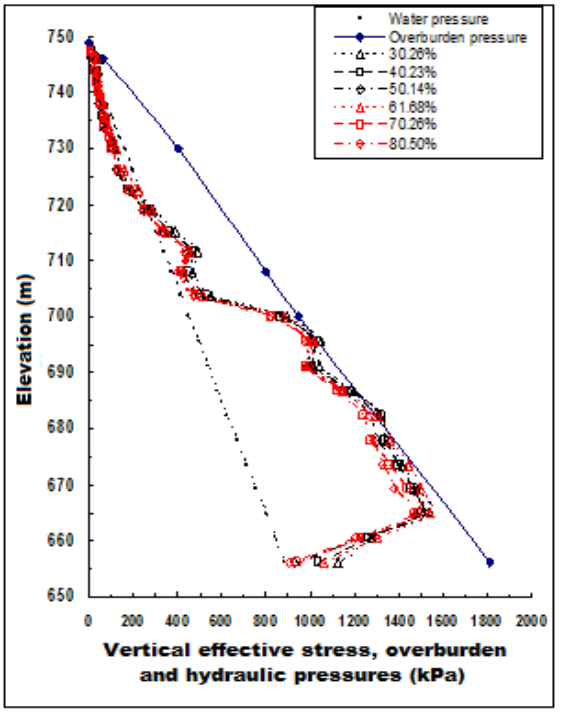

Wonorejo dam

Fig. 7. Position of hydraulic fracturing on Hyttejuvet model dam with clay core materials from Wonorejo dam.

References

[1] L. Zhang, J Du, Effects of abutment slopes on the performance of high rockfill dams. Canadian Geotechnical Journal Vol 34. No. 4. 1997, pp. 489-497.

[2] B. Loftquist, Earth pressure in a thin impervious core. Transaction of 4th International Congress on Large Dams, New Delhi, Vol 1, 1951, pp. 99-109.

[3] F. H. Kulhawy, T. M. Gurtowsky, Load transfer and hydraulic fracturing in zoned dams. Journal of Soil Mechanics and Foundation Engineering. ASCE. Vol.102. No. GT9, 1976, pp. 963-974.

[4] D. Djarwadi, K. B. Suryolelono, B. Suhendro, H. C. Hardiyatmo, Dimension effects of upstream filter of rock fill dam against hydraulic fracturing. Proceedings of the 3rd European Asian Civil Engineering Forum (EACEF) Yogyakarta, 2011, pp. G35-G40.

[5] R. Fell, C. F. Wan, M. Foster, Methods for Estimating the Probability of Failure of Embankment Dams by Internal Erosion and Piping through the Embankment. Uniciv Report R-428, 2004. University of New South Wales. Australia. ISBN: 85841 395.7.

[6] K. Y. Lo, K. Kaniaru, Hydraulic fracture in earth and rockfill dams. Canadian Geotechnical Journal. Vol. 27. No.4, 1990, pp. 496-506.

[7] J. Zhu, J.J. Wang, Investigation to arch action and hydraulic fracturing of core rockfill dam. Proceedings of the 4th International Conference on Dam Engineering. New Development in Dam Engineering. Nanjing, 2004. Taylor & Francis, pp. 1171-1180.

[8] B. Kjaernsli, I. Torblaa, I, Leakage through horizontal cracks in the core of Hyttejuvet dam. Norwegian Geotechnical Institute. Publication no. 80, 1968, pp. 39-47.

[9] J. L. Sherard, Embankment Dam Cracking. In Embankment Dam Engineering-The Casagrande Volume. New York. 1973. John Wiley & Sons.

[10] P. R. Vaughan, D. J. Kluth, M. W, Leonard, H. M. M, Pradoura, Cracking and Erosion of the Rolled Clay Core of Balderhead Dam and the Remedial Works Adopted for Its Repair. Transactions of Tenth International Congress on Large Dams. Montreal (3), 1970. pp.73-93.

[11] H. Vestad, Viddalsvatn Dam, a History of Leakages and Investigations. Transactions of Twelfth International Congress on Large Dams. Mexico. Vol 2, 1976, pp. 369-390.

[12] S. Cavounidis, K. Hoeg, Consolidation during construction of earth dams. Journal Geotechnical Engineering Division. ASCE. Vol 103. No 10, 1977, pp. 1055-1067.

[13] D. J. Naylor, D. J. Kinght, D. Ding, Coupled Consolidation Analysis of Construction and Subsequent Performance of Monasavu Dam. Journal of Computers and Geotechnics. No 6, 1988. pp. 95-129.

[14] E. E. Alonso, F. Battlle, A. Gens, A. Lloret, A. Consolidation Analysis of Partially Saturated Soil, Application to Earth Dam Construction. Proc 6th Intl Conf on Numerical Methods in Geomechanics. Innsbruck. Vol 2. 1988. pp. 1303-1308.

[15] K. L. A, Ng, J. C Small, J. C, A case study of hydraulic fracturing using finite element. Canadian Geotechnical Journal. Vol 36. 1999. pp. 861-875.

[16] D. Djarwadi, Analyses of hydraulic fracturing of the clay core of the rockfill dams on the various fine contents. PhD thesis. Gadjah Mada University. Yogyakarta. 2010. Indonesia (in Indonesian).
[17] J. M. Duncan, P. Byrne, K. S. Wong, P. Mabry, Strength, stress strain and bulk modulus parameters for finite element analysis of stress and movements in soil masses. Report no. UCB/GT/ 80-01. Dept of Civil Engineering. University of California. Berkeley. 1980. USA.
[18] S. W. Covarrubias, Cracking of earth and rock fill dams. PhD thesis. Harvard University. Cambridge. Massachusetts. 1969.

Available online at www.sciencedirect.com

ScienceDirect

Procedia Engineering 00 (2017) 000–000

Procedia Engineering

www.elsevier.com/locate/procedia

Sustainable Civil Engineering Structures and Construction Materials, SCESCM 2016

Back calculation of excessive deformation on deep excavation

Ma'ruf, M. F.[a]* and Darjanto, H.[b]

[a]*Civil Eng. Dept., Jember University, Jl. Kalimantan 37 Kampus Tegalboto, Jember,East Java, 68121, Indonesia*
[b]*Civil Eng. Dept. Narotama University, Klampis Ngasem, Sukolilo, Surabaya, East Java 60117, Indonesia*

Abstract

Excessive lateral deformation occurred during the excavation construction exceeded the design criteria. Scrutiny evaluation should be employed to investigate the factor triggering the problems. The evaluation was conducted using numerical analysis by means of PLAXIS 2D 2011. Back calculation modeling results showed that soil investigation did not capture the field condition properly. The existence of small pound and stream next to the field was not taken into account due to the distance of borehole location. Structural work was proposed to overcome the excessive lateral deformation.

Peer-review under responsibility of the organizing committee of SCESCM 2016.

Keywords: excessive deformation; deep excavation; numerical analysis;

1. Introduction

Deep excavation becomes a necessarily work in infrastructure and building project. Multi stories building should use underground structures for utilization as well as structural purposes. However, deep excavation is critical to both vertical and horizontal ground movement and basal heave as well. They have great influence to adjacent building and its earth structural work. It is therefore deep excavation work requires high precision in design as well as construction process to avoid failure.

The excavation failure can be either total or partial. The collapse of Nicoll Highway MRT is probably the most famous of the total deep excavation failure. It has been extensively investigated and documented. Whittle and his colleagues stated that the use of relatively thin jet grout piles and their specification was a lack along with low shear strength of marine clay to trigger the failure [1, 2]. Ishihara highlighted the requirement of closer spatial distance of

* Corresponding author. Tel.: +62-331-410241; fax: +62-331-410241.
E-mail address: farid.teknik@unej.ac.id

Peer-review under responsibility of the organizing committee of SCESCM 2016.

boring and sounding tests for deep seated deposit to reveal more precision deep soil characteristics [3]. Meanwhile the formal investigation report [4] indicated that the main reasons of failure as described below:

- Under design of the retaining wall.
- Under design of the strut whaler connection.
- Problems with instrumentation and monitoring process causes the incorrect back analysis during construction progress.

Under design that leads to lower factor of safety is typical reason of excavation failure. Three deep excavation failures of soft clay in Taiwan [5], the collapse of deep excavation in sensitive organic clay in Hangzhou, China [6], and two cases of excavation deteriorations in Kuala Lumpur, Malaysia [7] are the examples. They have inappropriate data collected causing misinterpretation of the soil properties. The use of improper soil parameters drives in under design of earth structure

This paper presents the case of the 13 m depth excavation supported by secant piles system. The failure did not yet occur. However, excess lateral deformation has developed on the retaining wall system. Investigation of the reasons and counter measure recommendation is discussed as well.

2. Project description

The construction of the 48 stories multi-purposes building required 12.8 m deep excavation. The site was situated at 120 m x 45 m area. Its layout can be seen in Fig.1. The towers were located in the middle of the site. Meanwhile, three stories basement occupied all the site area. The bottom basement was utilized as raft footing combined with bored pile. It was a single store warehouse building about 50 m from north border. A 3-stories building was neighboring along the South West to the West direction about 20 m from the boundary line. A small pound existed 15 m next to the North West corner continuously draining the water through a small stream along the North border.

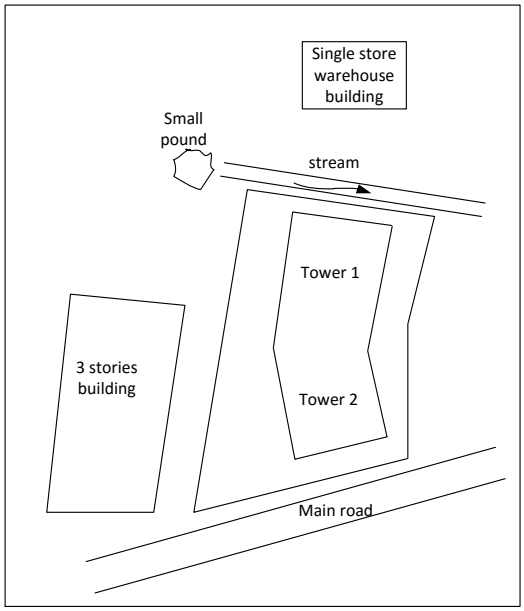

Fig. 1. Layout of the construction site

Four (4) boreholes and six (6) CPT tests were conducted. The location point of the test is presented in Fig.2a. The borehole locations were located along the tower building. The CPT tests were spread out off the borehole space. Fig.2b. and Fig. 2c show the CPT and SPT results respectively. The soil investigation results indicated that three

layers were identified. The soft to medium clay existed at 0 – 2 m depth. It was underlain by 13 m medium to stiff clay. This clay can be classified into expansive soil. The last identified stratum was stiff to very stiff clay. The ground water table did not exist along the boring data.

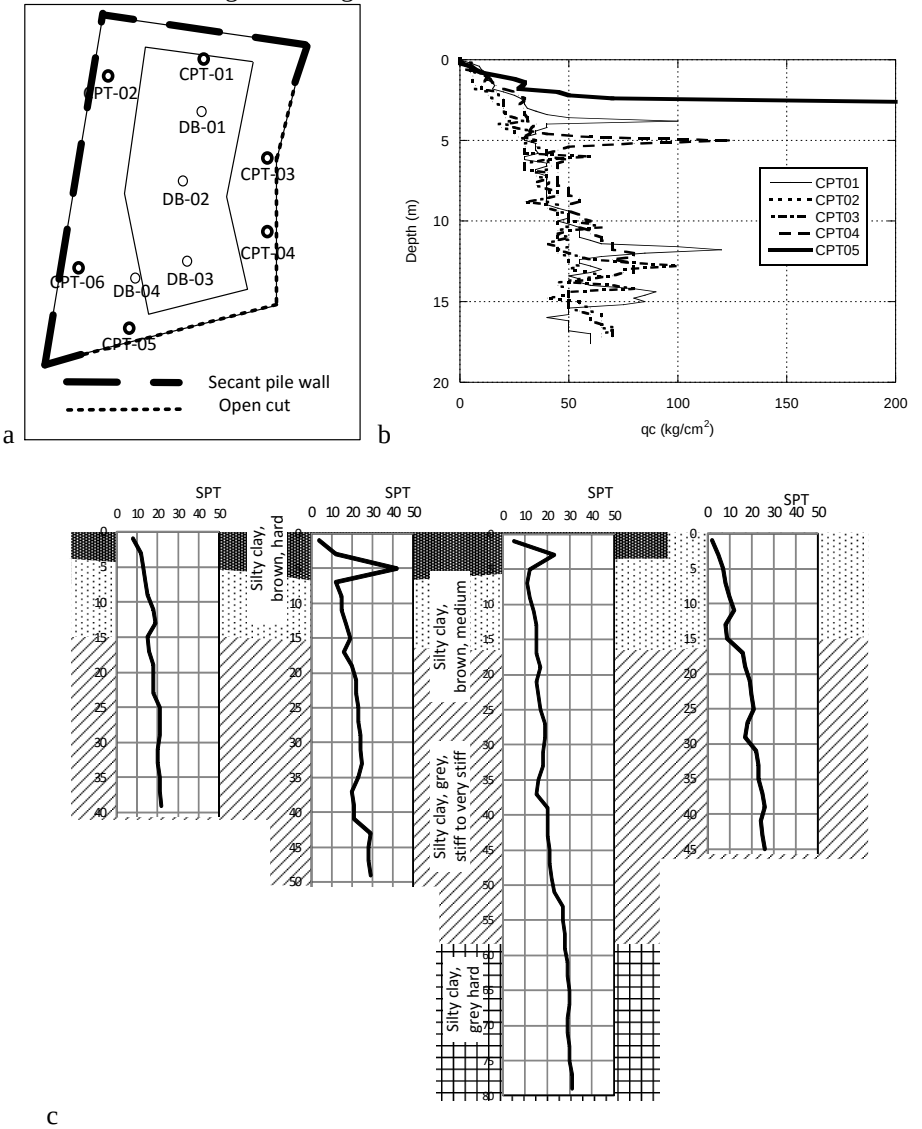

Fig. 2. (a) Location of borehole and CPT tests; (b) CPT results; (c) SPT and borehole results

3. Geotechnical recommendations

Based on the soil condition, the existing geotechnical recommendation related to the deep excavation can be described as follow:

- Excavation in the West and North side required cutting wall. The open cut can be applied in the other sides with the slope of 1.5V : 1H.
- The soldier pile system was recommended. The pile diameter was 800 cm and installed every 1200 cm with 20 m long. The pile should be able to retain minimum 500 kNm bending moment. The maximum design deflection was 120 mm at the top of the pile.
- For first 8 m excavation, a free standing soldier pile system was allowed. 1V:1H Counter front should exist from 8 m depth downward when removal of the ground for the tower was being conducted (Fig.3a.)
- Strut should be constructed before removal of the counter front (Fig. 3.b)
- Strut was permitted to be removed when the construction of the basement wall completed.
- The exposed slope should be immediately covered by minimum 75 mm thick of shotcrete.

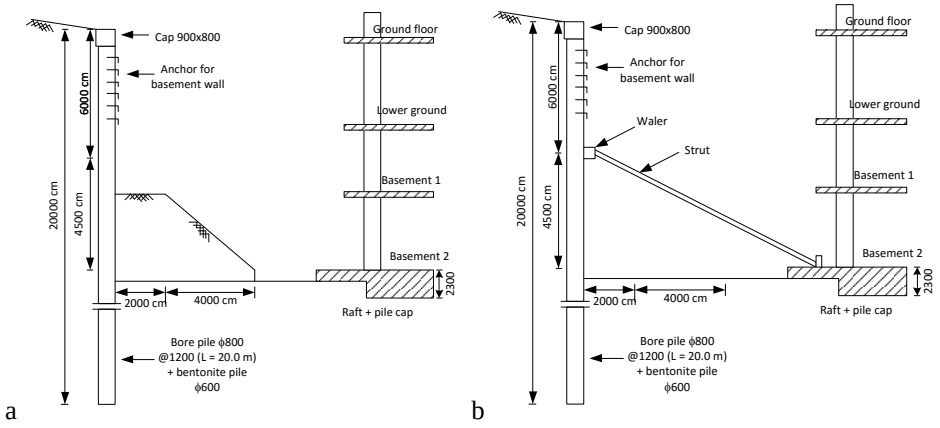

Fig. 3. The cut off wall system: (a) Counter front at 8 m depth; (b) Removal of counter front.

4. What went wrong?

The excavation work was started after soldier pile installation completed. The monitoring sensors were installed at the top of the pile cap according to the layout as described in Fig. 4a. The available monitoring data were started at days 13 after excavation work. The excavation sequence was started from the onset of tower 1 and extended into all direction to get 8 m depth dredging up. The 12.8 depth excavation was conducted by setting the ground counter front along the pile wall. Starting at M6 – M6' was a sloping excavation following arrow direction from – 12.8 m depth at M6 – M6' to ground level at the project boundary.

The deflection behavior along the excavation process can be evaluated in Fig.4b. The deflection of the wall exceeded the designed criteria at the middle of the North wall and at the first one-third of the West wall. Even it reached more than twice of the targeted deflection about 30 days afterward. This excessive deformation was a red warning and need a quick counter measure to prevent excavation failure.

5. Back analysis

Excessive lateral deformation of the wall indicated the first stage of the excavation failure. Slow counter measure action can lead to the catastrophic problem. Precise remediation required back analysis based on the recording data of the real condition. Finite element modeling was utilized for back analysis by means of commercial software PLAXIS 2D 2011.

5.1. Soil Parameters

Back analysis of the soldier pile wall system was based on finite element analysis. The soil behavior was modeled using Mohr Coulomb model. This model is the simplest one and requires minimum soil parameters. The soil parameter for the existing design based on the soil investigation report is presented in Table 1. The sensitivity analysis based on those parameters was conducted to capture the real deformation in the field.

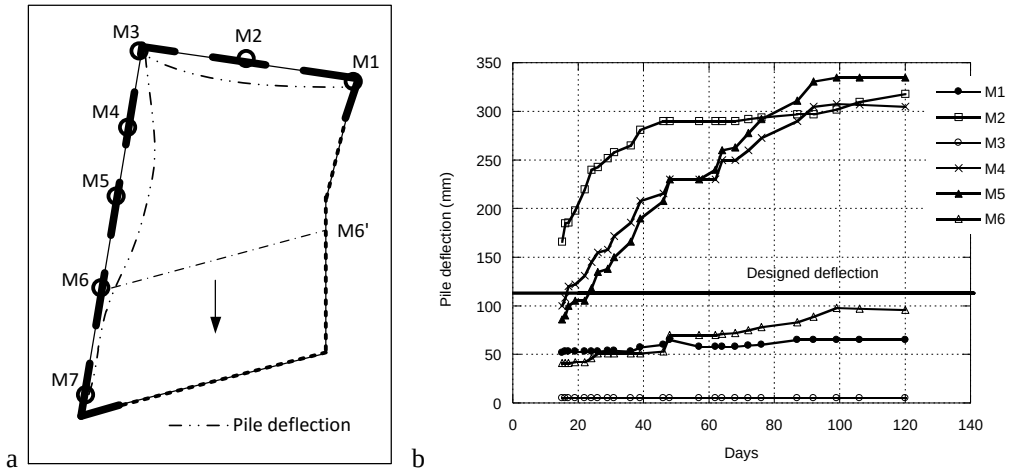

Fig. 4. (a) Monitoring points and deflection plan view; (b) Pile deflection curve.

Table 1. Soil parameters for existing design.

Parameter	Symbol	Layer 1	Layer 2	Layer 3
Name		Soft Clay	Clay	Stiff Clay
Material model		Mohr Coulomb	Mohr Coulomb	Mohr Coulomb
Type of material behavior		Undrained	Undrained	Undrained
Unsaturated unit weight (kN/m^3)	γ_{unsat}	16	16.8	17.2
Saturated unit weight (kN/m^3)	γ_{sat}	17	18	18
Stiffness modulus (kN/m^2)	E	7E3	9E3	12E3
Poisson ratio	υ	0.3	0.35	0.35
Cohesion (kN/m^2)	c	11	21	20
Friction angel (^{o})	ϕ	12	13	17

5.2. Geometry Modeling

Geometrical modeling of the excavation in PLAXIS is presented in Fig.5. The plane strain model was applied with 15 nodes for meshing. The uniform loading was applied to represent the 3 stories building. While fixed strut was installed to prevent continues deformation.

5.3. Model Simulation

The simulation was conducted twice. The first was sensitivity analysis to find the appropriate modeling parameters suit to the real deformation. The last one was to find the solution to prevent excessive deformation continuously occurred. Three parameters were utilized for sensitive analysis, namely stiffness modulus, cohesion, and friction angle. The results of the simulation can be seen in Fig.6. The parameters used to obtain field condition in which a 310 mm lateral deformation occurred are described in Table 2. Only layer 1 and layer 2 that significantly have effect of the wall deformation.

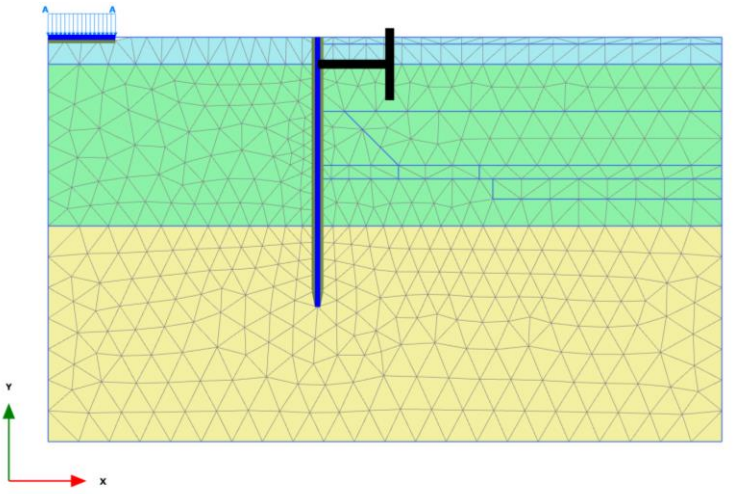

Fig. 5. Geometrical modeling and meshing in PLAXIS

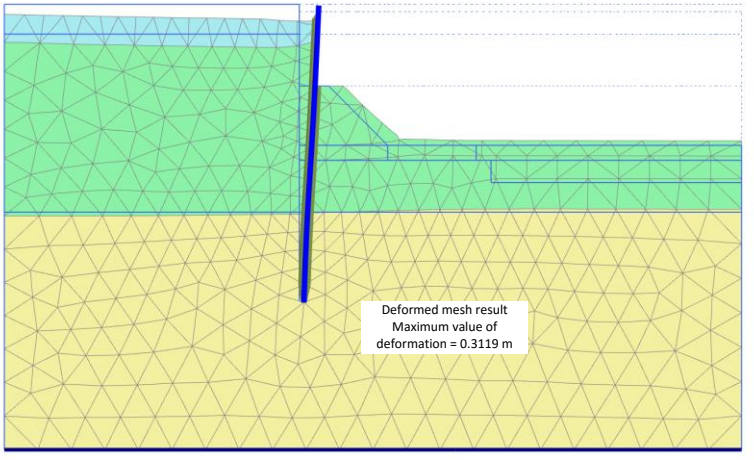

Fig. 6. Back analysis result

Table 1. Soil parameters after back analysis.

Parameter	Symbol	Layer 1	Layer 2	Layer 3
Name		Soft Clay	Clay	Stiff Clay
Stiffness modulus (kN/m^2)	*E*	2500	6E3	12E3
Cohesion (kN/m^2)	*c*	10	21	20
Friction angel (^{o})	ϕ	2	2	17

5.4. Structural Counter Measure

To prevent continuous deformation, strut is the most favorable structural counter measure. Strut can be installed without time consuming and the material is easily found in the surrounding construction site. The finite element

modeling is also utilized to predict the behavior of the excavation system when the strut is installed. The results of the simulation can be examined in Fig.7. It can be seen clearly that the excessive deformation is blocked at about 300 mm. it means that no additional deformation occurs.

6. Discussion

Back analysis simulates condition for different value of stiffness modulus, cohesion, and friction angle. The proper values of those parameters to get the real deformation are less than ones of the soil investigation results. However, those values still comply with the handbook of geotechnical design tables [8]. The very low value of friction angle can be understood as those two layers have very small portion of coarse soil. It means that the soil has no friction angle.

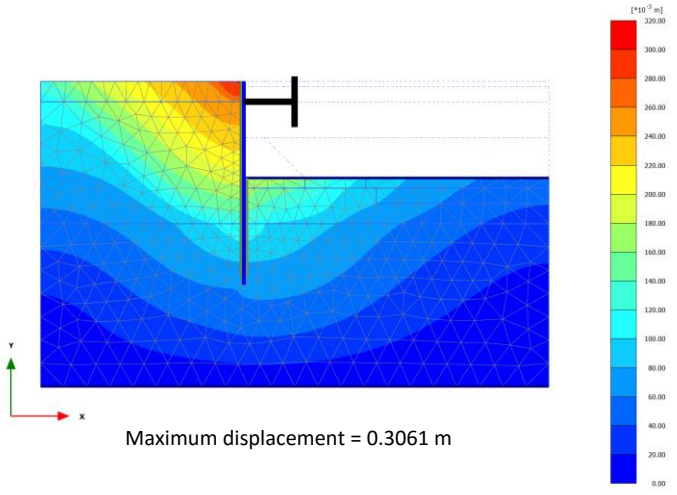

Fig. 7. Displacement distribution after strut installation

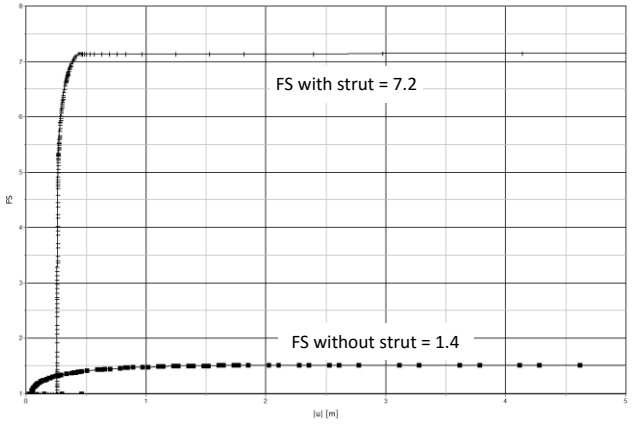

Fig. 8. Factor of Safety FS of the retaining wall system before and after back analysis

The excessive deformation maybe associated with the expansive characteristic of the soil. The water flow from the pound develops swelling effects on the soil that squeeze the wall away of the soil. Moreover, the stream next to

the retaining wall will reduce the soil strength significantly. It agrees with the result of the back analysis. The soil investigation results do not capture the effect of water to the soil strength since the point of the field test is relatively far from the pound.

The proposed solution to prevent continuous excessive deformation works well. It can be seen in Fig.8 that safety factor increases significantly when the strut is installed, even with very weak soil parameters. The excessive deformation does not continue to occur. In the field, excessive deformation and strut installation have changed the construction methods. The use of the building column to support the strut requires top down basement construction process (Fig.9). The lower basement should be constructed after the upper basement completed.

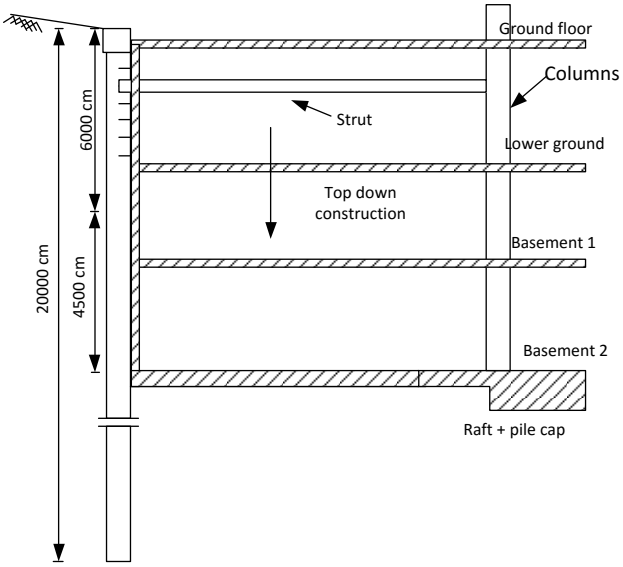

Fig. 9. Top down basement construction process

7. Concluding Remarks

Deep excavation requires careful examination when designing the supporting system. The information of the field is very important to interpret the soil investigation report. Lack of combining the field condition and soil investigation report interpretation can lead to construction failure.

References

[1] A.J. Whittle, R.V. Davies, Nicoll Highway Collapse: Evaluation of Geotechnical Factors Affecting Design of Excavation Support System, Proc. of Int. Conference of Deep Excavation, Singapore, 2006.
[2] G. Coral, A.J. Whittle, Re-Analysis of Deep Excavation Collapse Using a Generalized Effective Stress Soil Model, (ASCE Geotechnical Special Publications ; GSP 208)Proceedings of the 2010 Earth Retention Conference, 2010.
[3] K. Ishihara, Collapse of Braced Excavation in Singapore, Proceeding of TC302 Symposium Osaka 2011: International Symposium on Backwards Problem in Geotechnical Engineering and Monitoring of Geo-Construction, 2011, pp. 35- 50.
[4] A.M. Puzrin, E.E. Alonso, N.M. Pinyol, Braced Excavation Collapse: Nicoll Highway, Singapore, in A.M. Puzrin, E.E. Alonso, N.M. Pinyol (Eds.), Geomechanics of Failures, Springer, 2010, pp. 151 – 182.
[5] T.N. Do, C.Y. Ou, A. Lim, Evaluation of factors of safety against basal heave for deep excavations in soft clay using the finite element method, J. Geotech. Geoenviron. Eng , 139(2013) 2125 – 2135.
[6] R. Chen, Z. Li, Y. Chen, C. Ou, Q. Hu, M. Rao, M. (2014). "Failure Investigation at a Collapsed Deep Excavation in Very Sensitive Organic Soft Clay." J. Perform. Constr. Facil., 29(2015) 1-14.
[7] S.S. Liew, Y.E. Loh, Two Case Studies of Collapsed Temporary Excavation using Contiguous Bored Pile Wall, Proceeding of CIEHKIE-IEM Tripartied Seminar (Deep Excavation), Hong Kong, 21 May 2011.
[8] B.G. Look, Handbook of Geotechnical Investigation and Design Tables, Taylor and Francis, London, 2007.

Available online at www.sciencedirect.com

ScienceDirect

Procedia Engineering 00 (2017) 000–000

Procedia Engineering

www.elsevier.com/locate/procedia

Sustainable Civil Engineering Structures and Construction Materials, SCESCM 2016

Suggested graph of geotextile reinforcement against the several variation of field condition based on the soft clay soil in Java island area

Putu Tantri K.Sari[a], Yudhi Lastiasih[a], Sugiarto[b,*]

[a]*Civil Engineering Department, Institute Technologi of Sepuluh Nopember, Surabaya, 60111, Indonesia*
[b]*Civil Engineering Department Bakrie University, Jakarta, Indonesia*

Abstract

This paper described the behavior of reinforced embankments constructed on the soft clay subgrade with vary of compressible depth, embankment slope and embankment height. The stability of embankment using Bishop Methods, the resistance moment and the number of geotextile requirements in the vary condition are examined in this paper. It is shown that the vary condition of subgrade and embankment can significantly affect the embankment stability and also affect to number of reinforcement. So it needed a lot of time to do the design embankment reinforcement, especially when the construction carried out with a length of tens of kilometers. The major part of this paper is on the challenges to find the graph of the number of geotextile reinforcement which have been verified by the field condition. The graph is proposed to support the engineer and designer to design the embankment reinforce by geotextile to reduce time consuming due to a huge vary of field condition during construction.

Peer-review under responsibility of the organizing committee of SCESCM 2016.

Keywords: Geotextile; reinforcement embankment; slope stability; Bishop method; Limit equilibrium method.

1. Introduction

Construction of road and bridge infrastructure increasingly developed in Indonesia. A growing number of infrastructure developments led as less of stable and secure area to construct. That problem making it is inevitable that the road construction is performed in areas that have a relatively soft subgrade and tendency towards instability.

* Putu Tantri. Tel.: +6285731033116; fax: +62315928601.
E-mail address: tantrigeoteknik@gmail.com ; tantri@ce.its.ac.id

Peer-review under responsibility of the organizing committee of SCESCM 2016.

In addition, to avoid the flood water level and the adjustment of topography, the road construction is often carried out on a high embankment. Construction of roads with relatively high embankment on the soft soil subgrade can certainly raise some problems related to the stability of the road embankment.

Problems that often arise when the construction of the road with a high embankment and on soft soil is the stability against landslide. The performance of embankments constructed on soft clays has been studied by much research [5, 6, 8, 10, 12, 13, 15−17 and 21]. Some studies have also conducted to determine the condition of the embankment in the field by analyzing the test results of geotechnical instruments on road embankment in the field. Previous studies have also been conducted to determine the characteristics of geosynthetic installed as reinforcement embankment. The analysis shows that the use of geosynthetic can improve the stability of embankment.

The use of geosynthetic as one method of road embankment reinforcement is more developed. Usually the use of reinforcement with geotextile which is one type of geosynthetic is performed on the road embankment built on soft soil foundation. Geosynthetic reinforcement has been widely used to improve the stability of embankment on soft clay soil [1, 3, 4, 9, 14, 18, 19]. Geotextile layers increase the embankment stability by virtue of two primary function; tensile reinforcement and as drainage element reducing pore pressure. Properties and characteristics of the reinforcement embankment constructed on soft ground already widely understood and developed by researchers and implementers in the field.

The road construction is often conducted for many kilometers with each area have a different height of embankment. In addition, the subgrade under the embankment also has different characteristics. With the difference in height of embankment and type of subgrade, designer usually overwhelmed to do a reinforcement design of embankment. The calculation of the number of reinforcement geotextile design is usually done one by one in accordance with the variation height of the embankment and type of subgrade underneath. With so many variations of existing data of course will time consuming in doing design. Instead of the usual, the designer only have a limited time due to the process construction in the field should be implemented immediately. So it is not uncommon designer do a design that seemed perfunctory because it chased by the time. Design carelessly is certainly going to a very endanger the stability of embankment road, especially at the high embankment of landslide issues.

The main purpose of this study is to obtain the results of analysis of variations in the characteristics of the subgrade, embankment elevation variations for the required number of geotextile reinforcement. The main result of this study is in the form of a graph or code that will assist designer in making the design requirements for the number of reinforcements. The result of this analysis aims to avoid design errors due to varied data that planned as well as too short provided time to do the designing.

2. Brief description of variation data and methods

Variations of the data were used in this study such as: The high variation road embankment; Soft clay soil depth variations; Variations in the characteristics of the subgrade. The basis of the variation data was used from the approach of the data of road construction undertaken in Java Island, Indonesia. Locations used in the sampling data in this study were:

- Improvement of subgrade and reinforcement using geotextile on High way construction on Ngawi-Kertosono Pack. 2 (STA 111 + 250 s / d STA 118 + 700)
- Reinforcing embankment with geotextile on road development Porong-Gempol Toll
- The construction of the road embankment reinforcement embankment on the road section of Surabaya-Mojokerto

The data from in the three locations are expected to represent a variety of soft soil data on the island of Java in particular.

Highway roads embankment at Ngawi Kertosono have varied heights which is 2 meters to 7.5 meters, while on the road section Porong-Gempol highway also has an embankment height of between 2 meters to 7.8 meters. While on the road Surabaya-Mojokerto highway embankment heights are between 2 meters to 5 meters. The type of subgrade in the location to be reviewed are dominant clay which relatively soft with compressible soil depth are between 4 meters to 20 meters.

According to the different variations mentioned above, the stability of the embankment and reinforcement geotextile will analyzed in this research will be divided into several groups:

- Elevation embankments analyzed were 2 meters, 4 meters, 6 meters and 8 meters.
- The slopes of the embankment analyzed were 1: 1, 1:2 and 1: 3.
- The depths of soft soil analyzed were 5 meters, 10 meters, 15 meters and 20 meters.
- The characteristics of subgrade soil data were distinguished by the value of plasticity: Low Plasticity, Medium plasticity and high plasticity.

So from that variations will be analyzed as many as 32 types of data. Analysis of the stability of the embankment will be conducted using Limit Equilibrium Method with the concept of moment equilibrium method.

This method is very widely used by experts to analyze geotechnical landslide. LEM has developed since the early 20s century. Petterson (1915) present an analysis of the stability of embankments Stigberg Quay in Gotherberg, Sweden where the field is analyzed landslides which circle arc-shaped field of landslides mass calculation is done by the method of vertical slices. Furthermore the methods of calculation by using the method of slices continue to be developed by several researchers [12]. The development of computer calculations by auxiliary program began in the 1960s. The help of the computer program makes the development of mathematical formulas become well. Some researchers are beginning to develop a mathematical formula with aid a computer program [20].

2.1. Geotextile design

Allowable stress geotextile for reinforcement construction planning is defined as the ultimate tensile strength of age appropriate construction plan divided by the reduction factor is taken into account. The allowable stress values geotextile are in accordance with the following equation:

$$\sigma_{all} = \sigma_c \left(\frac{1}{f_d}.\frac{1}{f_{env}}.\frac{1}{f_m}.\frac{1}{f_c}\right) \quad (1)$$

Where σall as allowable stress geotextile; σc as the ultimate tensile strength according to age of geotextile construction; f_d as a reduction factor for mechanical damage; f_{env} are reduction factor by environmental conditions; f_m are reduction factor for the extrapolation of data geotextile tensile strength and fc are secure construction factor.

Another Formulation used in the calculation of allowable stress values geotextile are based on the AASHTO (2002). The tensile capacity of the reinforcement determined from constant load laboratory testing must also be adjusted using reduction factors to account for site-specific potential load of strength due to chemical and biological degradation (RF_d) and mechanical damage during installation (RF_{ID}). The allowable tensile strength of the reinforcement (T_{allow}) is the calculated as:

$$T_{allow} = \frac{T_{ult}}{RF} = \frac{T_{ult}}{RF_D x RF_{ID} x RF_{CR}} \quad (2)$$

All reduction factors must be based on product-specific testing. In no case should values for RF_D and RF_{ID} be less than 1.1. In the absence of such data, AASHTO (2002) recommends that RF not less than 7 or 3.5 for permanent and temporary wall structure, respectively. The magnitude of creep reduction factor (RF_{CR}) will vary with design life. Typically values may range from 1.5 to 3.0 with the lowest value corresponding to short lifetime. The maximum design load for a geosynthetic layer in a permanent reinforced wall application is typically reduced to a long-term allowable design load T_{des} where:

$$T_{des} = \frac{T_{allow}}{FS} \quad (3)$$

Here SF is an overall factor of safety to account for uncertainty in problem geometry, soil variability and applied loads and has a minimum value of 1.2. For reinforces slope, FS =1 since the overall factor of safety is accounted for in the stability analyses.

This research were used a method of slices approach together with the assumption of a circular failure surface. The potential failure surface must also include those passing partially through the reinforce soil mass and into the soil beyond the reinforced zone as well as those completely contained by the reinforced soil zone. A solution for the factor of safety using Bishop Methods of analysis carried out using the following equation:

$$FS = \left(\frac{Mr}{MD}\right)_{unreinforced} + \frac{\sum T_{allow} x R_t}{MD} \quad (4)$$

Where MR and MD are the resisting and driving moments for the unreinforced slope, respectively and Rt is the distance between the circular centre and the geotextile layer located.

Selection of geotextile for reinforcement influenced by two factors: internal and external factors. Internal factors consist of geotextile geotextile tensile strength, extension properties (creep), geotextile structure and resistance to environmental factors. Yet, not all available geotextile tensile strength can be utilized in planning and construction reinforcement. This study used a geotextile with ultimate tensile strength equivalent to 52 KN / m 'and 100 KN / m'.

2.2. Soil Profile

Soil data used in this study was based on ground investigation data were carried out at 3 road project mentioned above. The data obtained was recapitulated and the compressible soil depth is used to analyze. The next stage, data was correlated and compared with the empirical formula to obtain data that will be entered in an auxiliary program for slope stability analyses that is SLOPE/W. The main data which is entered into the SLOPE/W is the values of cohesion undrain at each layer of the subgrade. Due to the subgrade soil tested is dominant-type clay consistency then friction angle value is greatly small in close to zero. This study used a friction angle value for subgrade = 0. The cohesion undrains soil subgrade was divided into three types of plasticity: Low Plasticity; Medium Plasticity and High Plasticity. Cohesion value at each layer of soft clay soil is shown in Table 1.

Table 1. Soil subgrade data used in the analysis

Sub-grade Layer (1 meter per each layer)	Low Plasticity Cu (Kpa)	Medium Plasticity Cu (Kpa)	High Plasticity Cu (Kpa)
Layer 1	7.8	7.7	7.6
Layer 2	8.8	8.5	8.2
Layer 3	9.8	9.3	8.8
Layer 4	10.7	10	9.4
Layer 5	11.7	10.8	9.9
Layer 6	12.6	11.5	10.5
Layer 7	13.5	12.3	11
Layer 8	14.5	13	11.6
Layer 9	15.5	13.8	12.2
Layer 10	16.4	14.6	12.8
Layer 11	17.4	15.3	13.3
Layer 12	18.3	16	13.8
Layer 13	19.3	16.8	14.4
Layer 14	20.2	17.6	15
Layer 15	21.2	18.3	15.6
Layer 16	22	19	16.1

Layer 17	23	19.8	16.7
Layer 18	23.9	20.6	17.2
Layer 19	25	21.4	17.8
Layer 20	25.9	22.2	18.4

3. Analysis results and discussion

Analysis of embankment stability against sliding was done by using Bishop Simplification Method. Subgrade was assumed without performing soil improvement with prefabricated vertical drained (PVD) or other soil improvements. Therefore the calculation was done without considering the final and initial height of embankment. Subgrades used in this study were clay soil therefor the cohesion are very affect for the stability of the embankment.

3.1. Stability embankment analysis

The calculations of the number of reinforcement were performed by calculating the stability of the embankment by look at the value of safety factor and moment resistance that occur in the embankment. If the value of safety factor is smaller than 1 (SF <1), then the embankment has the possibility of landslide. The smaller the value of the safety factor, the smaller the embankment ability to resist the activating from the load received. The condition is caused by a resisting moment embankment is smaller than the driving moment of embankment.

In computing the number reinforcement requirement embankment by geotextile, the common reference used is the safety factor value. The calculation will be done by looking at the several times for the possibility of landslide by conducting a trial of some areas of Landslide that may occur. The smallest value of the safety factor is not a reference in this design. Landslide areas that produce the number reinforcement geotextile will be used in the reference design requirement of reinforcement number. So take a few trials to obtain most critical conditions. The experiments were performed on one of the heights of the embankment and one of the main conditions of the soil subgrade in one of the variations used. 180 iterations performed to prove that the value of the smallest safety factor is not necessarily the most critical condition landslide embankment.

Total reinforcement using geotextile requirement is highly dependent on the value of delta moment resistant. Therefor from the analysis results can be seen that the greatest value of delta moment resistance is not necessarily generated the smallest value of safety factor. In addition, it also shows that the highest number of geotextile is not generated by the smallest value of safety factor due to the value of moment resistance and activating moment also affected.

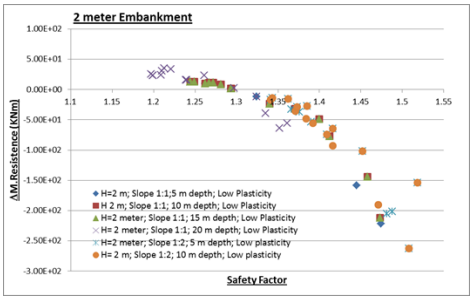

Fig. 1. Safety factor and delta Moment resistance of 2 meter embankment with vary condition.

The results of embankment stability analysis with a height of 2 meters showed that embankment is quite stable against the danger of sliding. Fig. 1 shows that the safety factor is greater than 1 so that the embankment is reasonably stable even without reinforcement performed. The stability of the embankment also occurs in all the variations used in this study. So for embankment 2 meter is not required reinforcement geotextile structurally as supporting landslide both internal and overall stability.

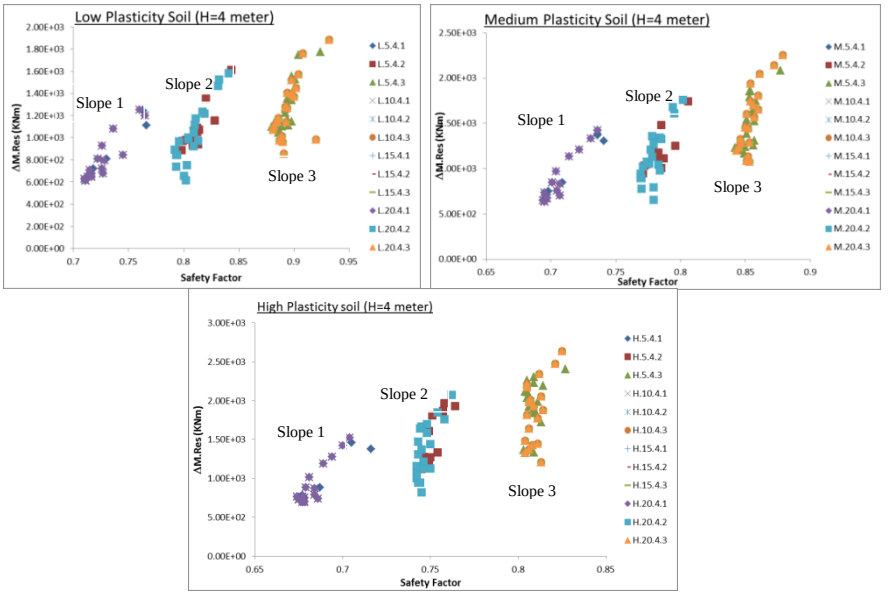

Fig. 2. Safety factor and delta moment resistance of 4 meter height embankment with various condition

The analysis result of the embankment higher than 2 meters showed that are need to reinforce as supporting against landslide. Fig. 2 shows the value of Safety factor and ΔMoment Resistance on 4 meter high embankment. Based on these graphs can be seen that the greater the slope of the embankment, the greater the value of the safety factor of the embankment. Plasticity value on the subgrade also affects the value of safety factor on the embankment. The higher the plasticity of land, the value of the safety factor in the embankment also will be smaller. This condition also occurs in embankment with 6 and 8 meters high. However, the 4 meters embankment high, the depth of subgrade is not much effect on the stability of landslide. The condition can be seen in the value of Safety factor with the different soil depths. This is caused by the deepest depth of landslide in the embankment as high as 4 meters is ± 5 meters (Fig. 3) therefor a depth of 10-20 meters soft ground does not effect of stability embankment

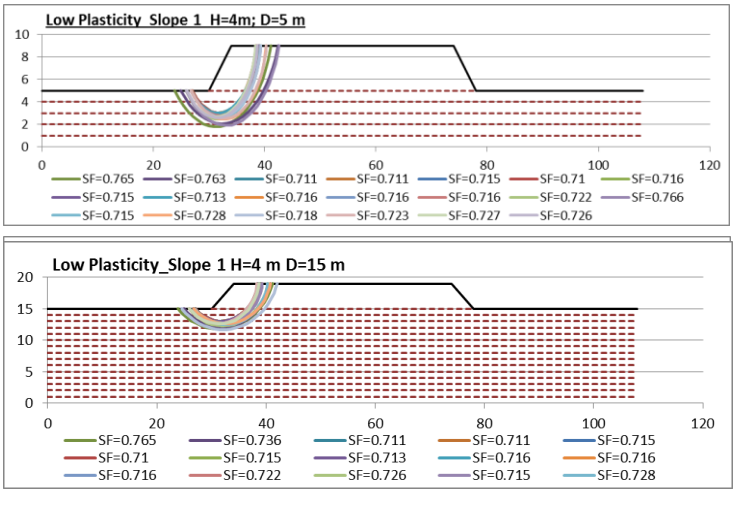

Fig. 3. The landslide depth of 4 meter embankment height with varies depth of soft soil subgrade.

From Fig. 3 it can be seen that the depth of the soft subgrade is not too big impact to the stability of the embankment and the depth of landslides area. The condition occurs at the height of the embankment is relatively low to moderate. So the higher the embankment, the depth of soft ground will increasingly affect the depth of landslide area. This condition can be seen in the results analysis of the embankment stability at a height of 6 and 8 meters. At the height of the embankment 6 meters, depth of sliding can occur for up to 5-7 meters. Such conditions affect the safety factor value that occurs. Results analysis of the embankment stability and the value of safety factor on the condition of soft soil depth of 5 meters are different when compared with the stability of the embankment and the value of safety factor on the condition of soft soil depth of 10 meters. While the results of the analysis at a depth of 10 soft soils to a depth deeper shows the relative same value of safety factor.

3.2. The number of geotextile reinforcement

The calculations of the required amount of geotextile were done by using two different geotextile tensile strength: 52 KNm' and 100 KNm'. In accordance with AASHTO standards (2002), the tensile strength of geotextile used in the design is influence by the reduction factor. The reduction factor is equal to 1.1-1.5 due to reduction because of installation errors; 2-2.5 due to reduction for their creep; 1.1-1.25 is the reduction due to the influence of biology; 1.1-1.2 is due to the influence of chemical reduction.

The numbers of geotextile used as a reference in this study are the sliding area that produced the highest amount of reinforcement. From the results shows that the slope of the embankment and the depth of the soft soil will affect the number of geotextile requirements. In addition, soil plasticity also affects the amount of geotextile requirements. The deeper the soft soil would produce relatively more required amount of reinforcement geotextile. However, this conclusion is dependent on the height of embankment on soft soil. The higher the embankment, the depth of landslides will be deeper so it will affect the number of geotextile. It shows that the depth of soft soil will affect the number of geotextile. At a height of 4 meters, the number of geotextile required at a depth of 5 and 10 meters produces the same amount of reinforcement. This was caused by a landslide depth is no more than 5 meters. Whereas at the height of embankment 6 and 8 meters, the number of geotextile requirements in the soft soil at a depth of 5 and 10 meters have a slightly different results. In 10 meters soft soil depth, the number of geotextile reinforcement will be relatively more. In addition, the greater the amount of soil plasticity produces more number of geotextile. The increasing number of geotextile also obtained in relatively steep slope of the embankment, namely the slope of 1: 1. The geotextile number is in great condition of geotextile tensile strength with the largest reduction factor.

In many variation of used then there are many variations result of the required amount of reinforcement geotextile. With the many results and lots of graphics then certainly will further confuse the designer. To facilitate the use, the chart number geotextile requirements then later simplified. The simplification is based on the existing conditions. In addition, the simplification also carried out under a range of the maximum and minimum number of geotextile reinforcement requirements based on size reduction factor used. The results of the simplification of the graph are then verified with the required amount of reinforcement geotextile on the embankment roads that have been applied in the field. Relationship Graph required amount of geotextile can be seen in Fig. 4.

The results on the above chart show the range of the required amount of geotextile on variations of soil plasticity. When the designer are brave enough to use with a geotextile reduction safety factor with great value, then the number of geotextile requirements as reinforcement embankment is relatively small when compared with the reduction factor when using small safety factor. Selection of range values for tensile strength reduction is based on the experience of the designer.

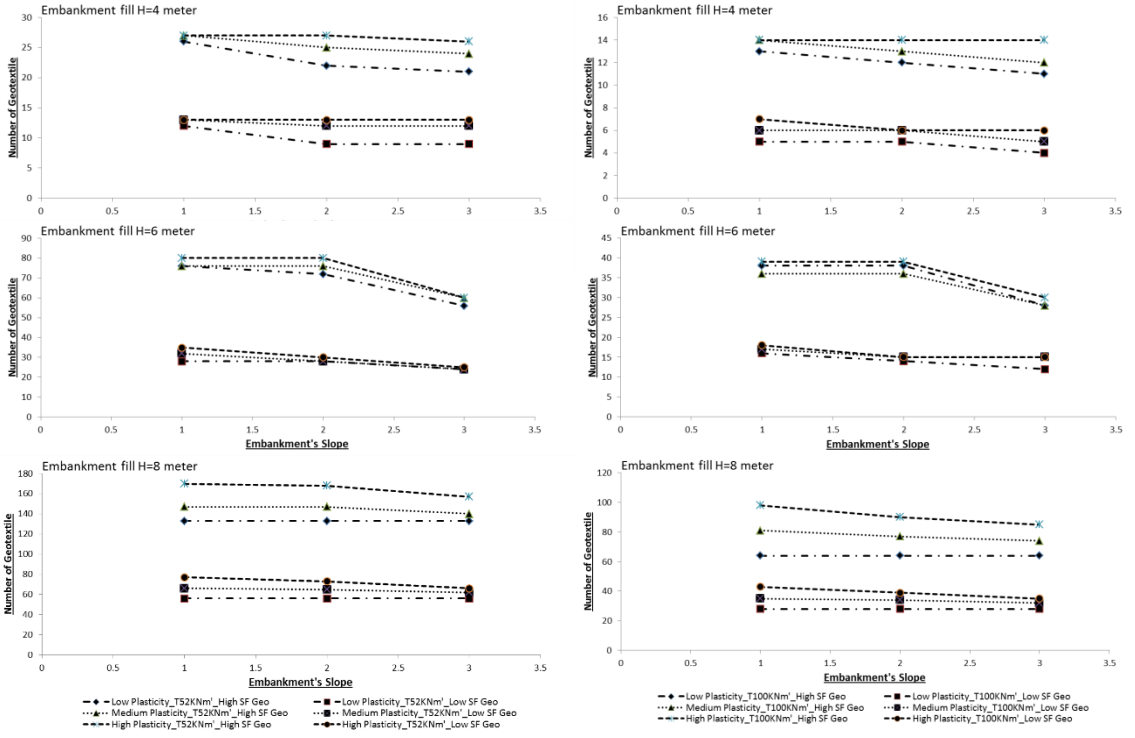

Fig. 4. Suggested graph of the geotextile requirements on varied conditions

The verification has made as consideration of the use of this chart. Verification is done on one of the road construction site that has been actually implemented. Such conditions are shows significant enough result. Total requirements reinforcement geotextile on the construction of toll roads Ngawi-Kertosono is as much as 15 sheets with an embankment height of 4 meters and 48 sheets at a height of 6 meters. Number of geotextile reinforcement is done on the road embankment when the subgrade is not improved by PVD so that the bearing capacity of subgrade under embankment does not increase. These results were consistent with the range of results obtained on the graph Fig. 13.

4. Summary and conclusion

In this paper, the amount ranges reinforcement requirements of embankment using geotextile on a variety of soil conditions has been obtained. Presentation of the results of the analysis with the variation used was a graph of the number geotextile requirements. From the graphs analysis results showing that the height of the embankment, embankment slope, soil type and depth of soft soil subgrade are very contribute significantly to the number of geotextile requirements. The higher the embankment of course, produces the greater number geotextile requirements. The smaller the slope of embankment, the number of geotextile requirements will be less. Geotextile a growing number are also found in embankment on the ground base with soft soil depth deeper.

This graph is expected to assist designer to do the design for reinforcement embankment using geotextile. Total requirements geotextile on the suggested graph is only done on the condition that relatively similar to the data used

in this study. Still need to be verified further to consummation this graph which is expected in accordance with the actual conditions that are often experienced designer in the field. In addition, the use of soil improvement methods that one of them is PVD will also greatly affect to the number of geotextile requirements. So it is still necessary to improve the graph to determine the influence of soil improvement with the number of geotextile.

References

[1] Bergado, D.T., Teerawattansuk, C., 2008. 2D and 3D numerical simulations of reinforces embankments on soft ground. Geotextiles and Geomembranes 26 (1), 39-55.
[2] Brand and R.P. Brenner, Elsevier Scientific Publishing Company. pp. 311–362.
[3] Briancon,L, Villard, P., 2008. Design of geosynthetic-reimforced platforms spanning localized sinkholes. Geotextiled and Geomembranes 26 (5), 416-428.
[4] Chen, Y-M., Cao, W.-P., Chen, R.-P., 2008. An Experimental Investigation of soil arching within basal reinforced and unreinforced piled embankments. Geotextiles and geomembranes 26(2), 164-174.
[5] Crawford, C.B., Fannin, R.J., and Kern, C.B. 1995. Embankment failures at Vernon, British Columbia. Canadian Geotechnical Journal, 32: 271–284.
[6] D'Appolonia, D.J., Lambe, T.W., and Poulos, H.G. 1971. Evaluation of pore pressures beneath an embankment. Journal of Soil Mechanics and Foundation Engineering, ASCE, 97: 881–897.
[7] Hoeg, K., Andersland, O.B., and Rolfsen, E.N. 1969. Undrained behaviour of quick clay under load tests at Astrum. Géotechnique, 19: 101–115.
[8] Humphrey, D.N., and Holtz, R.D. 1987. Reinforced embankments- a review of case histories. Geotextiles and Geomembranes, 6(4) : 129-144.
[9] Indraratna, B., Balasubramaniam, A.S., and Balachandran, S. 1992. Performance of test embankment constructed to failure on soft marine clay. Journal of Geotechnical Engineering, ASCE, 118: 12–33.
[10] Janbu, N. (1954). Aplication of composite slip surface for stability analysis. European conference on stability of earth slopes, Stockholm.
[11] Leroueil, S., Tavenas, F., Trak, B., La Rochelle, P., and Roy, M. 1978a. Construction pore pressures in clay foundations under embankments. Part I: the Saint-Alban test fills. Canadian Geotechnical Journal, 15: 54–65.
[12] Leroueil, S., Tavenas, F., Mieussens, C., and Peignaud, M. 1978b. Construction pore pressures in clay foundations under embankments. Part II: generalized behaviour. Canadian Geotechnical Journal, 15: 66–82.
[13] Li., A.L., Rowe, R.K., 2008, Effects of viscous behavioure of geosynthetic reinforcement and foundation soils on embankment performance. Geotextiles and Geomembranes 26 (4), 317-334.
[14] Loganathan, N., Balasubramaniam, A.S., and Bergado, D.T. 1993. Deformation analysis of embankments. Journal of Geotechnical Engineering, ASCE, 119: 1185–1206.
[15] Ortigao, J.A.R., Werneck, M.L.G., and Lacerda, W.A. 1983. Embankment failure on clay near Rio De Janeiro. ASCE Journal of the Geotechnical Engineering Division, 109, 11: 1460–1479.
[16] Parry, R.H.G., and Wroth, C.P. 1981. Shear stress-strain properties of soft clay. In Soft clay engineering. Edited by E.W.
[17] Rowe, R.K., Taechakumthorn, C., 2008. Combined effect of PVDs and reinforcement on embankments over state-sensitive soil. Geotextile and Geomembranes 26(3), 239-249.
[18] Sarsby, R.S., 2007. Use of 'Limited Sife Geotextiles' (LLGs) for basal reinforcement of embankment built on soft clay. Geotextile and geomembranes 25 (4-5), 302-310.
[19] Spencer, E. (1967). A method of analysis of the stability of embankments, Assuming parallel interslice forces. Geotechnique, Vo. 17, pp. 11-26.
[20] Tavenas, F., and Leroueil, S. 1980. The behaviour of embankments on clay foundations. Canadian Geotechnical Journal, 17: 236–260.